Equation (3.25) requires that the capillary be long enough to assure fully developed flow, where end effects are insignificant. However, because of entrance effects, the actual pressure profile along the length of the capillary exhibits curvature. The effect is shown schematically in Fig. 3.17 [31] and was corrected by Bagley [32] using the end correction e:

$$\tau_w = \frac{1}{2}\frac{(p_0 - p_L)}{(L/R + e)}. \tag{3.26}$$

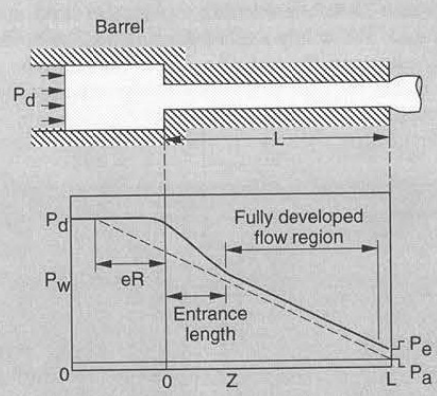


Figure 3.17 Entrance effects in a typical capillary viscometer

The correction e at a specific shear rate can be found by plotting pressure drop for various capillary L/D ratios as shown in Fig. 3.18 [31].

The equation for shear stress is then

$$\tau_{rz} = \frac{r}{R}\tau_w. \tag{3.27}$$

To obtain the shear rate at the wall the Weissenberg–Rabinowitsch [33] equation can be used

$$\dot{\gamma}_w = \frac{1}{4}\dot{\gamma}_{aw}\left(3 + \frac{d(\ln Q)}{d(\ln \tau)}\right) \tag{3.28}$$

where, $\dot{\gamma}_{aw}$ is the apparent or Newtonian shear rate at the wall and is written as

$$\dot{\gamma}_{aw} = \frac{4Q}{\pi R^3} \tag{3.29}$$

The shear rate and shear stress at the wall are now known. Therefore, using the measured values of the flow rate, Q, and the pressure drop, $p_0 - p_L$, the viscosity is calculated using

$$\eta = \frac{\tau_w}{\dot{\gamma}_w}. \tag{3.30}$$

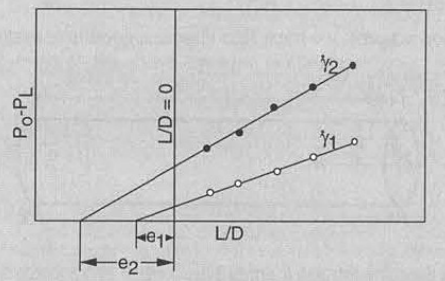


Figure 3.18 Bagley plots for two shear rates

3.2.3 The Cone-and-Plate Rheometer

The cone-and-plate rheometer is another rheological measuring device widely accepted in the polymer industry. Here, a disk of polymer is squeezed between a plate and a cone as shown in Fig. 3.19. When the disk is rotated, the torque and the rotational speed are related to the viscosity, and the force required to keep the cone at the plate is related to the first normal stress difference. The secondary normal stress difference is related to the pressure distribution along the radius of the plate.

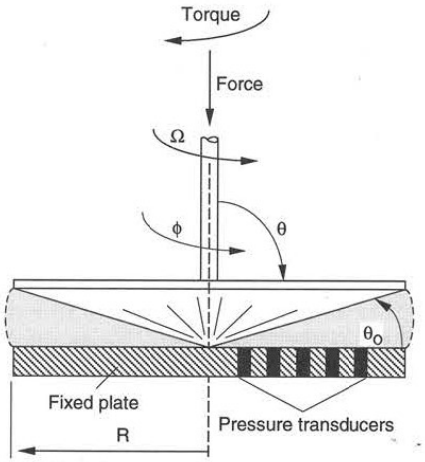


Figure 3.19 Schematic diagram of a cone-plate rheometer

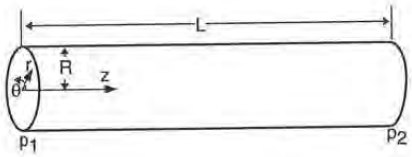
EG_000216549

ClearCorrect Exhibit 1038, Page 40 of 125

Examples

3.1 Derive the equation that describes the pressure driven velocity field inside a tube of constant diameter (Eq. (3.10)).

In our solution scheme, we must first choose a coodinate system:



Next we must state our assumption:

- no variations in the θ direction: $\frac{\partial}{\partial \theta} = v_\theta = 0$,
- steady state: $\frac{\partial}{\partial t} = 0$,
- no velocity in the radial direction: $v_r = 0$.

The continuity equation (Appendix 6) reduces to

$$\frac{\partial v_z}{\partial z} = 0$$

Using the reduced continuity equatien and the above assumptions, then only the z-component of the equation of motion (Appendix 6) is needed

$$0 = -\frac{\partial p}{\partial z} + \mu\left[\frac{1}{r}\frac{\partial}{\partial r}\left(r\frac{\partial v_z}{\partial r}\right)\right]$$

letting $\frac{\partial p}{\partial z} = \frac{\Delta p}{L}$ and integrating gives

$$r\frac{\partial v_z}{\partial r} = \frac{r^2}{2\mu}\left(\frac{\Delta p}{L}\right) + C_1$$

Since $\frac{\partial v_z}{\partial r} = 0$ *at* $r = 0, C_1 = 0$. Integrating again, we get

$$v_z = \frac{r^2}{4\mu}\left(\frac{\Delta p}{L}\right) + C_2$$

Since $v_z = 0$ *at* $r = R$, the above equation becomes

$$v_z = \frac{R^2 \Delta p}{4\mu L}\left[1 - \left(\frac{r}{R}\right)^2\right]$$

Problems

3.1 A single screw extruder can be modeled using a combination of shear flow (Fig. 3.3) and pressure flow between parallel plates (Fig. 3.4). Estimate the volumetric flow rate, Q, as a function of die pressure, Δp, with a Newtonian fluid assumption, using the notation in Fig.4.5 of the extrusion chapter.

3.2 Estimate the consistency index, m_0, and the power-law index, n, for the LDPE presented in Fig. 3.2.

3.3 Derive the equation that predicts the volumetric throughput during pressure flow through a slit (Eq. (3.7)).

3.4 Derive the the Hagen-Poiseuille equation for a power law fluid (Eq. (3.13)).

3.5 You are to extrude a polystyrene sheet through a die with a land length of 0.1 meters. What is the maximum speed you can extrude the sheet if the relaxation time of the polystyrene is 0.5 seconds for the given processing temperature ?

References

1. Macosko, C.W., *Rheology: Principles, Measurements and Applications*, VCH (1994), New York
2. Dealy, J.M., and K.F. Wissbrun, *Melt Rheology and Its Role in Plastics Processing*, Van Nostrand (1990), New York
3. Tanner, R.I., *Engineering Rheology*, Clarendon Press (1985), Oxford
4. Bird, R.B., R.C. Armstrong, and O. Hassager, *Dynamics of Polymeric Liquids*, 2nd Ed., Vol.1, John Wiley & Sons (1987), New York
5. Gordon, G.V., and M.T. Shaw, *Computer Programs for Rheologists*, Hanser Publishers (1994), Munich
6. Bird, R.B., and J.M. Wiest, *Annu. Rev. Fluid Mech.* (1995), *27*, 169
7. Giacomin, A.J., T. Samurkas, and J.M. Dealy, *Polym. Eng. Sci.* (1989), *29*, 499

EG_000216550

ClearCorrect Exhibit 1038, Page 41 of 125

8. Ostwald, W., *Kolloid-Z.* (1925), 36, 99
9. de Waale, A., *Oil and Color Chem. Assoc. Journal* (1923), 6, 33
10. Laun, H.M., *Rheol. Acta* (1978), *17*,1
11. Tadmor, Z., and R.B. Bird, *Polym. Eng. Sci.* (1974), *14*, 124
12. Agassant, J.-F., P. Avenas, J.-Ph. Sergent, and P.J. Carreau, *Polymer Processing: Principles and Modeling*, Hanser Publishers (1991), Munich
13. Vinogradov, G.V., A.Y., Malkin, Y.G. Yanovskii, E.K. Borisenkova, B.V. Yarlykov, and G.V. Berezhnaya, *J. Polym. Sci. Part A-2* (1972), *10*, 1061
14. Vlachopoulos, J., and M. Alam, *Polym. Eng. Sci.* (1972), *12*, 184
15. Hatzikiriakos, S.G., and J.M. Dealy, *ANTEC Tech. Papers* (1991), *37*, 2311
16. Spencer, R.S., and R.D. Dillon, *J. Colloid Inter. Sci.* (1947), *3*, 163
17. Denn, M.M., *Annu. Rev. Fluid Mech.* (1990), *22*, 13
18. Han, C.D. and K.W. Lem, *J. Appl. Polym. Sci.* (1984), 29, 1879
19. Castro, J.M. and C.W. Macosko, *AIChe J.* (1982), *28*, 250
20. Castro, J.M., S.J. Perry and C.W. Macosko, *Polymer Comm.* (1984), *25*, 82
21. Guth, E., and R. Simha, Kolloid-Zeitschrift (1936), 74, 266
22. Keunings, R., *Simulation of Viscoelastic Fluid Flow*, in *Computer Modeling for Polymer Processing*, Ed. C.L. Tucker III, Hanser Publishers (1989), Munich
23. Crocket, MJ., A.R., Davies, and K. Walters, *Numerical Simulation of Non-Newtonian Flow*, Elsevier (1984), Amsterdam
24. Debbaut, B., J.M. Marchal, and M.J. Crochet, *J. Non-Newtonian Fluid Mech.* (1988), *29*, 119
25. Dietsche, L., and J. Dooley, *SPE ANTEC* (1995), *53*, 188
26. Dooley, J., and K. Hughes, *SPE ANTEC* (1995), *53*, 69
27. Baaijens, J.P.W., *Evaluation of Constitutive Equations for Polymer Melts and Solutions in Complex Flows*, Ph.D. Thesis (1994), Eidhoven University of Technology, Eidhoven, The Netherlands
28. ASTM, 8.01, Plastics (I), ASTM (1994), Philadelphia
29. Hagen, G.H.L., *Annalen der Physik* (1839), *46*, 423
30. Poiseuille, L.J., *Comptes Rendus 11* (1840), 961
31. Dealy, J.M., *Rheometers for Molten Plastics*, Van Nostrand Reinhold Company (1982), New York
32. Bagley, E.B., *J. Appl. Phys.* (1957), *28*, 624
33. Rabinowitsch, B., *Z. Phys. Chem.* (1929), *145*, 1

4 Extrusion

During extrusion, a polymer melt is pumped through a shaping die and formed into a profile. This profile can be a plate, a film, a tube, or have any shape for its cross section. Ram-type extruders were first built by J. Bramah in 1797 to extrude seamless lead pipes. The first ram-type extruders for rubber were built by Henry Bewley and Richard Brooman in 1845. In 1846 a patent for cable coating was filed for trans-gutta-percha and cis-hevea rubber and the first insulated wire was laid across the Hudson River for the Morse Telegraph Company in 1849. The first screw extruder was patented by Mathew Gray in 1879 for the purpose of wire coating. However, the screw pump can be attributed to Archimedes, and the actual invention of the screw extruder in polymer processing by A.G. DeWolfe of the United States dates to the early 1860s. The first extrusion of thermoplastic polymers was done at the Paul Troester Maschinenfabrik in Hannover, Germany in 1935.

Although ram and screw extruders are both used to pump highly viscous polymer melts through passages to generate specified profiles, they are based on different principles. The schematic in Fig. 4.1 shows under what principles ram extruders, screw extruders, and other pumping systems work.

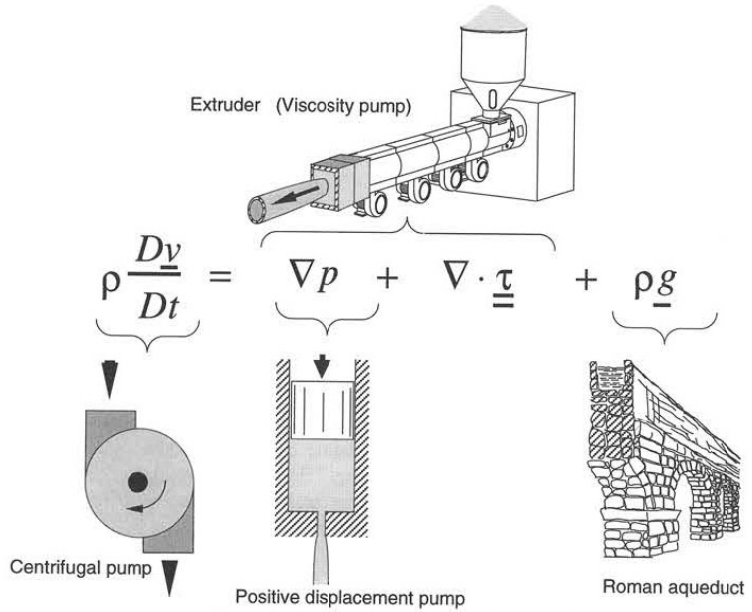


Figure 4.1 Schematic of pumping principles

EG_000216551

ClearCorrect Exhibit 1038, Page 42 of 125

The ram extruder is a positive displacement pump based on the pressure gradient term of the equation of motion. Here, as the volume is reduced, the fluid is displaced from one point to the other, resulting in a pressure rise. The gear pump, widely used in the polymer processing industry, also works on this principle. On the other hand, a screw extruder is a *viscosity pump* that works based on the pressure gradient term and the deformation of the fluid, represented as the divergence of the deviatoric stress tensor in Fig. 4.1. The centrifugal pump, based on the fluid inertia, and the Roman aqueduct, based on the potential energy of the fluid, are also represented in the figure and are typical of low viscosity liquids.

In today's polymer industry, the most commonly used extruder is the single screw extruder, schematically depicted in Fig. 4.2. The single screw extruder can either have a smooth inside barrel surface, called a *conventional single screw extruder*, or a grooved feed zone, called a *grooved feed extruder*. In some cases, an extruder can have a degassing zone, required to extract moisture, volatiles, and other gases that form during the extrusion process.

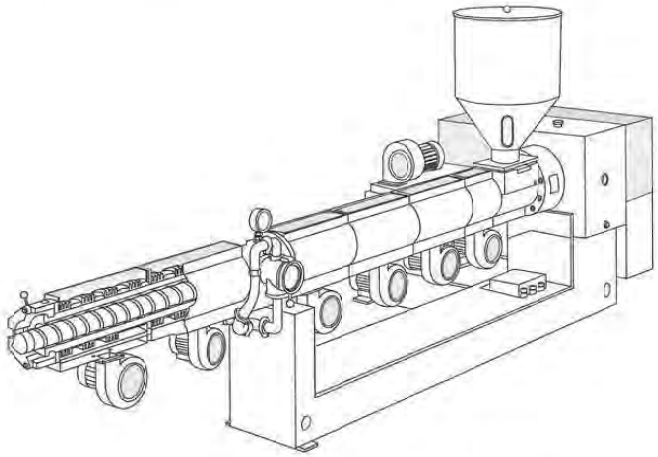


Figure 4.2 Schematic of a single screw extruder (Reifenhäuser)

Another important class of extruders are the twin screw extruders, schematically depicted in Fig. 4.3. Twin screw extruders can have co-rotating or counter-rotating screws, and the screws can be intermeshing or non-intermeshing. Twin screw extruders are primarily employed as mixing and compounding devices, as well as polymerization reactors. The mixing aspects of single and twin screw extruders are detailed in Chapter 5.

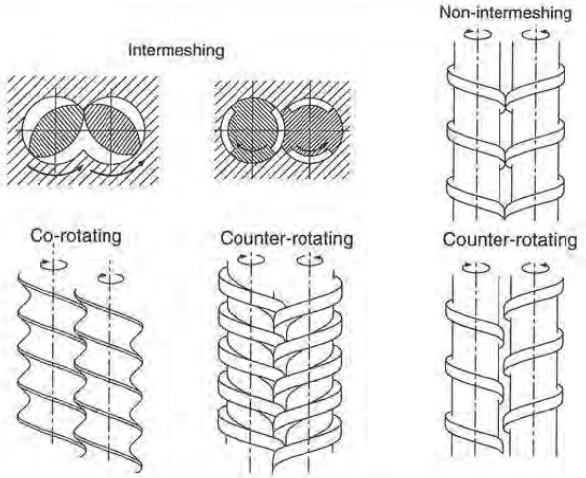


Figure 4.3. Schematic of different twin screw extruders

4.1 The Plasticating Extruder

The plasticating single screw extruder is the most common equipment in the polymer industry. It can be part of an injection molding unit and found in numerous other extrusion processes, including blow molding, film blowing, and wire coating. A schematic of a plasticating or three-zone, single screw extruder, with its most important elements, is in Fig. 4.4. Table 4.1 presents typical extruder dimensions and relationships common in single screw extruders.

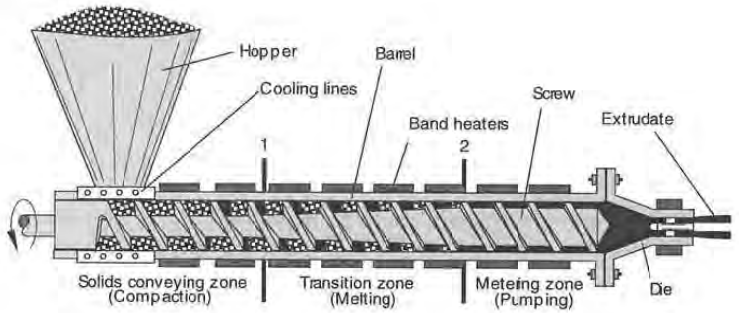


Figure 4.4 Schematic of a plasticating single screw extruder

EG_000216552

ClearCorrect Exhibit 1038, Page 43 of 125

Table 4.1 Typical extruder dimensions and relationships (the notation for Table 4.1 is defined in Fig. 4.5.)

L/D	Length to Diameter ratio 20 or less for feeding or melt extruders 25 for blow molding, film blowing and injection molding 30 or higher for vented extruders or high output extruders
D	Standard diameter
U.S. (inches)	0.75, 1.0, 1.5, 2, 2.5, 3.5, 4.5, 6, 8, 10, 12, 14, 16, 18, 20, and 24
Europe (mm)	20, 25, 30, 35, 40, 50, 60, 90, 120, 150, 200, 250, 300, 350, 400, 450, 500, and 600
ϕ	Helix angle 17.65° for a square pitch screw where L_s=D New trend: $0.8 < L_s/D < 1.2$
h	Channel depth in the metering section (0.05-0.07)D for D<30 mm (0.02-0.05)D for D>30 mm
β	Compression ratio: $h_{feed} = \beta h$ 2 to 4
δ	Clearance between the screw flight and the barrel 0.1 mm for D<30 mm 0.15 mm for D>30 mm
N	Screw speed 1-2 rev/s (60-120 rpm) for large extruders 1-5 rev/s (60-300 rpm) for small extruders
V_b	Barrel velocity (relative to screw speed) = πDN 0.5 m/s for most polymers 0.2 m/s for unplasticized PVC 1.0 m/s for LDPE

The plasticating extruder can be divided into three main zones:

- The solids conveying zone
- The melting or transition zone
- The metering or pumping zone

The tasks of a plasticating extruder are to:

- Transport the solid pellets or powder from the hopper to the screw channel
- Compact the pellets and move them down the channel
- Melt the pellets
- Mix the polymer into a homogeneous melt
- Pump the melt through the die

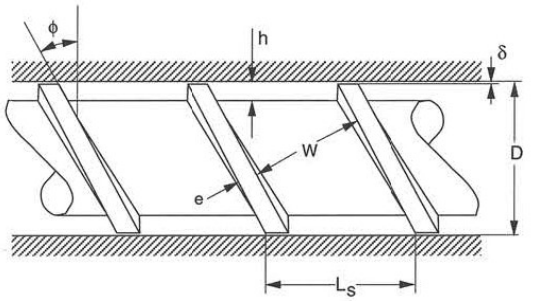


Figure 4.5 Schematic diagram of a screw section

The pumping capability and characteristic of an extruder can be represented with sets of *die and screw characterisctic curves*. Figure 4.6 presents such curves for a conventional (smooth barrel) single screw extruder.

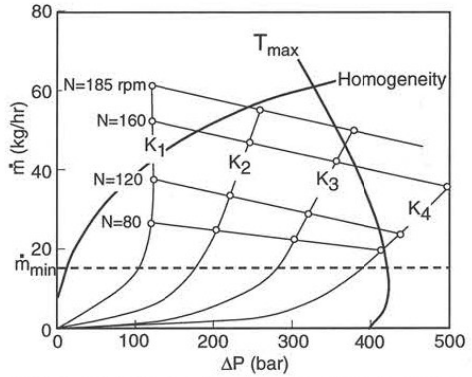


Figure 4.6 Screw and die characteristic curves for a 45 mm diameter extruder with an LDPE

The die characteristic curves are labelled K_1, K_2, K_3, and K_4 in ascending order of die restriction. Here, K_1 represents a low resistance die such as for a thick plate, and K_4 represents a restrictive die, such as is used for film. The different screw characteristic

EG_000216553

ClearCorrect Exhibit 1038, Page 44 of 125

curves represent different screw rotational speeds. In a screw characteristic curve the point of maximum throughput and no pressure build-up is called the point of *open discharge*. This occurs when there is no die. The point of maximum pressure build-up and no throughput is called the point of *closed discharge*. This occurs when the extruder is plugged.

Shown in Fig. 4.6 are also lines that represent critical aspects encountered during extrusion. The curve labeled T_{max} represents the conditions at which excessive temperatures are reached as a result of viscous heating. The feasibility line ($\dot{m}_{min}$) represents the throughput required to have an economically feasible system. The processing conditions to the right of the homogeneity line render a thermally and physically heterogeneous polymer melt.

4.1.1 The Solids Conveying Zone

The task of the solids conveying zone is to move the polymer pellets or powders from the hopper to the screw channel. Once the material is in the screw channel, it is compacted and transported down the channel. The process to compact the pellets and to move them can only be accomplished if the friction at the barrel surface exceeds the friction at the screw surface. This can be visualized if one assumes the matertial inside the screw channel to be a nut sitting on a screw. As we rotate the screw without applying outside friction, the nut (polymer pellets) rotates with the screw without moving in the axial direction. As we apply outside forces (barrel friction), the rotational speed of the nut is less than the speed of the screw, causing it to slide in the axial direction. Virtually, the solid polymer is then "unscrewed" from the screw.

ANALYSIS OF SOLIDS CONVEYING ZONE

The most complete analysis of the solids conveying zone in single screw extruders was performed by Darnell and Mol [1] and continued by Tadmor and Klein [2].

A useful limiting case is when the friction on the screw surface is negligible compared to the friction on the barrel, and when the pressure build-up in the screw channel is negligible (open discharge). These assumptions lead to a maximum mass throughput of

$$\dot{m} = \rho_{bulk}\pi D_b N \tan\phi\left(\frac{\pi}{4}\left(D_b^2 - D_s^2\right) - \frac{eh_{feed}}{\sin\phi}\right) \tag{4.1}$$

To maintain a high coefficient of friction between the barrel and the polymer, the feed section of the barrel must be cooled, usually with cold water cooling lines. The frictional forces also result in a pressure rise in the feed section. This pressure compresses the solids bed which continues to travel in down the channel as it melts in the transition zone. Figure 4.7 presents the pressure build-up in a conventional, smooth barrel extruder. In these extruders, most of the pressure required for pumping and mixing is generated in the metering section.

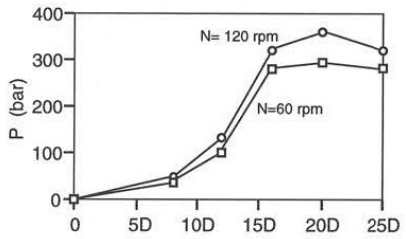


Figure 4.7 Conventional extruder pressure distribution

The simplest mechanism for ensuring high friction between the polymer and the barrel surface is grooving its surface in the axial direction [3, 4]. Extruders with a grooved feed section are called *grooved feed extruders*. To avoid excessive pressures that can lead to barrel or screw failure, the length of the grooved barrel section must not exceed 3.5D. A schematic diagram of the grooved section in a single screw extruder is presented in Fig. 4.8. The key factors that propelled the development and refinement of the grooved feed extruder were the processing problems, excessive melt temperature, and reduced productivity posed by high viscosity and low coefficients of friction typical of high molecular weight polyethylenes and polypropylenes.

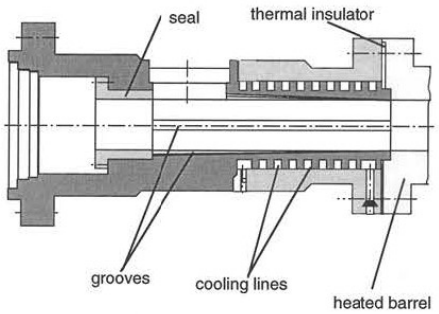


Figure 4.8 Schematic diagram of the grooved feed section of a single screw extruder

In a grooved feed extruder, the conveying and pressure build-up tasks are assigned to the feed section. Figure 4.9 presents the pressure build-up in a single screw extruder with a grooved feed section. The high pressures in the feed section lead to the main advantages over conventional systems. With grooved feed systems, there is a higher productivity and a higher melt flow stability and pressure invariance. This is demonstrated with the screw characteristic curves in Fig. 4.10, which presents screw characteristic curves for a 45 mm

EG_000216554

ClearCorrect Exhibit 1038, Page 45 of 125

diameter grooved feed extruder with comparable mixing sections and die openings as shown in Fig. 4.6.

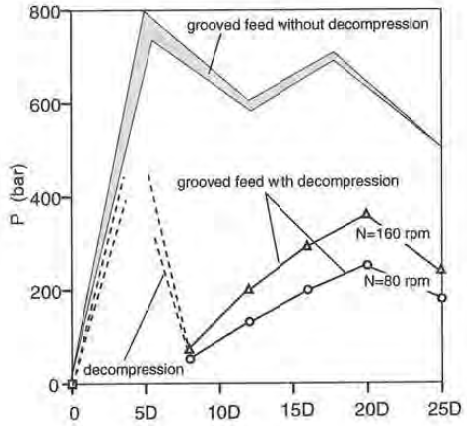


Figure 4.9 Grooved feed extruder pressure distribution

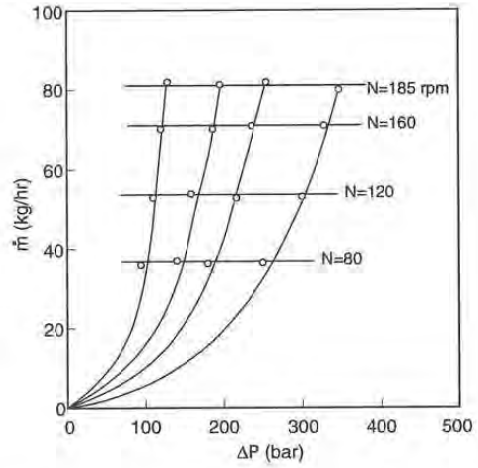


Figure 4.10 Screw and die characteristic curves for a grooved feed 45 mm diameter extruder with an LDPE

The behavior of the two extruders in Figs. 4.6 and 4.10 are best compared if the throughput and the pressure build-up are non-dimensionalized. The dimensionless throughput is

$$\hat{m} = \frac{\dot{m}}{\rho N D^3} \tag{4.2}$$

and the dimensionless pressure build-up is

$$\Delta\hat{p} = \frac{\Delta p D}{m N^n L_c} \tag{4.3}$$

where L represents the total channel length and for a 25 L/D extruder is

$$L_c = \frac{25D}{\sin(\phi)} \tag{4.4}$$

where ϕ is assumed to be 17.65° (square pitch). Figure 4.11 presents the results shown in Figs. 4.6 and 4.10 after having been non-dimensionalized using Eqs. (4.2 and 4.3). The figure clearly shows the higher productivity of the grooved feed extruder where the throughput is at least 50% more than that observed with the conventional system for a comparable application. Used with care, Fig. 4.11 can also be used for scale-up.

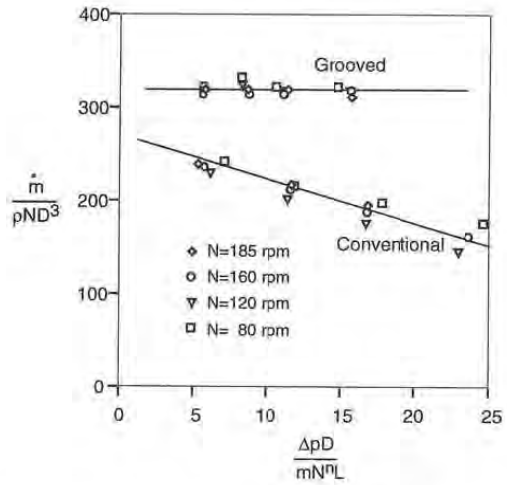


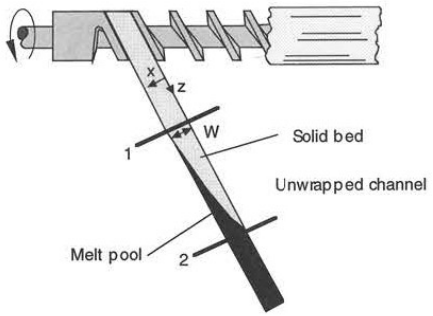
Fig. 4.11 Dimesionless screw charactristic curves for conventional and grooved feed extruders

EG_000216555

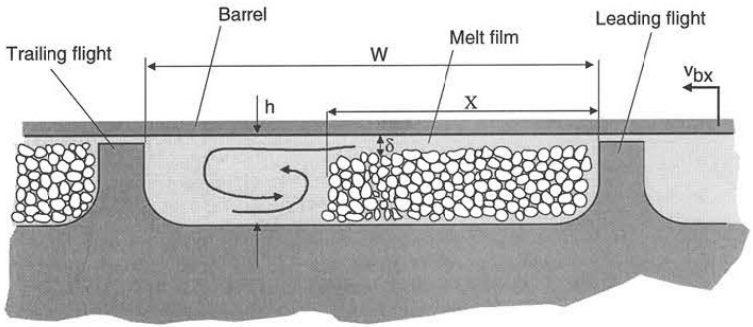
ClearCorrect Exhibit 1038, Page 46 of 125

4.1.2 The Melting Zone

The melting or transition zone is the portion of the extruder where the material melts. The length of this zone is a function of the material properties, screw geometry and processing conditions. During melting, the size of the *solid bed* shrinks as a *melt pool* forms at its side, as depicted in Fig. 4.12a which shows the polymer unwrapped from the screw channel.



(a)



(b)

Figure 4.12 (a) Solids bed in an unwrapped screw channel and (b) screw channel cross section

Figure 4.12b presents a cross section of the screw channel in the melting zone. The solid bed is pushed against the leading flight of the screw as freshly molten polymer is wiped from the *melt film* into the melt pool by the relative motion between the solids bed and the barrel surface.

screw extruder is the well known Tadmor Model [5]. Using the Tadmor Model, one can accurately predict the solid bed profile in the single screw extruder. Figure 4.13 presents the experimental and predicted solids bed profile of an LDPE in a single screw extruder. The material properties and processing conditions used in the calculations are given in Table 4.2.

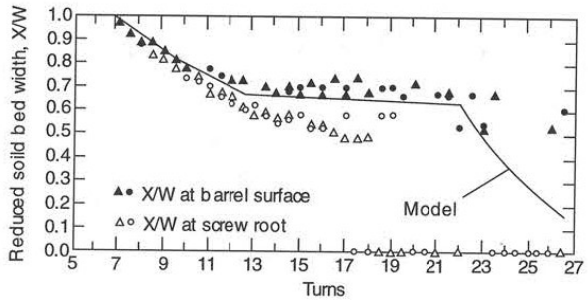


Figure 4.13 Predicted (Tadmor Model) and experimental solids bed profile

Table 4.2 Extruder parameters, processing conditions, and material proprerties for the solids bed profile results in Fig. 4.13

Extruder Geometry:

Square pitch screw, D=63.5mm, L/D=26.5, W=54.16mm
Feed zone - 12.5 turns h_1=9.4mm
Transition zone - 9.5 turns h_1=9.4mm h_2=3.23mm
Metering zone - 4.5 turns h_2=3.23mm

Processing Conditions:

T_0=24°C T_b=149 °C N=60 rpm Δp=204 bar $\dot{m}$=61.8 kg/hr

Material properties (LDPE):

Viscosity: n=0.345 a=0.01 °C^{-1} m_0=5.6x10^4 Pa-s^n
T_m=110 °C

Thermal: k_m=0.1817 W/m°C C_m=2.596 kJ/kg°C C_s=2.763 kJ/kg°C
ρ_{bulk}=595 kg/m^3 ρ_s=915.1 kg/m^3 ρ_m=852.7 + 5.018x10^{-7}p - 0.4756T
λ=129.8 kJ/kg

EG_000216556

ClearCorrect Exhibit 1038, Page 47 of 125

TADMOR'S MELTING MODEL

The Tadmor Model presented in this section was derived using the notation shown in Figs. 4.12a and 4.12b. The non-Newtonian temperature dependent viscosity of the polymer is described by

$$\eta = m_0 e^{-a(T-T_m)}|\dot{\gamma}|^{n-1} \tag{4.5}$$

The solids bed width X in a constant channel depth section is calculated using

$$\frac{X}{W} = \frac{X_0}{W}\left[1 - \frac{\psi(z-z_0)}{2h}\right]^2 \tag{4.6}$$

and in a tapered section with a taper $A = \frac{h_1 - h_2}{z_1 - z_2}$ is given as a function of the channel depth

$$\frac{X}{W} = \frac{X_0}{W}\left[\frac{\psi}{A} - \left(\frac{\psi}{A} - 1\right)\sqrt{\frac{h_0}{h}}\right]^2 \tag{4.7}$$

The dimensionless volumetric flow rate ψ is given by

$$\psi = \frac{\Phi}{v_{sz}\rho_{bulk}\sqrt{X_0}} \tag{4.8}$$

where v_{sz} is the velocity of the solid bed in the down-channel direction

$$v_{sz} = \frac{\dot{m}}{\rho_{bulk} W h} \text{ and} \tag{4.9}$$

$$\Phi = \left\{\frac{v_{bx}\rho_m U_2\left[k_m(T_b - T_m) + U_1/2\right]}{2\left[C_s(T_m - T_0) + C_m\overline{\Theta}(T_b - T_m) + \lambda\right]}\right\}^{1/2} \tag{4.10}$$

$$U_2 = 2\left[\frac{1 - b' - e^{-b'}}{b'(e^{-b'} - 1)}\right] \tag{4.11}$$

$$b' = \frac{-a(T_b - T_m)}{n} \tag{4.12}$$

$$U_1 = 2m_0 v_j^{n+1}\delta^{1-n}\frac{\left(e^{-b'} + b' - 1\right)}{b'^2}\left(\frac{b'}{1 - e^{-b'}}\right)^{n+1} \tag{4.13}$$

The speed v_j is the relative velocity between the barrel and the solid bed

$$v_j = \sqrt{v_{bx}^2 + (v_{bz} - v_{sz})^2} \tag{4.14}$$

The dimensionless temperature and the film thickness are defined by

$$\overline{\Theta} = \frac{b'/2 + e^{-b'}\left(1 + 1/b'\right) - 1/b'}{b' + e^{-b'} - 1} \tag{4.15}$$

and

$$\delta = \left\{\frac{\left[2k_m(T_b - T_m) + U_1\right]X}{v_{bx}U_2\rho_m\left[C_s(T_m - T_{s0}) + C_m\overline{\Theta}(T_b - T_m) + \lambda\right]}\right\}^{1/2} \tag{4.16}$$

From experiment to experiment there are always large variations in the experimental solids bed profiles. The variations in this section of the extruder are caused by slight variations in processing conditions and by the uncontrolled solids bed break-up towards the end of melting. This effect can be eliminated by introducing a screw with a barrier flight that separates the solids bed from the melt pool. The Maillefer screw and barrier screw in Fig. 4.14 are commonly used for high quality and reproducibility. The Maillefer screw maintains a constant solids bed width, using most effectively the melting with melt-removal mechanism, while the barrier screw uses a constant channel depth with a gradually decreasing solids bed width.

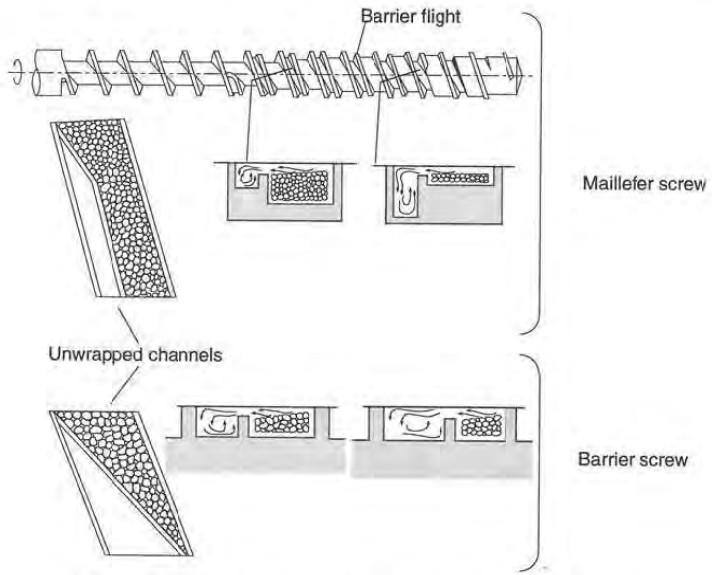


Figure 4.14 Schematic diagram of screws with different barrier flights

EG_000216557

ClearCorrect Exhibit 1038, Page 48 of 125

4.1.3 The Metering Zone

The metering zone is the most important section in melt extruders and conventional single screw extruders that rely on it to generate pressures sufficient for pumping. The pumping capabilites in the metering section of a single screw extruder can be estimated by solving the equation of motion with appropriate constitutive laws. For a Newtonian fluid in an extruder with a constant channel depth, the screw and die characteristic curves for different cases are represented in Fig. 4.15. The figure shows the influence of the channel depth on the screw characterisctic curves. A restrictive extrusion die would clearly work best with a shallow channel screw, and a less restrictive die would render the highest productivity with a deep channel screw.

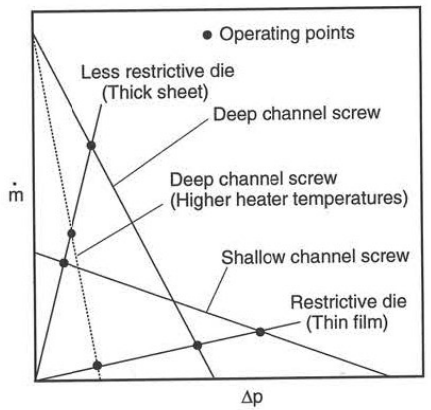


Figure 4.15 Screw characteristic curves (Newtonian)

ANALYTICAL SCREW CHARACTERISTICS CURVES (NEWTONIAN)

For a Newtonian material, the analytical solution is given by Tadmor [2]. It is

$$Q=\frac{V_{bz}W(h-\delta)}{2}F_d+\frac{Wh^3}{12\eta_0}\left(-\frac{\partial p}{\partial z}\right)F_p(1+f_L) \tag{4.17}$$

where the down channel velocity is,

$$V_{bz}=\pi NDcos(\phi) \tag{4.18}$$

$$tan(\phi)=\frac{L_s}{\pi D} \tag{4.19}$$

and the leakage flow factor is

$$f_L=\left(\frac{\delta}{h}\right)^3\frac{e}{W}+\frac{\left(1+\frac{e}{W}\right)\left[\frac{1+e/W}{tan^2\phi}-\frac{6\eta_0V_{bz}(h-\delta)}{h^3(\partial p/\partial z)}\right]}{1+\left(\frac{h}{\delta}\right)^3\frac{e}{W}} \tag{4.20}$$

The drag and pressure shape factors F_d and F_p are necessary to account for the no-slip boundary condition on the channel walls, and can be approximated using functions valid for $(h/W)<0.6$ given by [6]

$$F_d\approx 1-0.571\frac{h}{W} \tag{4.21}$$

and

$$F_p\approx 1-0.625\frac{h}{W} \tag{4.22}$$

In both the grooved barrel and the conventional extruder, the diameter of the screw determines the metering or pumping capacity of the extruder. Figure 4.16 presents typical normalized mass throughput as a function of screw diameter for both systems.

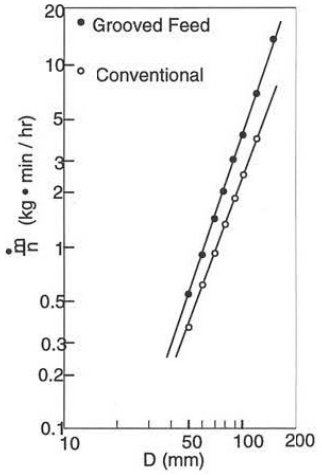


Figure 4.16 Throughput for conventional and grooved feed extruders

EG_000216558

ClearCorrect Exhibit 1038, Page 49 of 125

4.2 Extrusion Dies

The extrusion die shapes the polymer melt into its final profile. The extrusion die is located at the end of the extruder and it is used to extrude:

- Flat films and sheets
- Pipes and tubular films for bags
- Filaments and strands
- Hollow profiles for window frames
- Open profiles

As shown in Fig. 4.17, depending on the functional needs of the product, several rules of thumb can be followed when designing an extruded plastic profile. These are:

- Avoid thick sections. Thick sections add to the material cost and increase sink marks caused by shrinkage.
- Minimize the number of hollow sections. Hollow sections add to die cost and make the die more difficult to clean.
- Generate profiles with constant wall thickness. Constant wall thickness in a profile makes it easier to control the thickness of the final profile and results in a more even crystallinity distribution in semi-crystalline profiles.

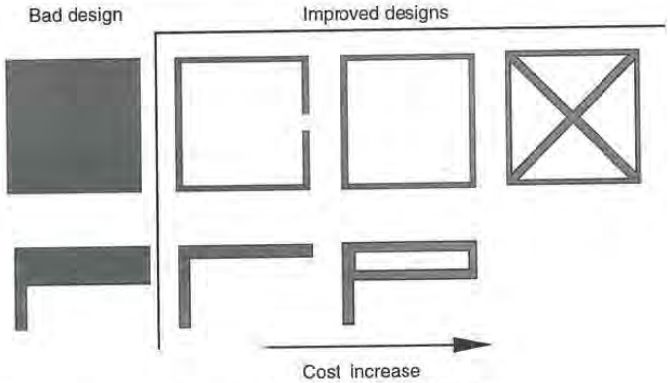


Figure 4.17 Extrusion profile designs

4.2.1 Sheeting Dies

One of the most widely used extrusion dies is the *coat-hanger sheeting die*. A sheeting die, such as depicted in Fig. 4.18 is formed by the following elements:

- Manifold: evenly distributes the melt to the approach or land region
- Approach or land: carries the melt from the manifold to the die lips
- Die lips: perform the final shaping of the melt

- Flex lips: for fine tuning when generating a uniform profile

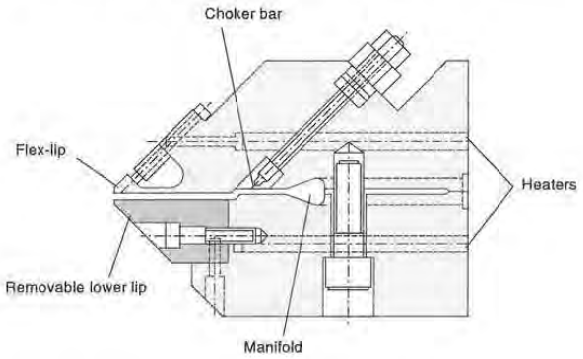


Figure 4.18 Cross section of a coat-hanger die

To generate a uniform extrudate geometry at the die lips, the geometry of the manifold must be specified appropriately. Figure 4.19 presents the schematic of a coat-hanger die with a pressure distribution that corresponds to a die that renders a uniform extrudate. It is important to mention that the flow though the manifold and the approach zone depend on the non-Newtonian properties of the polymer extruded. So the design of the die depends on the shear thinning behavior of polymer. Hence, a die designed for one material does not necessarily work for another.

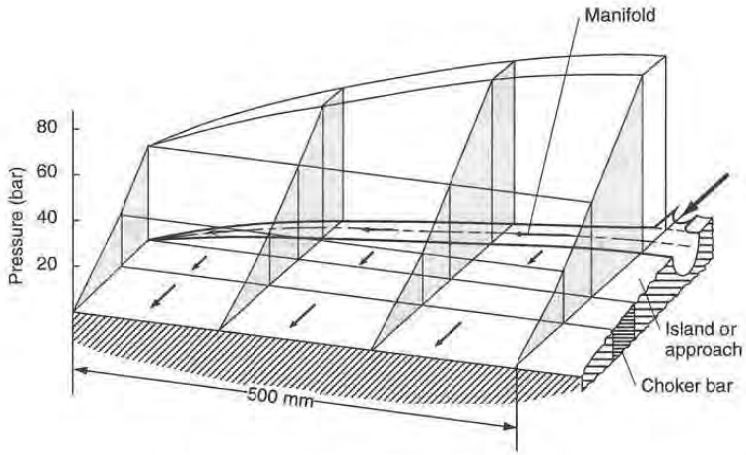


Figure 4.19 Pressure distribution in a coat-hanger die

EG_000216559

ClearCorrect Exhibit 1038, Page 50 of 125

ANALYTICAL COAT-HANGER DIE

For the isothermal flow of a power-law fluid, using the notation in Fig. 4.20, we can perform a mass balance and solve the equation of motion for the manifold (flow in a tube) and the approach (flow between parallel plates) region. For uniform flow in the die lips, the design equation for a coat-hanger sheeting die is given by [5]

$$R(x)=\left\{\frac{[(3+s)/\pi]^n h^{2n+1}(W-x)^n}{2^n(s+2)^n\left(\frac{dL}{dl}\right)}\right\}^{\frac{1}{3n+1}} \tag{4.23}$$

where $s=1/n$. For a manifold with a straight axis the manifold curvature can be computed using

$$\frac{dL}{dl}=-\sin\alpha \tag{4.24}$$

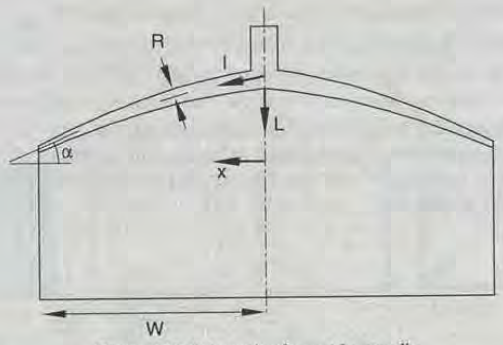


Figure 4.20 Schematic of a coat-hanger die

4.2.2 Tubular Dies

In a tubular die, the polymer melt exits through an annulus. These dies are used to extrude plastic pipes and tubular film. The film blowing operation is discussed in more detail in Chapter 7.

The simplest tubing die is the spider die, depicted in Fig. 4.21. Here, a symmetric mandrel is attached to the body of the die by several legs. The polymer must flow around the spider legs causing weld lines along the pipe or film. These weld lines, visible streaks along the extruded tube, are weaker regions.

To overcome weld line problems, the cross-head tubing die is often used. Here, the die design is similar to that of the coat-hanger die, but wrapped around a cylinder. This die is depicted in Fig. 4.22. Since the polymer melt must flow around the mandrel, the extruded tube exhibits one weld line. In addition, although the eccentricity of a mandrel can be

controlled using adjustment screws, there is no flexibility to perform fine tuning such as in the coat-hanger die. This can result in tubes with uneven thickness distributions.

The spiral die, commonly used to extrude tubular blown films, eliminates weld line effects and produces a thermally and geometrically homogeneous extrudate. The polymer melt in a spiral die flows through several feed ports into independent spiral channels wrapped around the circumference of the mandrel. This type of die is schematically depicted in Fig. 4.23.

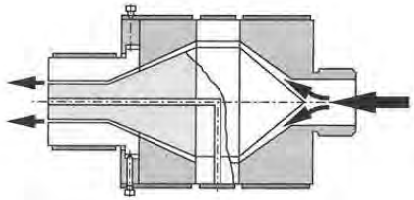


Figure 4.21 Schematic of a spider leg tubing die

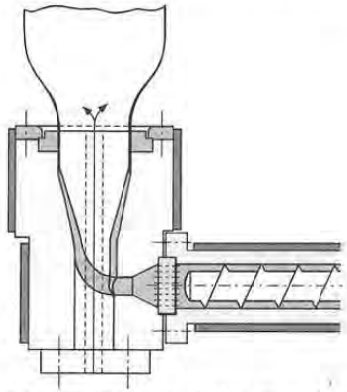


Figure 4.22 Schematic of a cross-head tubing die used in film blowing

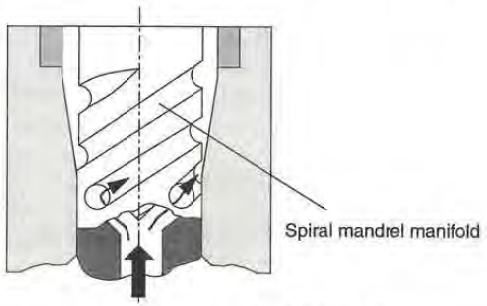


Figure 4.23 Schematic of a spiral die

EG_000216560

ClearCorrect Exhibit 1038, Page 51 of 125

Examples

4.1 Reproduce the predicted solids bed profile for the solids conveying section in the system found in Fig. 4.13. Use the data presented in Table 4.2.

From the conditions given in Table 4.2, we can first compute the barrel velocity with respect to the screw using

$$v_b = \pi Dn = \pi(0.0635)(1) = 0.1995\ m/s$$

The down and cross channel velocities are

$$v_{bz} = v_b \cos\phi = (0.1995)\cos(17.65) = 0.1901\ m/s$$
$$v_{bx} = v_b \sin\phi = (0.1995)\sin(17.65) = 0.0605\ m/s$$

The velocity of the solids bed is computed using Eq. (4.9)

$$v_{sz} = \frac{(61.8/3600)}{(595)(0.05416)(0.0094)} = 0.0567\ m/s$$

The relative speed between the solids bed and the barrel is calculated using Eq. (4.14)

$$v_j = \sqrt{(0.0605)^2 + (0.1901 - 0.0567)^2} = 0.1465\ m/s$$

and using Eqs. (4.12), (4.11), and (4.15), we can compute

$$b' = \frac{-0.01(149-110)}{0.345} = -1.1304$$

$$U_2 = 2\left[\frac{1+1.1304-e^{1.1304}}{-1.1304\left(e^{1.1304}-1\right)}\right] = 0.8155$$

$$\overline{\Theta} = \frac{-1.1304/2 + e^{1.1304}(1+1/(-1.1304)) - 1/(-1.1304)}{-1.1304 + e^{1.1304} - 1} = 0.7002$$

If we neglect the pressure effects, we can compute the melt density using an average temperature of 129.5 °C as

$$\rho_m = 852.7 - 0.4756(129.5) = 791.1\ kg/m^3$$

Using Eqs. (4.13), (4.16), (4.10), and (4.8), we can compute

$$U_1 = 2(5.6x10^4)(0.1465)^{1.345}\delta^{0.655}\left(\frac{e^{1.1304}-1.1304-1}{(-1.1304)^2}\right)\left(\frac{-1.130}{1-e^{1.1304}}\right)^{1.1304}$$

$$U_1 = 2786.8\delta^{0.655}$$

$$\delta = \left\{\frac{[2(0.1817)(149-110)+U_1]X}{(0.0605)(0.8155)(791.1)[2763(110-24)+2596(0.7002)(149-110)+129800]}\right\}^{1/2}$$

$$\delta = 2.418x10^{-4}\left[(14.7+U_1)X\right]^{1/2}$$

$$\Phi = \left\{\frac{(0.0605)(791.1)(0.8155)[(0.1817)(149-110)+U_1/2]}{2[(2763)(110-24)+(2596)(0.7002)(149-110)+129800]}\right\}^{1/2}$$

$$\Phi = 4.72x10^{-3}\left[14.17+U_1\right]^{1/2}$$

$$\psi = \frac{4.72x10^{-3}\left[14.17+U_1\right]^{1/2}}{(0.0567)(595)\sqrt{0.05416}}$$

$$\psi = 6.01x10^{-4}\left[14.17+U_1\right]^{1/2}$$

Assuming melting begins at the 7th turn,

$$z_0 = \frac{(7-1)(0.0635)}{\sin(17.65)} = 1.26\ m$$

at which point $X_0 = W$, Eq. (4.6) can be written as

$$\frac{X}{W} = \left[1 - 53.19\psi(z-1.26)\right]^2$$

U_1, δ, ψ and X must be solved simultaneously from the end of the 6th turn to the middle of the 12th turn. The results are tabulated below.

Turns	z	δ (m)	U_1 (N/s)	ψ	X (m)	X/W
7.0	1.466	0.0002967	13.63	0.003169	0.05416	1.0000
7.5	1.571	0.0002905	13.44	0.003158	0.05227	0.9651
8.0	1.675	0.0002844	13.26	0.003147	0.05043	0.9311
8.5	1.780	0.0002783	13.07	0.003137	0.04863	0.8979
9.0	1.885	0.0002723	12.88	0.003126	0.04688	0.8656
9.5	1.990	0.0002664	12.70	0.003115	0.04517	0.8340
10.0	2.094	0.0002605	12.52	0.003105	0.04350	0.8032

EG_000216561

ClearCorrect Exhibit 1038, Page 52 of 125

Turns	z	δ (m)	U_1 (N/s)	ψ	X (m)	X/W
10.5	2.199	0.0002548	12.33	0.003094	0.04188	0.7733
11.0	2.304	0.0002490	12.15	0.003083	0.04030	0.7441
11.5	2.408	0.0002434	11.97	0.003073	0.03876	0.7156
12.0	2.513	0.0002378	11.79	0.003062	0.03726	0.6880
12.5	2.618	0.0002323	11.61	0.003052	0.03580	0.6610

4.2 Draw the screw characteristic curve for a 45 mm diameter melt extruder for a rotational speed of 60 rpm. The extruder has a square pitch, an L/D of 20, a constant channel depth of 2.5 mm, a channel width of 37.88 mm, and a clearance of 0.15 mm. Assume a Newtonian viscosity of 100 Pa-s.

From the above conditions we can first compute the down channel velocity using

$$v_{bz} = \pi DN\cos\phi = \pi(0.045)(1)\cos(17.65) = 0.1347\ m/s$$

and the channel length using

$$L_c = \frac{(L/D)D}{\sin\phi} = \frac{20(0.045)}{\sin(17.65)} = 2.968\ m$$

Using Eqs. (4.21-22) we can compute the drag and pressure shape factors as

$$F_1 \approx 1 - 0.571\left(\frac{0.0025}{0.03788}\right) = 0.9623$$

$$F_p \approx 1 - 0.625\left(\frac{0.0025}{0.03788}\right) = 0.9587$$

and Eq. (4.20) is used to compute the leakage flow factor as

$$f_L = \left(\frac{0.00015}{0.0025}\right)^3 \frac{0.005}{0.03788} + \frac{\left(1+\dfrac{0.005}{0.03788}\right)\left[\dfrac{1+\dfrac{0.005}{0.03788}}{\tan^2 17.65} - \dfrac{6(100)(0.1347)(0.0025-0.00015)}{(0.0025)^3(\Delta p/2.968)}\right]}{1+\left(\dfrac{0.0025}{0.00015}\right)^3 \dfrac{0.005}{0.03788}}$$

$$f_L = 0.0066 - \frac{6.67x10^4}{\Delta p}$$

With Eq. (4.17) we can now calculate the flow rate

$$Q = \left[\frac{(0.1347)(0.03788)(0.0025-0.00015)}{2}(0.9623) - \frac{(0.03788)(0.0025)^3}{12(100)(2.968)}(0.9587)\Delta p(1+f_L)\right]$$

which is converted to kg/h using ρ=1000kg/m^3

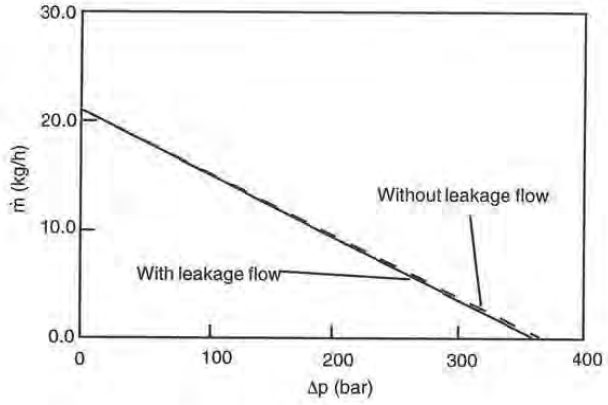
$$\dot{m} = Q\rho = Q(1000)(3600)$$

$$\dot{m} = 20.736 - 5.724x10^{-7}\Delta p\left(1.0066 - \frac{6.67x10^4}{\Delta p}\right)$$

The screw characteristic curve without the effect of leakage flow reduces to

$$\dot{m} = 20.736 - 5.724x10^{-7}\Delta p$$

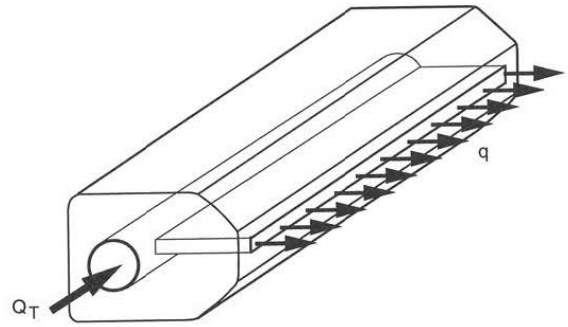
Both curves are plotted in the figure below.



4.3 Formulate a design equation for the end-fed sheeting die shown below such that the extruded sheet is of uniform thickness. Your job is to specify the length of the approach zone or die land as a function of the manifold direction to achieve uniform flow. The manifold diameter is constant and the flow can be assumed isothermal with a Newtonian viscosity of η.

EG_000216562

ClearCorrect Exhibit 1038, Page 53 of 125

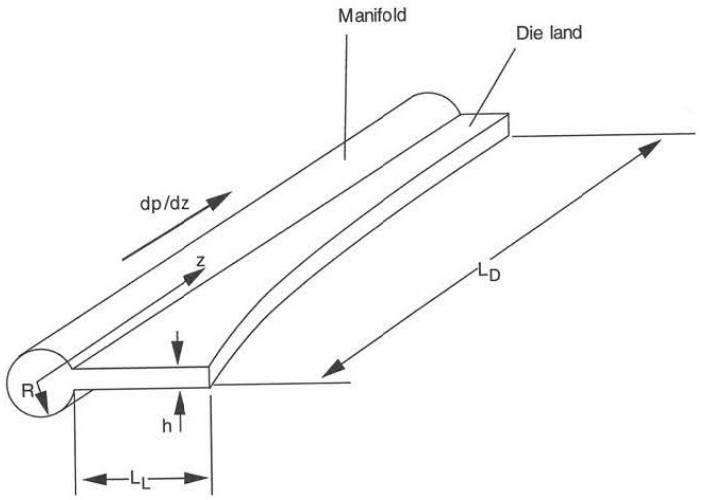


After assigning a coordinate system, and assuming the notation presented in the figure below, the flow of the manifold can be represented using the Hagen-Poiseuille equation as

$$Q = \frac{\pi R^4}{8\eta}\left(-\frac{dp}{dz}\right)$$

and the flow in the die land (per unit width) using slit flow

$$q = \frac{h^3}{12\eta}\left(-\frac{dp}{dl}\right) = \frac{h^3}{12\eta}\left(\frac{p}{L_l}\right)$$

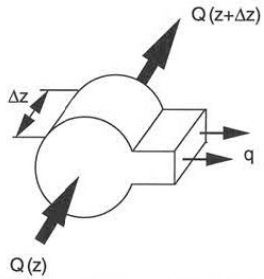


A manifold that leads to a uniform sheet must deliver a constant throughput along the die land. Performing flow balance within the differental element shown below results in

$$Q(z+\Delta z) - Q(z) - q(z)\Delta z = 0$$

and letting Δz-->0 results in

$$\frac{dQ}{dz} = -q = \text{constant}$$



If we then integrate and let $Q = Q_T$ at $z = 0$ and $Q = 0$ at $z = L_D$ we get

$$Q(z) = Q_T\left(1 - \frac{z}{L_D}\right)$$

Hence,

$$\frac{dQ}{dz} = -\frac{Q_T}{L_D} = -\frac{h^3}{12\eta}\frac{p(z)}{L_l(z)}$$

which results in

$$L_l(z) = \frac{h^3}{12\eta}\frac{L_D}{Q_T}p(z)$$

where $p(z)$ is unknown. We can now rewrite the manifold equation as

$$\frac{dp}{dz} = -\frac{8\eta}{\pi R^4}Q_T\left(1 - \frac{z}{L_D}\right)$$

and then, letting $p = p_0$ at $z = 0$, we get

EG_000216563

ClearCorrect Exhibit 1038, Page 54 of 125

$$p = p_0 - \frac{8\eta Q_T L_D}{\pi R^4}\left[\left(\frac{z}{L_D}\right) - \frac{1}{2}\left(\frac{z}{L_D}\right)^2\right]$$

which leads to a land length of

$$L_l = \frac{h^3 L_D p_0}{12\eta Q_T} - \frac{2h^3 L_D^2}{3\pi R^4}\left[\left(\frac{z}{L_D}\right) - \frac{1}{2}\left(\frac{z}{L_D}\right)^2\right]$$

Problems

4.1 How would the profile presented in Example 1 be affected by using a more restrictive die which reduces the mass throughput by 20% ?

4.2 Reproduce the predicted solids bed profile for the transition and metering sections in the system presented in Table 4.2.

4.3 How would the profile presented in Example 1 be affected if you increase the barrel temperature from 149 to 160 °C ?

4.4 How many turns are required to melt a solids bed for a system similar to the one in Example 1, but using a screw with a constant channel depth of 9.4 mm? How does your result compare to the melting in the three-zoned plasticating extruder?

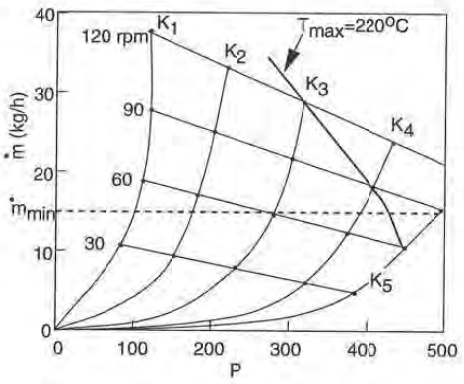
4.5 You are to extrude a 100 mm wide HDPE sheet using a single screw extruder with 45 mm diameter screw equipped with distributive and dispersive mixing heads. The screw characteristic curve is in the figure below.* The die can be approximated with a 100 mm wide and 100 mm long slit. Typical power-law constants for HDPE at 180 °C are m=20,000 Pa-s^n and n=0.41. Use a specific gravity for HDPE of 0.95.

On the graph below, draw the die characteristic curves for dies with 1 mm and 1.5 mm slits.

Explain the difference between the analytical and the experimental die characteristic curves.

Is it feasible to extrude a sheet through a 1.5 mm slit ? If so, what screw speed would you choose ? What about a 1 mm thick slit ?

* Courtesy of ICIPC, Medellín, Colombia.

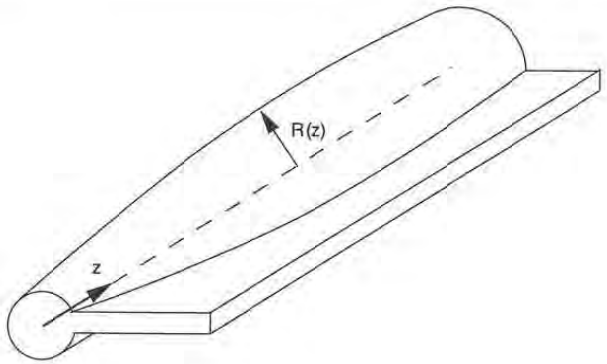


4.6 Plot the screw characteristic curve for the extruder in Example 4.2 once the clearance increases to 0.25 mm as a result of wear.

4.7 Plot the dimensionless screw characteristic curves for the extruder in Example 2 with a clearance of 0, 0.15, and 0.25 mm.

4.8 Plot the dimensionless screw characteristic curves for the extruder of Example 2 with a channel depth of 1.5, 2.5, and 5 mm.

4.9 Formulate the design equation for an end-fed sheeting die such as the one in Example 3. Unlike the example, the new die should have a variable radius manifold as in the figure below. In this case, the axial distance from the manifold center to the die exit must be constant.



EG_000216564

ClearCorrect Exhibit 1038, Page 55 of 125

4.10 Formulate the design equation for a coat-hanger die such as shown in Fig.4.20, but with a contant manifold angle α and a Newtonian fluid assumption. Derive an equation for R(x) which results in uniform flow.

4.11 Plot the manifold radius function, Eq. (4.23), for different power law indices, n, a die width of 50 cm, a die thickness of 1 mm and a constant manifold angle of 30°.

4.12 Plot the manifold radius function, Eq. (4.23), for different manifold angles, a die width of 50 cm, a die thickness of 1 mm, and a power-law index of 0.5.

References

1. Darnell, W.H., and E.A.J Mol, *Soc. Plastics Eng. J.* (1956), *12*, 20
2. Tadmor, Z., and I. Klein, *Engineering Principles of Plasticating Extrusion*, Van Nostrand Reinhold Company (1970), New York
3. Menges, G., W. Predöhl, R. Hegele, U. Kosel, and W. Elbe, Plastverarbeiter (1969), (20) 79 and 188
4. Menges, G., U. Kosel, R. Hegele, and W. Elbe, SPE ANTEC (1972), 784
5. Z. Tadmor, and C.G. Gogos, *Principles of Polymer Processing*, John Wiley & Sons (1979), New York
6. Rauwendaal, C., *Polymer Extrusion*, Hanser Publishers (1990), Munich

5 Mixing

The quality of the finished product in almost all polymer processes depends in part how well the material was mixed. Mixing can occur in internal mixers or in processing (e.g., in single and twin screw extruders). Both the material properties and the formability of the compound into shaped parts are highly influenced by the mixing quality. Hence, a better understanding of the mixing process helps one optimize processing conditions and increase part quality.

The process of polymer blending or mixing is accomplished by distributing or dispersing a minor or secondary component within a major component serving as a matrix. The major component can be thought of as the continuous phase, and the minor components as distributed or dispersed phases in the form of droplets, filaments or agglomerates.

When creating a polymer blend, one must always keep in mind that the blend will probably be remelted in subsequent processing or shaping processes. For example, a rapidly cooled system, frozen as a homogenous mixture, can separate into phases because of coalescence when re-heated. For all practical purposes, such a blend is not processable. To avoid this, special macromolecules are commonly used to compatibilize the boundary layers between phases [1].

The mixing can be *distributive* or *dispersive*. The morphology development of polymer blends is determined by three competing mechanisms: distributive mixing, dispersive mixing, and coalescence. Figure 5.1 presents a model, proposed by Macosko and co-workers [1,2], that helps us visualize the mechanisms governing morphology development in polymer blends.

5.1 Distributive Mixing

Distributive mixing or laminar mixing of compatible liquids is usually characterized by the distribution of the droplet or secondary phase within the matrix. This distribution is achieved by imposing large strains on the system such that the interfacial area between phases increases and the local dimensions, or striation thicknesses, of the secondary phases decrease. This concept is shown in Fig. 5.2 [3]. Here we have a Couette flow device with the secondary component having an initial striation thickness of δ_0. As the inner cylinder rotates, the secondary component is distributed through the systems with constantly decreasing striation thickness.

EG_000216565

ClearCorrect Exhibit 1038, Page 56 of 125

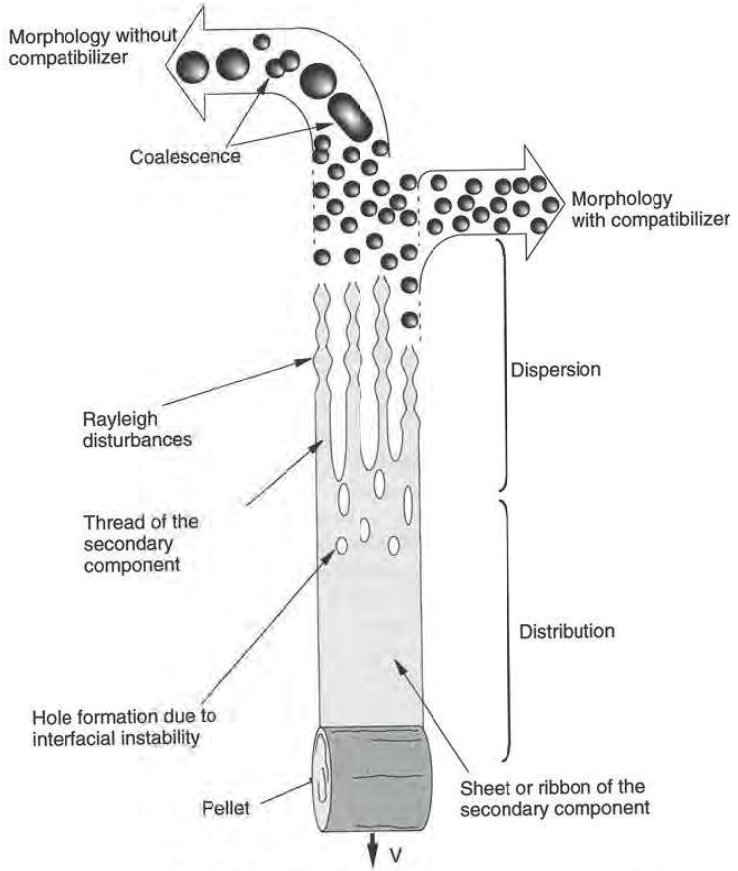


Figure 5.1 Mechanism for morphology development in polymer blends

5.1.1 Effect of Orientation

Imposing large strains on the system may not homogenize the mixture sufficiently. The type of mixing device, initial orientation, and position of the fluid components play a significant role in the quality of mixing. For example, the mixing mechanism shown in Fig. 5.2 homogeneously distributes the melt within the region contained by the streamlines cut across by the initial secondary component. Figure 5.3 [4] shows another variation of initial orientation and arrangement of the secondary component. Here, the secondary phase cuts across all streamlines, which can lead to a homogeneous mixture throughout.

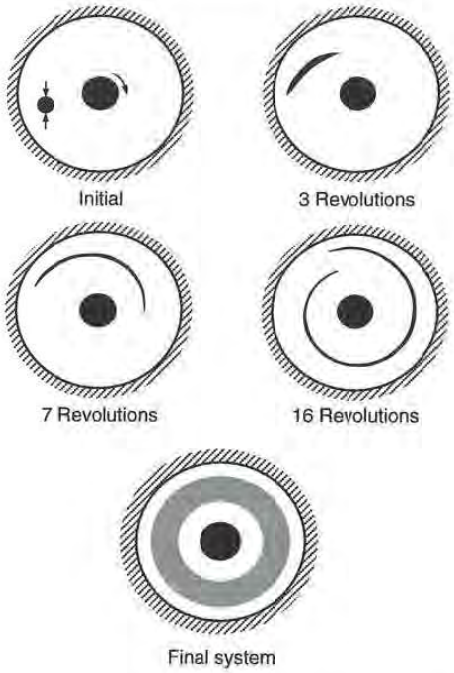


Figure 5.2 Experimental results of distributive mixing in Couette flow, and schematic of the final mixed system

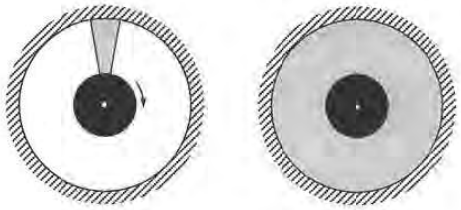


Figure 5.3 Distributive mixing in Couette flow

EG_000216566

ClearCorrect Exhibit 1038, Page 57 of 125

ESTIMATING DISTRIBUTIVE MIXING

Distributive mixing can be quantified by the reduction in striation thickness. For a sphere deformed into an ellipsoid, the striation thickness can be related to the total strain using

$$\delta = 2R(1 + \gamma^2)^{-1/4}. \tag{5.1}$$

Another common way of quantifying mixing is by following the growth of the interface between the primary and secondary fluids. In simple shear, a simple relation exists between the interfacial area, the strain and the orientation of the area of the secondary fluid with respect to the flow direction [5]:

$$\frac{A}{A_0} = \gamma \cos \alpha \tag{5.2}$$

where A_0 is the initial interfacial area, A is the final interfacial area, γ is the total strain and α the angle between the surface normal vector and the flow direction. Figure 5.4 [6] demonstrates this.

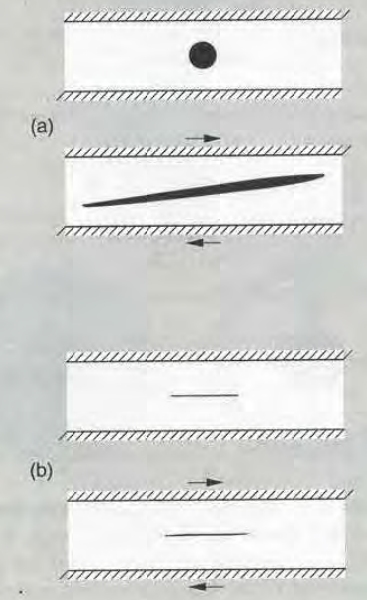


Figure 5.4 Effect of initial surface orientation on distributive mixing

Here, both cases (a) and (b) build with equal initial areas, A_0, and undergo the same amount of strain, $\gamma = 10$. The circular secondary component in (a) has a surface that is randomly oriented, between 0 and 2π, whereas most of the surface of the elongated secondary component in case (b) is oriented at $\frac{\pi}{2}$ so that of the interfacial area hardly changes. An ideal case would have been a long slender secondary component with a surface oriented in the flow direction or vertically between the parallel plates. Hence, the maximum interface growth inside a simple shear mixer can be achieved if the direction of the interface is maintained in an optimal orientation ($\cos \alpha = 1$). In a simple shear flow, this would require a special stirring mechanism that would maintain the interface between the primary and secondary fluid components in a vertical position. Using this concept, Erwin [7] demonstrated that the upper bound for the ideal mixer is found in a mixer that applies a plane strain extensional flow or pure shear flow to the fluid. In such a system the growth of the interfacial areas follows the relation given by

$$\frac{A}{A_0} = e^{\gamma/2} \tag{5.3}$$

In Erwin's ideal mixer, the amount of mixing increases exponentially compared to a linear increase if the orientation of the fluids' interfaces remain undisturbed.

5.2 Dispersive Mixing

Dispersive mixing in polymer processing involves breaking a secondary immiscible fluid or an agglomerate of solid particles and dispersing them throughout the matrix. Here, the imposed strain is not as important as the imposed stress which causes the system to break up. Hence, the type of flow inside a mixer plays a significant role in the break up of solid particle clumps or fluid droplets in dispersion.

5.2.1 Break Up of Particulate Agglomerates

The most common example of dispersive mixing of particulate solid agglomerates is the dispersion and mixing of carbon black into a rubber compound. The dispersion of such a system is schematically represented in Fig. 5.5. However, the break-up of particulate agglomerates is best explained using an ideal system of two small spherical particles that must be separated and dispersed during mixing.

EG_000216567

ClearCorrect Exhibit 1038, Page 58 of 125

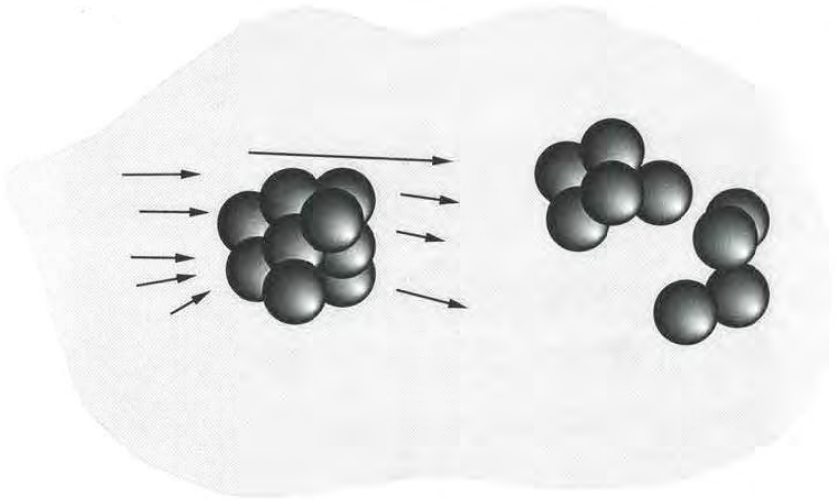


Figure 5.5 Break-up of particulate agglomerates during flow

If the mixing device generates a simple shear flow, as shown in Fig. 5.6, the maximum separation forces on the particles occur when they are oriented in a 45° position as they continuously rotate during flow. The magnitude of the force trying to separate the "agglomerate" is given by [8]

$$F_{shear} = 3\,\pi\,\eta\dot{\gamma}\,r^2 \tag{5.4}$$

where η is the viscosity of the carrier fluid, $\dot{\gamma}$ the magnitude of the strain rate tensor, and r the radii of the particles.

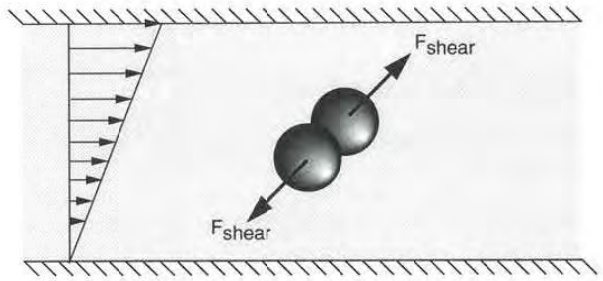


Figure 5.6 Force applied to a two-particle agglomerate in simple shear

However, if the flow field generated by the mixing device is purely elongational, such as shown in Fig. 5.7, the particles always are oriented at 0 °; the position of maximum force. The magnitude of the force for this system is given by

$$F_{elong} = 6\,\pi\,\eta\dot{\gamma}\,r^2 \tag{5.5}$$

which is twice the maximum tangential force producing simple shear. In addition, in an elongational flow, the agglomerate is always oriented in the direction of maximum force generation, whereas in simple shear flow, the agglomerate tumbles quickly through the position of maximum force.

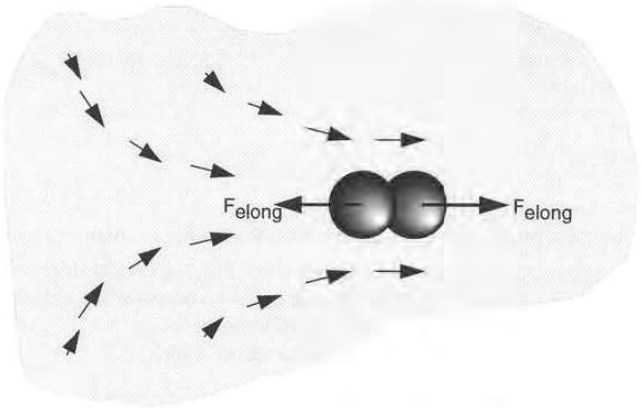


Figure 5.7 Force applied to a two-particle agglomerate in an elongational flow

The above analysis makes it clear that for mixing processes requiring break-up and dispersion of agglomerates, elongation is the preferred mode of deformation. This is only valid if the magnitude of the rate of deformation tensor can be kept the same in elongation as in shear. Hence, when optimizing mixing devices, it is important to know which mode of deformation dominates, which can be accomplished by computing a *flow number* [9], defined by

$$\lambda = \frac{\dot{\gamma}}{\dot{\gamma} + \omega} \tag{5.6}$$

where $\dot{\gamma}$ is the magnitude of the rate of deformation tensor and ω the magnitude of the vorticity tensor. A flow number of 0 implies pure rotational flow, a value of 0.5 represents simple shear flow, and pure elongational flow is implied when λ equals 1.

EG 000216568

ClearCorrect Exhibit 1038, Page 59 of 125

5.2.2 Break-Up of Fluid Droplets

Droplets in an incompatible matrix tend to be spherical as a result of their natural tendency to maintain the lowest possible surface to volume ratio. However, a flow field within the mixer applies a stress on the droplets, causing them to deform. If this stress is high enough, it eventually causes the drops to disperse. The droplets disperse when the surface tension can no longer maintain their shape in the flow field and the filaments break up into smaller droplets. This phenomena of dispersion and distribution continues to repeat itself until the stresses of the flow field can no longer overcome the surface tension of the new droplets formed.

As can be seen, the mechanism of fluid agglomerate break-up are similar in nature to solid agglomerate break-up in the sense that both rely on forces to disperse them. Hence, elongation is also the preferred mode of deformation when breaking up fluid droplets and threads, making the flow number, λ, indispensable when quantifying mixing processes.

A parameter commonly used to determine whether a droplet disperses is the capillary number defined by

$$Ca = \frac{\tau R}{\sigma_s} \tag{5.7}$$

where τ is the flow induced or deviatoric stress, R the characteristic dimension of the droplet and σ_s the surface tension acting on the drop. The capillary number is the ratio of flow stresses to droplet surface stresses. Droplet break-up occurs when a critical capillary number, Ca_{crit}, is reached. This break-up is clearly shown in Fig. 5.8 [10], which depicts the disintegration of a Newtonian thread in a Newtonian matrix.

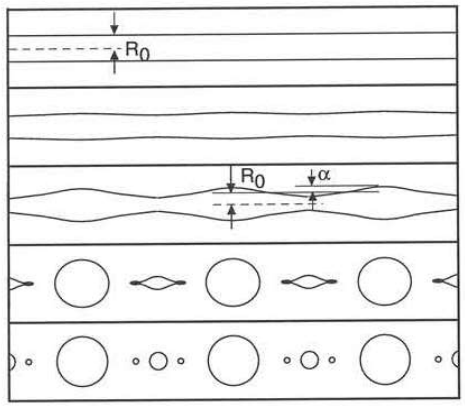


Figure 5.8 Disintegration of a Newtonian 0.35 mm diameter castor oil thread in a Newtonian silicon oil matrix. Redrawn from photographs taken every second

Because of the continuously decreasing thread radius, the critical capillary number is reached at some specific point in time. As a result of the competing deviatoric stresses and surface forces, the cylindrical shape becomes unstable and small disturbances at the surface lead to a growth of capillary waves, commonly called *Rayleigh disturbances*. Disturbances with various wavelengths form on the cylinder surface, but only those with a wavelength exceeding the circumference ($2\pi R_0$) of the thread lead to a monotonic decrease of the interfacial area.

Figure 5.9 [11] shows the critical capillary number as a function of viscosity ratio, ϕ, and flow type, described by the mixing parameter λ. For a viscosity ratio of 1 the critical capillary number is of order 1 [12]. Distributive mixing is implied when Ca is much greater than Ca_{crit} since the interfacial stress is much smaller than shear stresses. For such a case, the capillary waves which cause droplet break-up would not develop. Dispersive mixing is implied when Ca approaches its critical value or when interfacial stresses nearly equal the deviatoric stresses causing droplet break-up. In addition, break-up can occur only if enough time elapses.

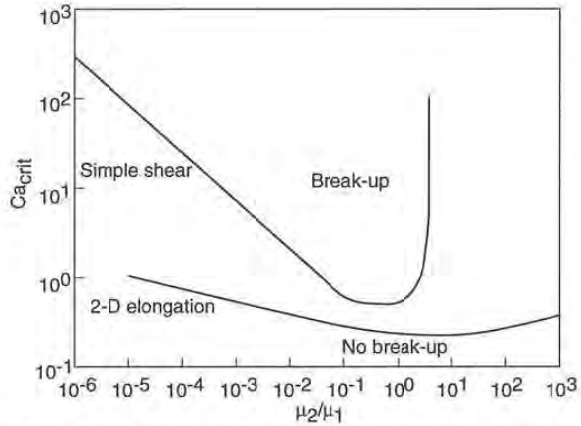


Figure 5.9 Critical capillary number for drop break-up as a function of viscosity ratio in a simple shear and a 2-D elongational flow

BREAK-UP TIME OF INCOMPATIBLE FLUIDS DURING DISPERSION

The time required for break-up, t_b, can be computed using

$$t_b = \frac{5.61}{q} \tag{5.8}$$

where q is given by

EG_000216569

ClearCorrect Exhibit 1038, Page 60 of 125

$$q = \frac{\sigma_s \Omega}{2\eta_1 R_0} \quad (5.9)$$

and Ω is a dimensionless growth rate represented in Fig. 5.10. The break-up time decreases as the critical capillary number is exceeded. The reduced break-up time t_b^* can be approximated using [11]

$$t_b^* = t_b \left(\frac{Ca}{Ca_{crit}} \right)^{-0.63} \quad (5.10)$$

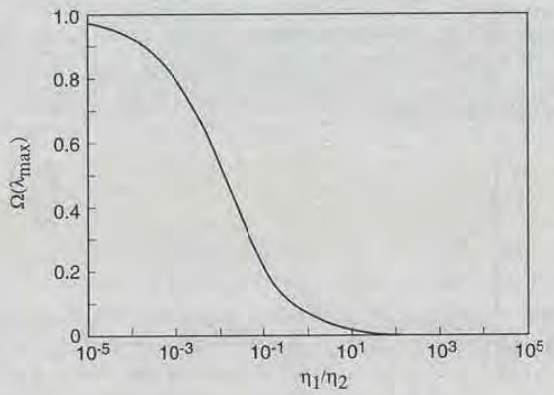


Figure 5.10 Dominant growth rate of interfacial disturbances as a function of viscosity ratio

As mentioned before, surface tension plays a large role in mixing, especially when dealing with dispersive mixing, when the capillary number approaches its critical value. Because of the stretching of the interfacial area caused by distributive mixing, the local radii of the suspended components decrease as surface tension starts to play a role. Once the capillary number goes below its critical value, only slight deformations occur and internal circulation maintains an equilibrium elliptical droplet in the flow. The mixing process then reduces to the distribution of the dispersed droplets.

5.3 Mixing Devices

The final properties of a polymer component are heavily influenced by blending or mixing during processing or as a separate step in the manufacturing process. As

mentioned earlier, when measuring the quality of mixing, one must also evaluate the mixing efficiency. For example, the amount of power required to achieve the highest mixing quality for a blend may be unachievable. This section presents mixing devices commonly encountered in polymer processing.

In general, mixers can be classified into two categories: internal batch mixers and continuous mixers. Internal batch mixers, such as the Banbury mixer, are the oldest mixing devices in polymer processing but are slowly being replaced by continuous mixers. This is because most continuous polymer processes involve mixing in addition to their normal processing tasks. Typical examples are single and twin screw extruders that often have mixing heads or kneading blocks incorporated into their systems.

5.3.1 Banbury Mixer

The Banbury mixer, shown in Fig. 5.11, is perhaps the most commonly used internal batch mixer. Internal batch mixers are high intensity mixers that generate complex shearing and elongational flows which work especially well in the dispersion of solid particle agglomerates within polymer matrices. One of the most common applications for high intensity internal batch mixing is the break-up of carbon black agglomerates into rubber compounds. The dispersion of agglomerates depends strongly on mixing time, rotor speed, temperature, and rotor blade geometry [13]. Figure 5.12 [14,15] shows the fraction of undispersed carbon black versus time in a Banbury mixer at 77 rpm and 100 °C. The broken line in the figure represents the fraction of particles smaller than 500 nm.

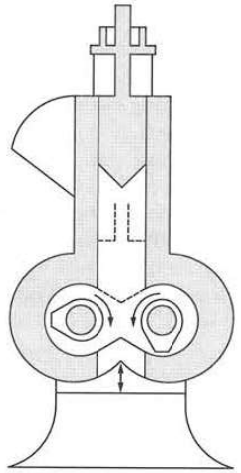


Figure 5.11 Schematic diagram of a Banbury mixer

EG_000216570

ClearCorrect Exhibit 1038, Page 61 of 125

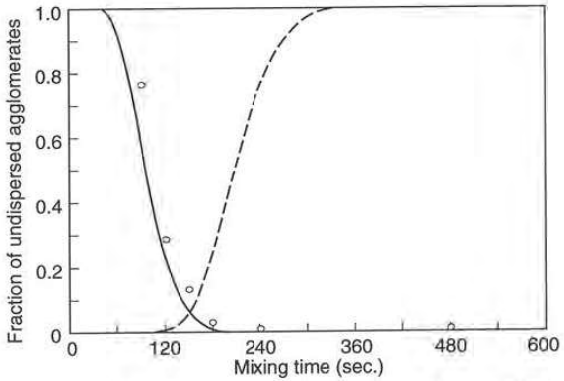


Figure 5.12 Fraction of undispersed carbon black, of size above 9 μm, as a function of mixing time inside a Banbury mixer; (O) denotes experimental results and solid line theoretical predictions; thebroken line denotes the fraction of aggregates below 500 nm in size

5.3.2 Mixing in Single Screw Extruders

One task of a single screw extruder is to mix polymers with additives and to homogenize the melt before pumping it through the die. As discussed in the previous chapter, even without a mixing section, there is a cross flow component in the polymer melt traveling down the channel in a single screw extruder. This cross flow component acts as a stirring mechanism which causes mixing. By circulating the fluid from the top of the channel to the bottom, and vice versa, the cross-channel component re-orients the interfaces between the primary and secondary fluids, enhancing mixing during extrusion.

Mixing caused by the cross-channel flow component can be further enhanced by introducing pins in the flow channel. These pins can either sit on the screw as shown in Fig. 5.13 [16], or the barrel as shown in Fig. 5.14 [17]. The extruder with the adjustable pins on the barrel is called a QSM-extruder.* In both cases the pins disturb the flow by re-orienting the surfaces between fluids and by creating new surfaces by splitting the flow. The pin type extruder is especially useful for mixing high viscosity materials such as rubber compounds; thus, it is often used in *cold feed rubber extruders*, a machine widely used to produce rubber profiles .

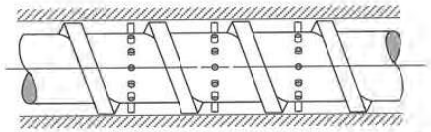


Figure 5.13 Pin mixing section on the screw of a single screw extruder

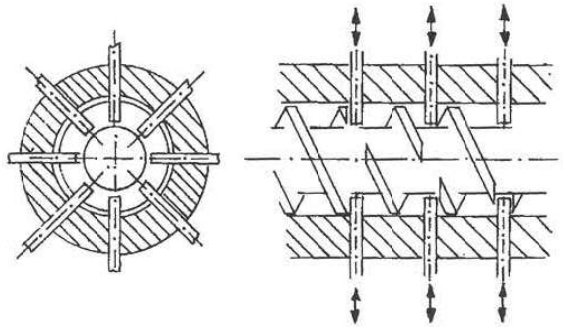


Figure 5.14 Pin barrel extruder

For lower viscosity fluids, such as thermoplastic polymer melts, often the mixing action caused by the cross-flow is insufficient to re-orient, distribute, and disperse the mixture, so one must use special mixing sections. Re-orientation of the interfaces between primary and secondary fluids and distributive mixing can be induced by any disruption in the flow channel. Figure 5.15 [16] presents commonly used distributive mixing heads for single screw extruders. These mixing heads introduce several disruptions in the flow field which improve mixing.

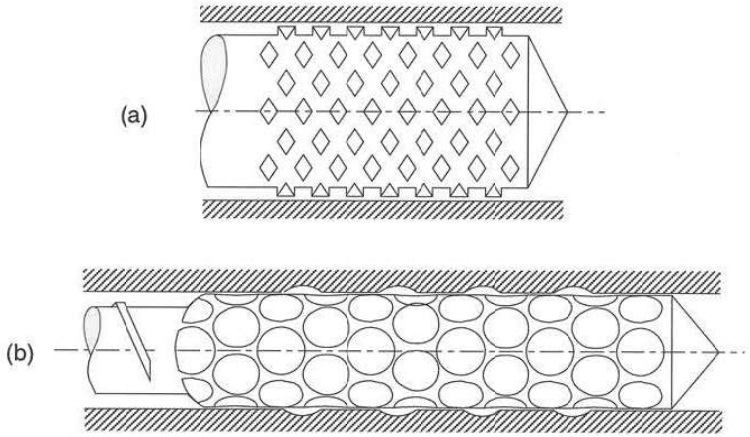


Figure 5.15 Distributive mixing sections: (a) pineapple mixing section, (b) cavity transfer mixing section

EG_000216571

ClearCorrect Exhibit 1038, Page 62 of 125

As mentioned earlier, dispersive mixing is required when breaking particle agglomerates or when surface tension effects exist between primary and secondary fluids. To disperse such systems, the mixture must be subjected to large stresses. Barrier-type screws are often sufficient to apply high stresses; however, more intensive mixing results from a mixing head. When using barrier screws or a mixing head as shown in Fig. 5.16 [16] the mixture is forced through narrow gaps, causing high stresses in the melt. Most dispersive and distributive mixing heads result in flow resistance, causing viscous heating and pressure losses during extrusion.

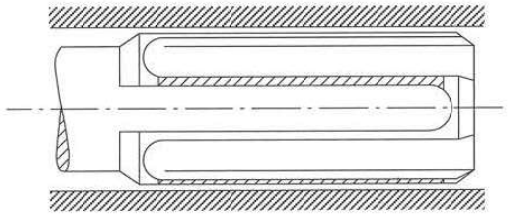


Figure 5.16 Maddock or Union Carbide mixing section

Current dispersive mixing heads have two important drawbacks. One, they rely mostly on shear rather than elongational stresses, and two, the material passes over the high stress region only once. As already discussed earlier, elongational deformation achieves dispersion more effectively than shear, but also, in terms of energy and power consumption, simple shear flows are significantly inferior to any extensional flow.

Recently, a new mixing technology was developed that eliminates these disadvantages of existing single screw extruder mixing heads [17]. The new mixing head has wedged-shaped pushing flights with a large gap, and wedged-shaped slots within the flights, as shown in Fig. 5.17. The wedge shapes generate strong elongational deformations with little viscous dissipation. Experiments performed on PS/HDPE blends show that such a mixing head can break down the dispersed PS phase to an average of 2 μm droplets, with negligible pressure losses and viscous dissipation. The size of the dispersed phase is comparable to co- and counter-rotating twin screw extruders, as discussed in section 5.3.5.

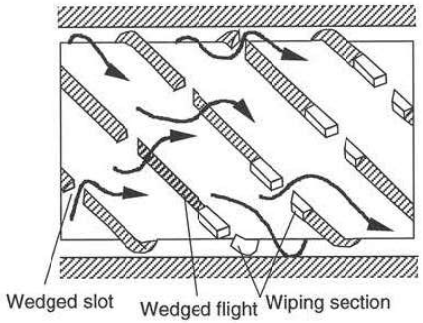


Figure 5.17 CRD mixing section

5.3.3 Static Mixers

Static mixers or motionless mixers are pressure-driven, continuous mixing devices through which the melt is pumped, rotated, and divided, leading to effective mixing without movable parts and mixing heads. One of the most commonly used static mixers is the twisted tape static mixer schematically shown in Fig. 5.18. As the fluid is rotated by the dividing wall, the interfaces between the fluids increase. The interfaces are then re-oriented by 90° once the material enters a new section. The stretching and re-orientation sequence is repeated until the number of striations is so high that a nearly homogeneous mixture is achieved. Figure 5.19 shows a sequence of cuts down a Kenics static mixer.

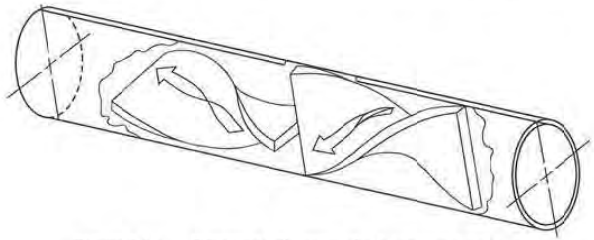


Figure 5.18 Schematic diagram of a Kenics static mixer

The number of striations increase from section to section by 2, 4, 8, 16, 32..., or simply by $N = 2^n$, where N is the number of striations and n the number of sections in the mixer.

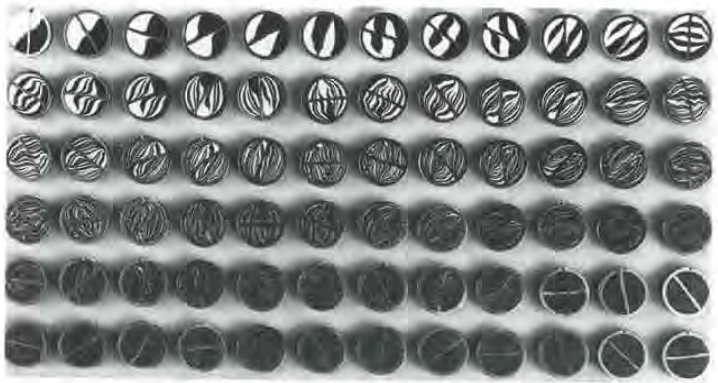


Figure 5.19 Experimental progression of the layering of colored resins in a Kenics static mixer. Courtesy of Chemineer, Inc.

EG_000216572

ClearCorrect Exhibit 1038, Page 63 of 125

Similar to dispersive mixers in single screw extrusion, a major drawback of existing static mixers is that their main mode of deformation is shear rather than elongation. Recently, a new dispersive static mixer was developed that generates elongational deformations, which lead to higher dispersive mixing [18]. Figure 5.20 presents a schematic of the new dispersive static mixer.

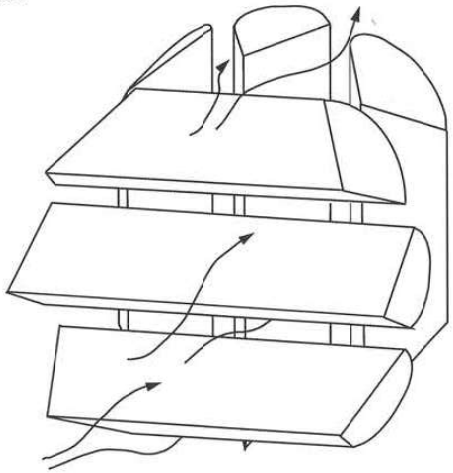


Figure 5.20 Schematic diagram of a disperive static mixer

5.3.4 Cokneader

The cokneader is a single screw extruder with pins on the barrel and a screw that oscillates in the axial direction. Figure 5.21 shows a schematic diagram of a cokneader. The pins on the barrel wipe the entire surface of the screw, making it the only self-cleaning single-screw extruder. This reduces residence time, which makes it appropriate for processing thermally sensitive materials. The pins on the barrel also disrupt the solids bed creating a *dispersed melting* [19], which improves the overall melting rate and reduces the material temperature.

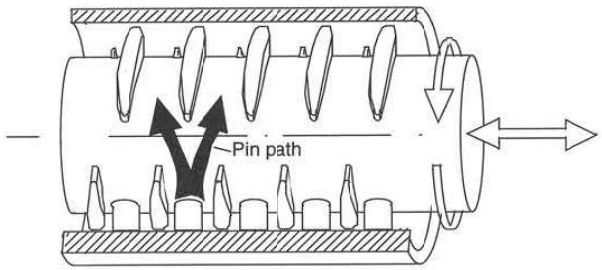


Figure 5.21 Schematic diagram of a cokneader

A simplified analysis of a cokneader gives the following number of striations per L/D [20]

$$N_s = 2^{12} \tag{5.11}$$

so that over a section of 4D the number of striations is $2^{12(4)} = 2.8E14$. A detailed discussion on the cokneader is given by Rauwendaal [20] and Elemans [21].

5.3.5 Twin Screw Extruders

In the past two decades, twin screw extruders have developed into the most popular continuous mixing devices. In general, they can be classified into intermeshing or non-intermeshing, and co-rotating or counter-rotating twin screw extruders. The intermeshing twin screw extruders are *self-cleaning* which evens out the polymer residence time. The main characteristic of this configuration is that the screw surfaces slide past each other, constantly removing polymer stuck to the screw.

In the last two decades, the co-rotating twin screw extruder systems have established themselves as efficient continuous mixers for most processes, including reactive extrusion. In essence, the co-rotating systems have a high pumping efficiency caused by the double transport action of the two screws. The counter-rotating systems generate high temperature pulses, making them inappropriate for reactive extrusion, but they generate high stresses because of the calendering action between screws, making them efficient machines to disperse pigments and lubricants.*

Several studies evaluate the mixing capabilities of twin screw extruders. Two recent studies by Lim and White [22, 23] evaluated morphology development in a 30.7 mm screw diameter co-rotating [24] and a 34 mm screw diameter counter-rotating [13] intermeshing twin screw extruder. In both studies, they dry-mixed a 75/25 blend of polyethylene and polyamide 6 pellets and then fed into the hopper at 15 kg/hour. Small samples were taken along the axis of the extruder and evaluated using optical and electron microscopy.

The blend dispersion is manifested by the reduction of the characteristic size of the polyamide 6 phase. Figure 5.22 is a plot of the weight average and number average domain size of the polyamide 6 phase along the screw axis with one kneading-pump element and three special mixing elements.

Using a co-rotating twin screw extruder with three kneading disk blocks, a final morphology with polyamide 6 weight average phase sizes of 2.6 μm was achieved. Figure 5.23 shows the morphology development along the screw axes. When comparing counter-rotating (Fig. 5.22) with co-rotating (Fig. 5.23), both achieve similar final mixing quality. However, the counter-rotating extruder achieved the final morphology much earlier in the screw than the co-rotating twin screw extruder. A possible explanation for this is that the blend traveling through the counter-rotating configuration melted earlier than in the co-rotating geometry. In addition, the phase size was slightly smaller, possibly as a result of the calendering effect between the screws in the counter-rotating system.

EG_000216573

* There seems to be considerable disagreement about co- versus counter- rotating twin screw extruders between different groups in the polymer processing industry and academic community.

ClearCorrect Exhibit 1038, Page 64 of 125

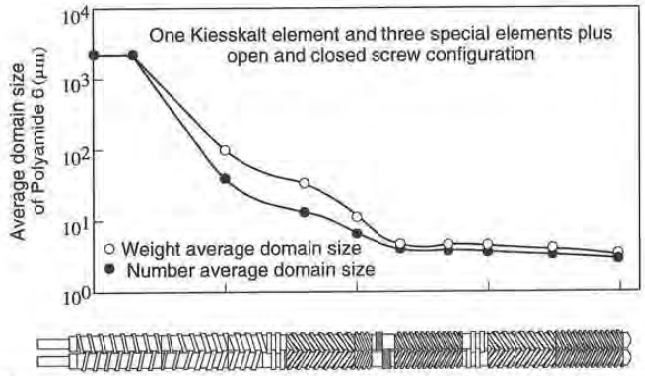


Figure 5.22 Number and weight average of polyamide 6 domain sizes along the screws for a counter-rotating twin screw extruder with special mixing elements

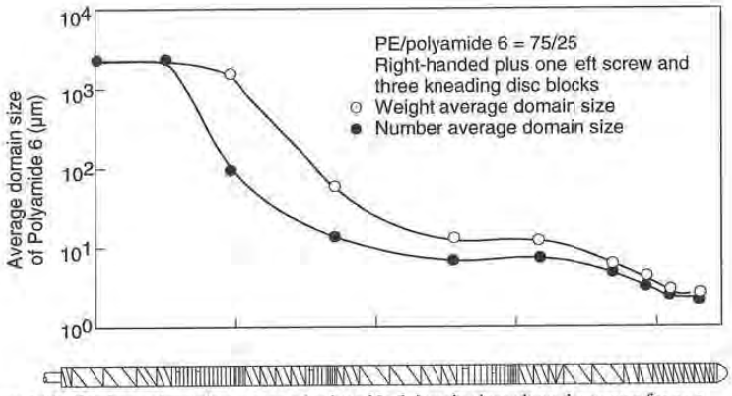


Figure 5.23 Number and weight average of polyamide 6 domain sizes along the screws for a co-rotating twin screw extruder with special mixing elements

Examples

5.1 You are to use a 45 mm diameter single screw extruder to create a polycarbonate/polypropylene polymer blend. The maximum screw rotation is 160 rpm and the screw channel depth is 4mm. Assuming a barrel temperature of 300 °C, a surface tension, σ_s between the two polymers of 8×10^{-3} N/m, and using the viscosity curves given in Figs. 5.24 and 5.25, determine:

- If one can disperse 20% PC into 80% PP
- If one can disperse 20% PP into 80% PC
- The minimum size of the dispersed phase

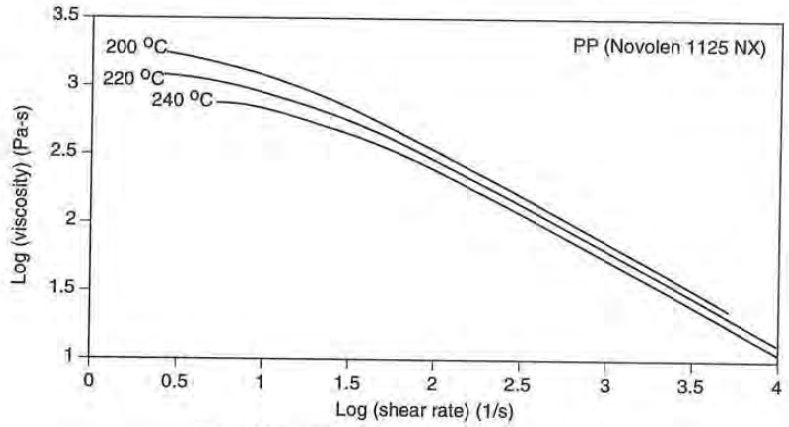


Figure 5.24 Viscosity curves for a polypropylene

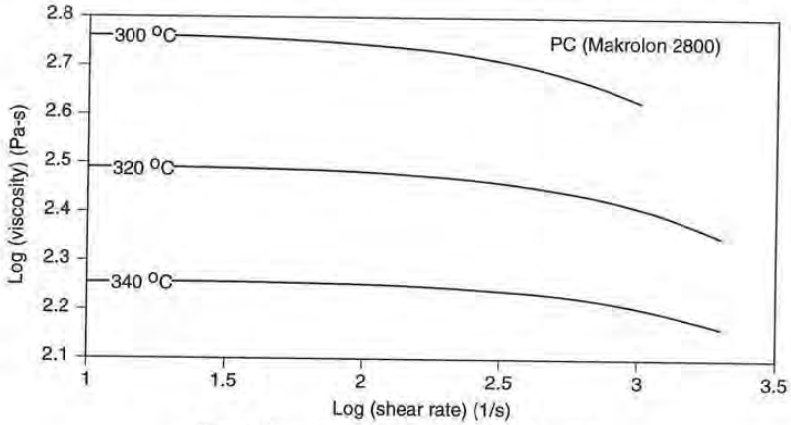


Figure 5.25 Viscosity curves for a polycarbonate

We start this problem by first calculating the average speed in the extruder using

$$v_0 = \pi DN = \pi(45)(160)(1/60) = 377 \frac{\text{mm}}{s}$$

which results in an average rate of deformation of

$$\dot{\gamma} = \frac{v_0}{h} = \frac{377}{4} = 94 \frac{1}{s}$$

From the viscosity curves we get $\eta_{PC} \approx 600\ Pa-s$ *and* $\eta_{PP} \approx 150\ Pa-s$.
Using Fig. 5.9 we can deduce that one cannot disperse polycarbonate into

EG_000216574

ClearCorrect Exhibit 1038, Page 65 of 125

polypropylene using a single screw extruder that only induces shear deformation, since $\eta_{PC}/\eta_{PP} > 4$. On the other hand, one can disperse polypropylene into polycarbonate using the same single screw extruder.

Using Fig. 5.9 we can see that dispersive mixing for a $\eta_{PP}/\eta_{PC} = 0.25$ will occur at $Ca_{crit} \approx 0.7$. Hence, neglecting the effects of coalescencewe can calculate the minimum size of the dispersed phase using

$$Ca_{crit} = 0.7 = \frac{\tau R}{\sigma_s} = \frac{600(94)R}{8x10^{-3}} \longrightarrow D = 2R = 0.2\mu m$$

To achieve this dispersion we must maintain the stresses for an extended period.

Problems

5.1 Estimate the striation thickness of a 3mm diameter pigmented polystyrene pellet in a polystyrene matrix after traveling through a 20 turn, 45 mm diameter, 5 mm constant channel depth, single screw extruder. Assume open discharge conditions. Use 100 rpm rotational speed.

5.2 Someone in your company proposes to use an existing square pitch 150 mm diameter plasticating single screw extruder as a mixing device for a 40/60 PP/PS polymer blend. The metering section is 5 turns long and has a channel depth of 10 mm. Will dispersion of the polypropylene occur for a screw rotation of 60 rpm ? Will there be enough time for dispersion ? Assume open discharge and a temperature of 220 °C. Use viscosity data given in Example 5.1, and in Fig. 5.26.

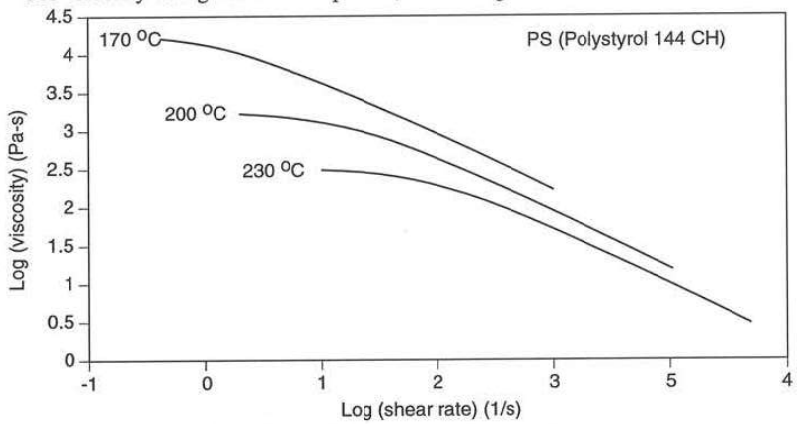


Figure 5.26 Viscosity curves for a polystyrene.

5.3 Someone in your company proposes to use an existing square pitch 150 mm diameter plasticating single screw extruder as a mixing device for a 40/60 PS/PP polymer blend. The metering section is 5 turns long and has a channel depth of 10 mm. Will dispersion of the polystyrene occur for a screw rotation of 60 rpm ? Assume open discharge and a temperature of 220 °C. Use viscosity data given in Figs. 5.24 and 5.26.

5.4 An internal batch mixer maintains shear rates, $\dot{\gamma}$, of 100 s^{-1} for extended periods. In the mixer you want to disperse LDPE in a PS matrix at 170 °C. What is the size of the dispersed phase? Will the PS still be transparent? Use viscosity data given in Figs. 5.26 and 5.27.

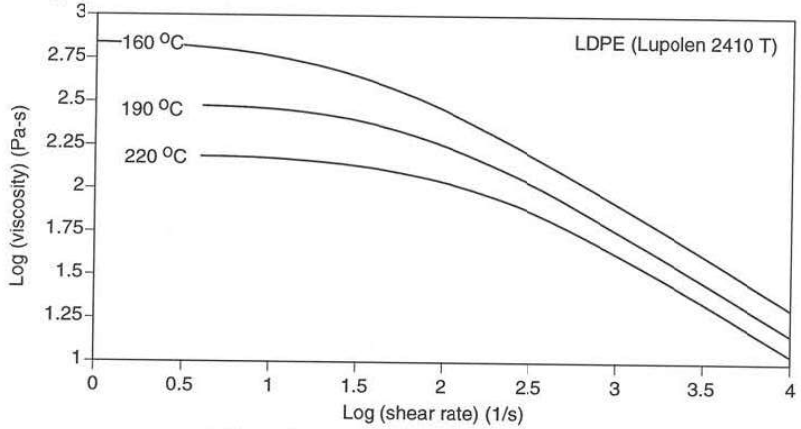


Figure 5.27 Viscosity curves for a low density polyethylene.

References

1. Sundararaj, U., and C.W. Macosko, *Macromolecules* (1995), *28*, 2647
2. Scott, C.E., and C.W. Macosko, *Polymer Bulletin* (1991), *26*, 341
3. Gramann, P.J., L. Stradins, and T.A. Osswald, *Intern. Polymer Processing* (1993), 8, 287
4. Tadmor, Z., and C.G. Gogos, *Principles of Polymer Processing*, John Wiley & Sons (1979), New, York
5. Erwin, L., *Polym. Eng. & Sci.* (1978), *18*, 572
6. Rauwendaal, C., *Mixing in Polymer Processing*, Marcel Dekker, Inc. (1991), New York
7. Erwin, L., *Polym. Eng. & Sci.* (1978), *18*, 738
8. Tadmor, Z., *Ind. Eng. Fundam.* (1976), *15*, 346
9. Cheng, J., and I. Manas-Zloczower, *Internat. Polym. Proc.* (1990), 5, 178
10. Sundararaj, U., and C.W. Macosko, *Macromolecules* (1995), *28*, 2647
11. Grace, H.P., *Chem. Eng. Commun.* (1982), *14*, 225
12. Janssen, J.M.H., Ph.D. Thesis (1993), Eindhoven University of Technology, The Netherlands
13. Biswas, A., and T.A. Osswald (1994), unpublished research
14. Cox, R.G., *J. Fluid Mech.* (1969), 37, 3, 601–623
15. Boonstra, B.B., and A.I. Medalia, *Rubber Age* (1963), 3, 4

EG_000216575

ClearCorrect Exhibit 1038, Page 66 of 125

16. Rauwendaal, C., *Polymer Extrusion*, Hanser Publishers (1990), Munich
17. Rauwendaal, C, T.A. Osswald, P.J. Gramann, and B.A. Davis, *SPE ANTEC Tech. Pap.* (1998), 56
18. Gramann, P..J., B.A. Davis, T.A. Osswald and C. Rauwendaal (1998), Patent Pending
19. Rauwendaal, C., *SPE ANTEC Tech. Pap.* (1993), *39*, 2232
20. Rauwendaal, C., *Mixing in Reciprocating Extruders*, A chapter in *Mixing and Compounding of Polymers*, Eds. I. Manas-Zloczower and Z. Tadmor, Hanser Publishers (1994), Munich
21. Elemans, P.H.M., Modeling of the cokneater, A chapter in *Mixing and Compounding of Polymers*, Eds. I. Manas-Zloczower and Z. Tadmor, Hanser Publishers (1994), Munich
22. Lim, S. and J.L. White, *Intern. Polymer Processing* (1993), *8*, 119
23. Lim, S. and J.L. White, *Intern. Polymer Processing* (1994), *9*, 33
24. Stone, H.A. and L.G. Leal, *J. Fluid Mech.* (1989), 198, 399–427

6 Injection Molding

Injection molding is the most important process used to manufacture plastic products. Today, more than one-third of all thermoplastic materials are injection molded and more than half of all polymer processing equipment is for injection molding. The injection molding process is ideally suited to manufacture mass produced parts of complex shapes requiring precise dimensions. The process goes back to 1872 when the Hyatt brothers patented their stuffing machine to inject cellulose into molds. However, today's injection molding machines are mainly related to the reciprocating screw injection molding machine patented in 1956. A modern injection molding machine with its most important elements is shown in Fig. 6.1. The components of the injection molding machine are the plasticating unit, clamping unit, and the mold.

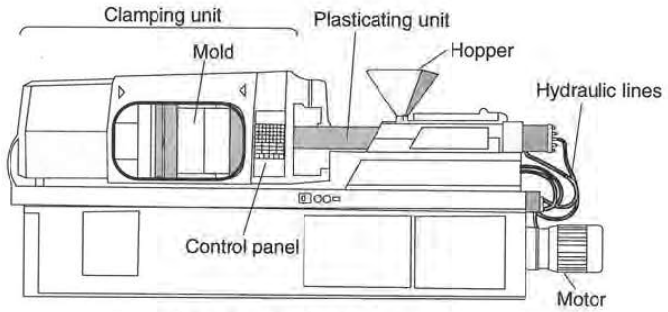


Figure 6.1 Schematic of an injection molding machine

Today, injection molding machines are classified by the following international convention*

Manufacturer type T / P

where T is the clamping force in metric tons and P is defined as

$$P = \frac{v_{max} p_{max}}{1000} \tag{6.1}$$

where v_{max} is the maximum shot size in cm^3 and p_{max} is the maximum injection pressure in bar. The clamping forced T can be as low as 1 metric ton for small machines, and as high as 11,000 tons.

* The old US convention uses MANUFACTURER T-v where T is the clamping force in British tons and v the shot size in ounces of polystyrene

EG_000216576

ClearCorrect Exhibit 1038, Page 67 of 125

6.1 The Injection Molding Cycle

The sequence of events during the injection molding of a plastic part, as shown in Fig. 6.2, is called the injection molding cycle. The cycle begins when the mold closes, followed by the injection of the polymer into the mold cavity. Once the cavity is filled, a holding pressure is maintained to compensate for material shrinkage. In the next step, the screw turns, feeding the next shot to the front of the screw. This causes the screw to retract as the next shot is prepared. Once the part is sufficiently cool, the mold opens and the part is ejected. Fig. 6.3 presents the sequence of events during the injection molding cycle. The figure shows that the cycle time is dominated by the cooling of the part inside the mold cavity. The total cycle time can be calculated using

$$t_{cycle} = t_{closing} + t_{cooling} + t_{ejection} \tag{6.2}$$

where the closing and ejection times, $t_{closing}$ and $t_{ejection}$, can last from a fraction of second to a few seconds, depending on the size of the mold and machine.

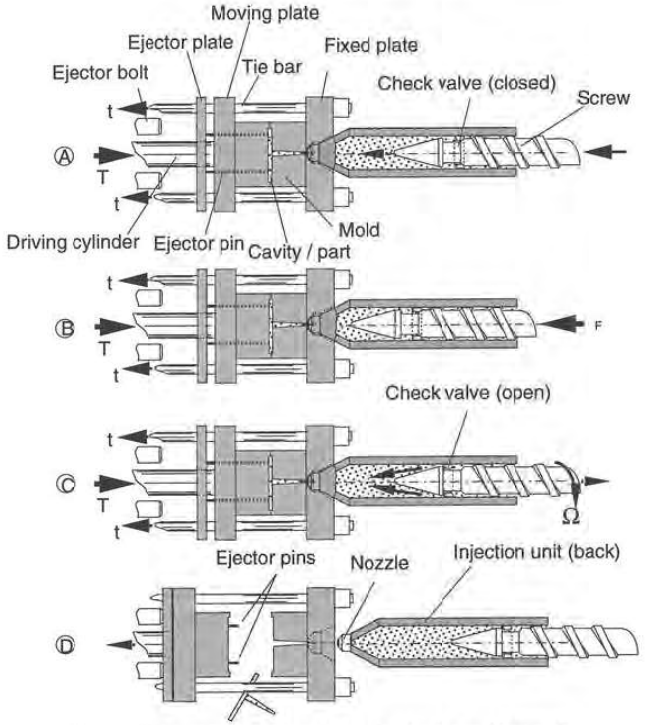


Figure 6.2 Sequence of events during an injection molding cycle

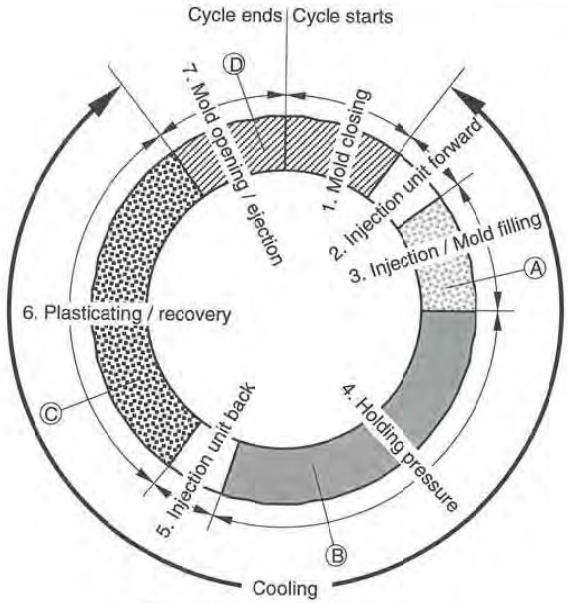


Figure 6.3 Injection molding cycle

ESTIMATING COOLING TIME DURING INJECTION MOLDING

The cooling time for a plate-like part of thickness h can be estimated using [1]

$$t_{cooling} = \frac{h^2}{\pi\alpha} \ln\left(\frac{8}{\pi^2}\frac{T_M - T_W}{T_D - T_W}\right) \tag{6.3}$$

and for cylindrical geometry of diameter D using

$$t_{cooling} = \frac{D^2}{23.14\alpha} \ln\left(0.692\frac{T_M - T_W}{T_D - T_W}\right) \tag{6.4}$$

In Eqs. (6.3) and (6.4), α represents thermal diffusivity, T_M represents the melt temperature, T_W the mold temperature, and T_D the average part temperature at ejection.

Using the average part temperature history and the cavity pressure history, the process can be followed and assessed using the PvT diagram as depicted in Fig. 6.4. [2-3]. To follow the process on the PvT diagram, we must transfer both the temperature and the pressure at

EG_000216577

ClearCorrect Exhibit 1038, Page 68 of 125

matching times. The diagram reveals four basic processes: an isothermal injection (0-1) with pressure rising to the holding pressure (1-2), an isobaric cooling process during the holding cycle (2-3), an isochoric cooling after the gate freezes with a pressure drop to atmospheric (3-4), and then isobaric cooling to room temperature (4-5).

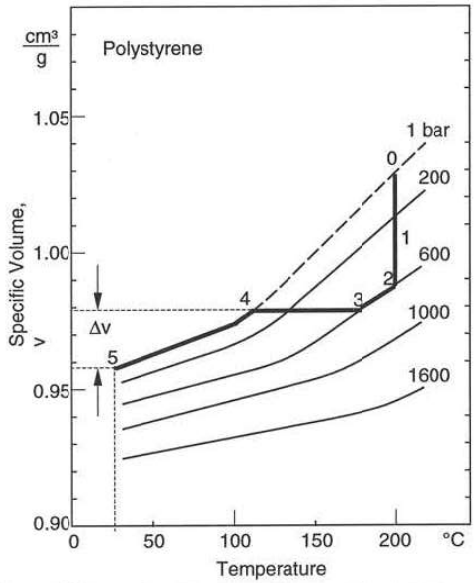


Figure 6.4 Trace of an injection molding cycle in a PvT diagram

The point on the PvT diagram where the final isobaric cooling begins (4), controls the total part shrinkage, Δv. This point is influenced by the two main processing conditions - the melt temperature, T_M and the holding pressure, P_H, as depicted in Fig. 6.5. Here the process in Fig. 6.4 is compared to one with a higher holding pressure. Of course, there is an infinite combination of conditions that render acceptable parts, bound by minimum and maximum temperatures and pressures. Figure 6.6 presents *the molding diagram* with all limiting conditions. The melt temperature is bound by a low temperature that results in a *short shot* or unfilled cavity and a high temperature that leads to material degradation. The hold pressure is bound by a low pressure that leads to excessive shrinkage or low part weight, and a high pressure that results in *flash*. Flash results when the cavity pressure force exceeds the machine clamping force, leading to melt flow across the mold parting line. The holding pressure determines the corresponding clamping force required to size the injection molding machine. An experienced polymer processing engineer can usually determine which injection molding machine is appropriate for a specific application. For the untrained polymer processing engineer, finding this appropriate holding pressure and its corresponding mold clamping force can be difficult.

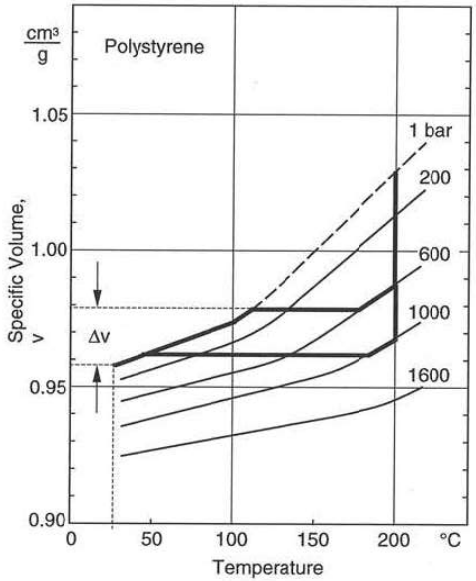


Figure 6.5 Trace of two different injection molding cycles in a PvT diagram

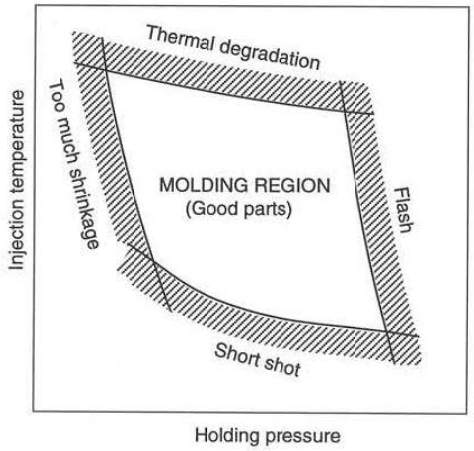


Figure 6.6 The molding diagram

EG_000216578

ESTIMATING INJECTION PRESSURE AND CLAMPING FORCE

To aid the polymer processing engineer in finding required injection pressures and corresponding mold clamping forces, Stevenson [4] generated a set of dimensionless groups and corresponding graphs for non-isothermal mold filling of non-Newtonian polymer melts.

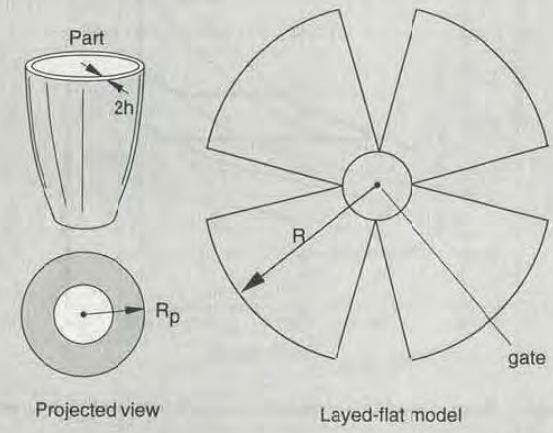


Fig.6.7 Lay-flat representation of an injection molded part

Using the notation in Fig. 6.7 and a viscosity defined by $\eta = m_0 e^{-a(T-T_{ref})}|\dot{\gamma}|^{n-1}$, four dimensionless groups are defined.

- The dimensionless temperature β determines the intensity of the coupling between the energy equation and the momentum balance. It is defined by

$$\beta = a(T_i - T_m) \tag{6.5}$$

where T_i and T_m are the injection and mold temperatures respectively.

- The dimensionless time τ is the ratio of the filling time, t_{fill}, and the time for thermal equilibrium via conduction, defined by

$$\tau = \frac{t_{fill} k}{h^2 \rho C_p} \tag{6.6}$$

- The Brinkman number Br is the ratio of the energy generated by viscous dissipation and the energy transported by conduction. For a non-isothermal, non-Newtonian model it is

$$Br = \frac{m_0 e^{-aT_i} h^2}{k(T_i - T_m)} \left(\frac{R}{t_{fill} h} \right)^{n+1} \tag{6.7}$$

- The power-law index n of the Ostwald and deWaale model reflects the shear thinning behavior of the polymer melt.

Once the dimensionless parameters are calculated, the dimensionless injection pressures $\left(\frac{\Delta p}{\Delta p_l}\right)$ and dimensionless clamping forces $\left(\frac{F}{F_l}\right)$ are read from Figs. 6.8 to 6.11. The isothermal pressure and force are computed using

$$\Delta p_l = \frac{m_0 e^{-aT_i}}{1-n} \left[\frac{1+2n}{2n} \frac{R}{t_{fill} h} \right]^n \left(\frac{R}{h} \right) \tag{6.8}$$

and

$$F_l = \pi R^2 \left(\frac{1-n}{3-n} \right) \Delta p_l \tag{6.9}$$

Since the part area often exceeds the projected area, Fig. 6.12 can be used to correct the computed clamping force.

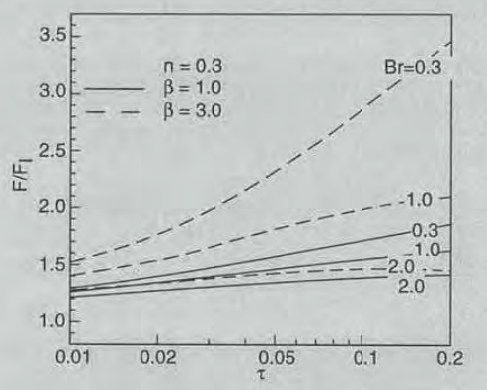


Fig. 6.8 Dimensionless clamping force versus dimensionless groups

EG_000216579

ClearCorrect Exhibit 1038, Page 70 of 125

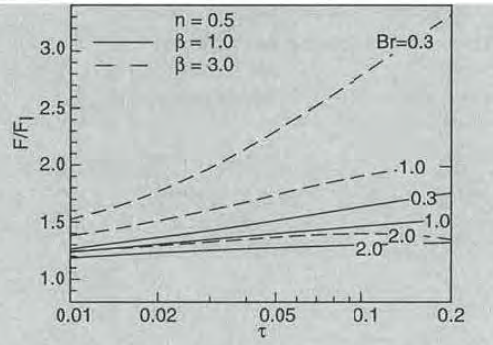


Fig. 6.9 Dimensionless clamping force versus dimensionless groups

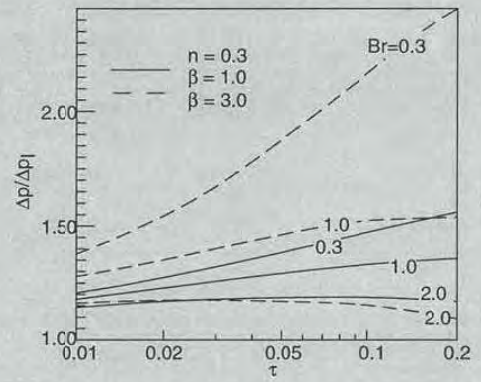


Fig. 6.10 Dimensionless injection pressure versus dimensionless groups

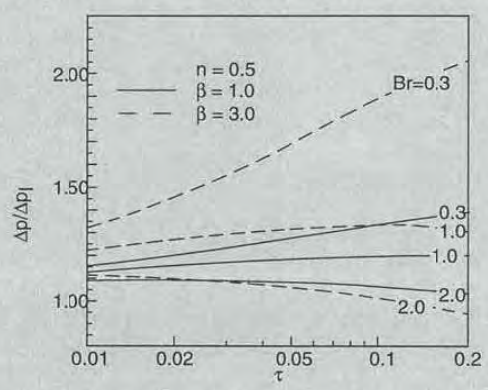


Fig. 6.11 Dimensionless injection pressure versus dimensionless groups

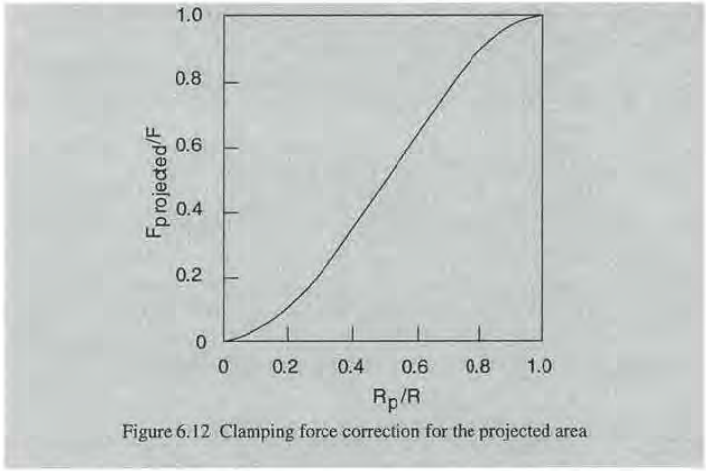


Figure 6.12 Clamping force correction for the projected area

With difficulty, one can control and predict the component's shape and residual stresses at room temperature. For example, *sink marks* in the final product are caused by material shrinkage during cooling, and residual stresses can lead to environmental stress cracking under certain conditions [5].

Warpage in the final product is often caused by processing conditions that lead to asymmetric residual stress distributions through the part thickness. The formation of residual stresses in injection molded parts is attributed to two major coupled factors: cooling and flow stresses. The first and most important is the residual stress formed as a result of rapid cooling.

RESIDUAL STRESSES IN AN INJECTION MOLDED PART

The parabolic temperature distribution through the thickness of a solidified injection molded part leads to a parabolic residual stress distribution, compressive in the outer surfaces of the component and tensile in the core. Assuming no residual stress build-up during phase change, a simple function based on the parabolic temperature distribution, can be used to approximate the residual stress distribution in thin sections [6]:

$$\sigma = \frac{2}{3}\,\alpha E\,(T_s - T_f)\left(\frac{6z^2}{4L^2} - \frac{1}{2}\right). \qquad (6.10)$$

Here, T_f is the final temperature of the part, E is the modulus, α the thermal expansion coefficient, L the half thickness and T_s denotes the solidification temperature: glass transition temperature for amorphous thermoplastics or the melting temperature for semi-crystalline polymers. Figure 6.13 [7]

EG_000216580

ClearCorrect Exhibit 1038, Page 71 of 125

compares the compressive stresses measured on the surface of PMMA moldings to those predicted by Eq. 6.10.

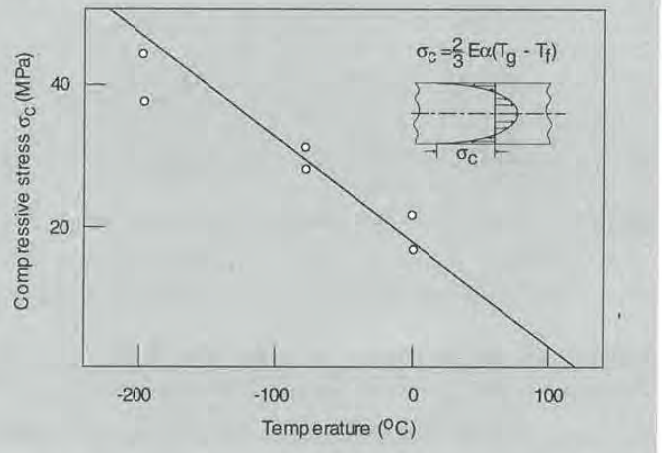


Figure 6.13 Comparison between computed, Eq. (6.10), and measured compressive stresses on the surface of injection molded PMMA plates

6.2 The Injection Molding Machine

6.2.1 The Plasticating and Injection Unit

A plasticating and injection unit is shown in Fig. 6.14. The major tasks of the plasticating unit are to melt the polymer, to accumulate the melt in the screw chamber, to inject the melt into the cavity, and to maintain the holding pressure during cooling.

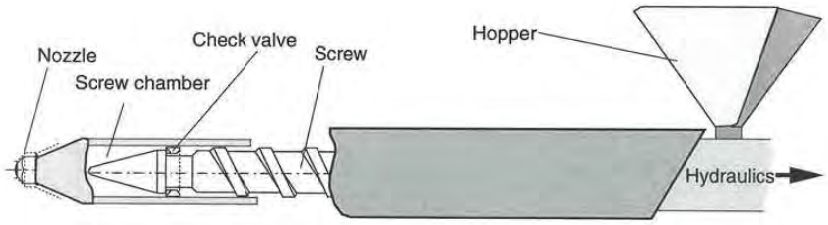


Figure 6.14. Schematic of the plasticating unit

The main elements of the plasticating unit follow:

- Hopper
- Screw
- Heater bands
- Check valve
- Nozzle

The hopper, heating bands and the screw are similar to a plasticating single screw extruder, except that the screw in an injection molding machine can slide back and forth to allow for melt accumulation and injection. This characteristic gives it the name *reciprocating screw*. The maximum stroke in a reciprocating screw is 3D.

Although the most common screw used in injection molding machines is the three-zone plasticating screw, two stage vented screws are often used to extract moisture and monomer gases just after the melting stage.

The check valve, or non-return valve, is at the end of the screw and enables it to work as a plunger during injection and packing without allowing polymer melt back flow into the screw channel. A check valve and its function during operation is depicted in Fig. 6.2, and in Fig. 6.14. A high quality check valve allows less then 5% of the melt back into the screw channel during injection and packing.

The nozzle is at the end of the plasticating unit and fits tightly against the sprue bushing during injection. The nozzle type is either open or shut-off. The open nozzle is the simplest, rendering the lowest pressure consumption.

6.2.2 The Clamping Unit

The job of a clamping unit in an injection molding machine are to open and close the mold, and to close the mold tightly to avoid flash during the filling and holding. Modern injection molding machines have two predominant clamping types: mechanical and hydraulic.

Figure 6.15 presents a toggle mechanism in the open and closed mold positions. Although the toggle is essentially a mechanical device, it is actuated by a hydraulic cylinder. The advantage of using a toggle mechanism is that as the mold approaches closure the available closing force increases and the closing decelerates significantly. However, the toggle mechanism only transmits its maximum closing force when the system is fully extended.

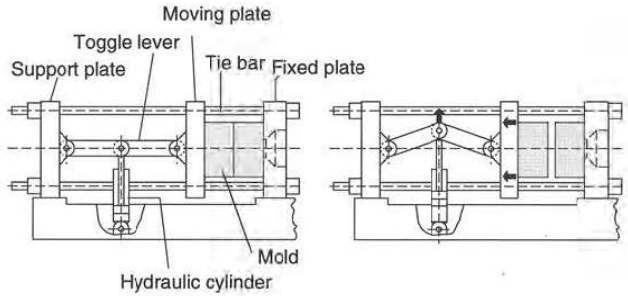


Figure 6.15. Clamping unit with a toggle mechanism

EG_000216581

ClearCorrect Exhibit 1038, Page 72 of 125

Figure 6.16 presents a schematic of a hydraulic clamping unit in the open and closed positions. The advantages of the hydraulic system is that a maximum clamping force is attained at any mold closing position and that the system can take different mold sizes without major system adjustments.

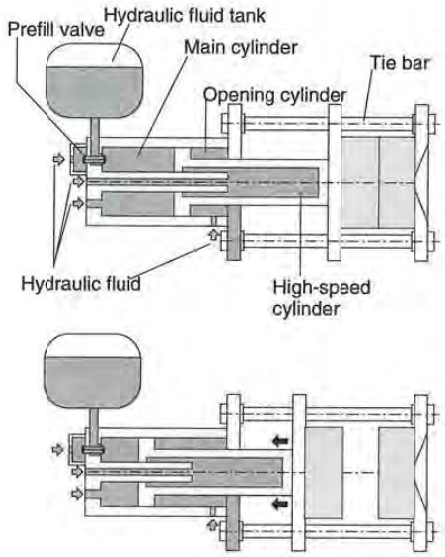


Figure 6.16 Hydraulic clamping unit

6.2.3 The Mold Cavity

The central point in an injection molding machine is the mold. The mold distributes polymer melt into and throughout the cavities, shapes the part, cools the melt and ejects the finished product. As depicted in Fig. 6.17, the mold is custom-made and consists of the following elements:

- Sprue and runner system
- Gate
- Mold cavity
- Cooling system (thermoplastics)
- Ejector system

During mold filling, the melt flows through the sprue and is distributed into the cavities by the runners, as in Fig. 6.18.

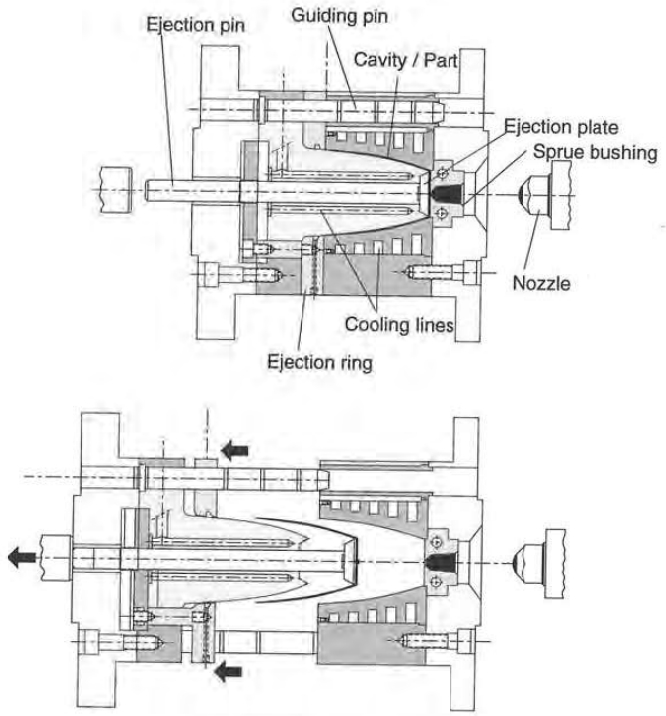


Figure 6.17 An injection mold

The runner system in Fig. 6.18 (a) is symmetric where all cavities fill at the same time causing the polymer to fill all cavities in the same way. The disadvantage of this balanced runner system is that the flow paths are long, leading to high material and pressure consumption. On the other hand, the asymmetric runner system shown in Fig. 6.18(b) leads to parts of different quality. Equal filling of the mold cavities can also be achieved by varying runner diameters. There are two types of runner systems - cold and hot. Cold runners are ejected with the part, and are trimmed after mold removal. The advantage of the cold runner is lower mold cost. The hot runner keeps the polymer at its melt temperature. The material stays in the runners system after ejection, and is injected into the cavity in the following cycle. There are two types of hot runner system: externally and internally heated. The externally heated runners have a heating element surrounding the runner that keeps the polymer isothermal. The internally heated runners have a heating element running along the center of the runner, maintaining a polymer melt that is warmer at its center and possibly solidified along the outer runner surface. Although a hot runner system considerably increases mold cost, its advantages include elimination of trim and lower pressures for injection.

EG_000216582

ClearCorrect Exhibit 1038, Page 73 of 125

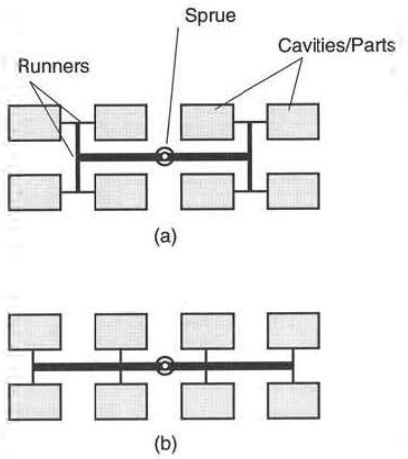


Figure 6.18 Schematic of different runner system arrangements

When large items are injection molded, the sprue sometimes serves as the gate, as shown in Fig. 6.19. The sprue must be subsequently trimmed, often requiring further surface finishing. On the other hand, a pin-type gate (Fig. 6.19) is a small orifice that connects the sprue or the runners to the mold cavity. The part is easily broken off from such a gate, leaving only a small mark that usually does not require finishing. Other types of gates, also shown in Fig. 6.19, are film gates, used to eliminate orientation and disk or diaphragm gates for symmetric parts such as compact discs.

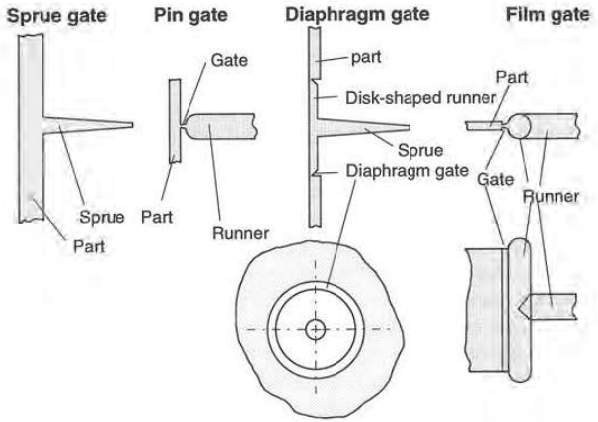


Figure 6.19 Schematic of different gating systems

6.3 Related Injection Molding Processes

Although most injection molding processes are covered by the conventional process description discussed earlier in this chapter, there are several important molding variations including:

- Multi-color
- Multi-component
- Co-injection
- Gas-assisted
- Injection-compression

Multi-color injection molding occurs when two or more components are injected through different runner and gate systems at different stages during the molding process. Each component is injected using its own plasticating unit. The molds are often located on a turntable. Multi-color automotive stop lights are molded this way.

In principle, the multi-component injection molding process is the same as the multi-color process. Here, either two incompatible materials are molded or one component is cooled sufficiently so that the two components do not adhere to each other. For example, to mold a ball and socket system, the socket of the linkage is molded first. The socket component is allowed to cool somewhat and the ball part is injected inside it. This results in a perfectly movable system. This type of injection molding process is used to replace tedious assembling tasks and is becoming popular in countries where labor costs are high.

In contrast to multi-color and multi-component injection molding, co-injection molding uses the same gate and runner system. Here, the component that ends as the outer skin of the part is injected first, followed by the core component. The core component displaces the first and a combination of the no-slip condition between polymer and mold and the freezing of the melt creates a sandwiched structure as depicted in Fig. 6.20.

In principle, the gas-assisted injection molding process is similar to two-component injection molding. Here, the second or core component is nitrogen, which is injected through a needle into the polymer melt, blowing the melt out of the way and depositing it against the mold surfaces.

Injection-compression molding first injects the material into a partially opened mold, and then squeezes the material by closing the mold. Injection-compression molding is used for polymer products that require a high quality surface finish, such as compact discs and other optically demanding components.

EG_000216583

ClearCorrect Exhibit 1038, Page 74 of 125

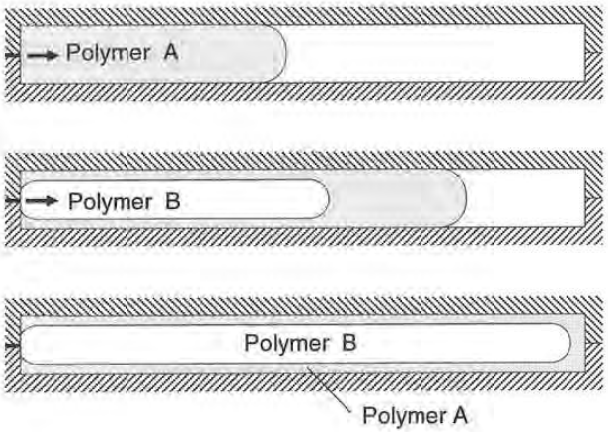


Figure 6.20 Schematic of the co-injection molding process

6.4 Computer Simulation in Injection Molding

Today, computer simulation is commonly used to predict mold filling, fiber orientation, thermal history, residual stresses and warpage in complex parts. It is common practice, to determine gate location, balance the runner system, relocate or eliminate possible weldlines, reduce shrinkage and warpage, and optimize the properties of the finished product before ever cutting a piece of metal, through the use of simulation packages.

In injection molding, researchers are making progress on solving three-dimensional orientation for complex realistic applications [8,9]. Commercially available programs solve for the non-isothermal, non-Newtonian filling and orientation in non-planar injection molded parts. They used the Hele–Shaw model [10] to simulate the mold filling. For example, Fig. 6.21 presents the filling pattern and weldline location during molding of a complex lawn-mover housing. Orientation in the finished product is computed using tensor representations. The injection molded part is divided into layers to include complex flow and heat transfer phenomena that take place during filling. Figure 6.22 presents the fixed finite element mesh used to represent a plate and the predicted filling pattern during molding. The same figure presents the computed fiber orientation distribution in three different layers within the part.

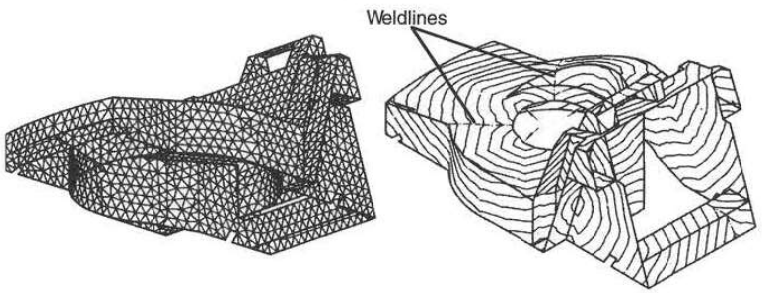


Figure 6.21 Finite element mesh and predicted filling pattern for a lawn-mover housing

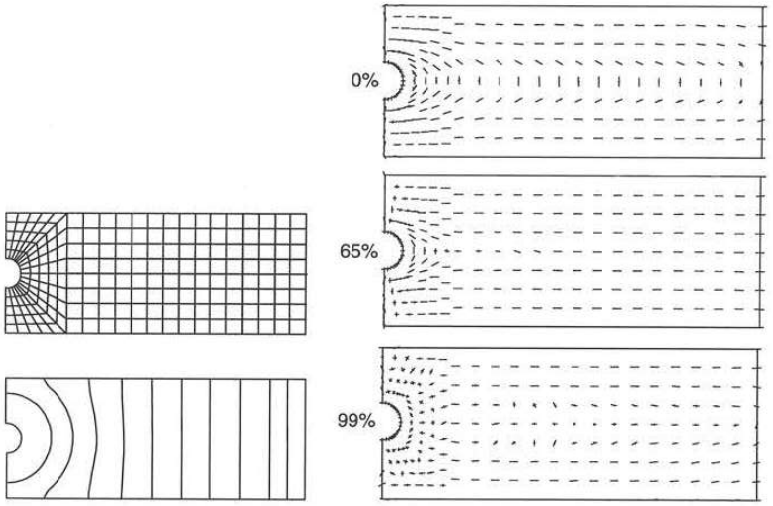


Figure 6.22 Finite element mesh, predicted filling pattern and computed fiber orientation in three different layers (0% corresponds to the center and 100% to the surface of the part)

Examples

6.1 Consider the multi-cavity injection molding process shown in Fig. 6.23. To achieve equal part quality, the filling time for all cavities must be balanced. For the case in question, balance your cavities by solving for the runner radius, R_2. For a balanced runner system the flow rates into all cavities must match. For a given flow rate Q, length L, and radius R_1, you must also solve for the pressures at the runner system

EG 000216584

ClearCorrect Exhibit 1038, Page 75 of 125

junctures. Assume an isothermal flow of a non-Newtonian shear thinning polymer. Compute the radius R_2 for a part molded of polystyrene with a consistency index (m) of 2.8×10^4 Pa-s^n and a power law index (n) of 0.28. Use values of L=10 cm, R_1=3 mm, and $Q = 20$ cm^3/s.

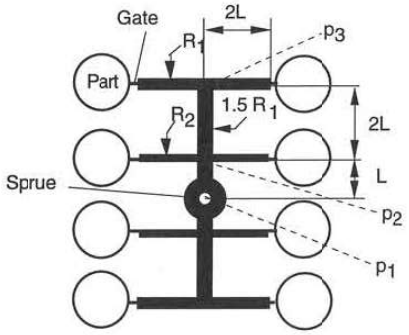


Figure 6.23 Runner system lay cut

The flow through each runner section is governed by the Hagen-Poiseuille equation:

$$Q = \frac{\pi R^3}{s+3}\left(\frac{R\,\Delta p}{2\,m\,L}\right)^s$$

The various sections can be represented using

Section 1: $$4Q = \frac{\pi(1.5R_1)^3}{s+3}\left[\frac{1.5R_1(P_1 - P_2)}{2\,m\,L}\right]^s$$

Section 2: $$2Q = \frac{\pi(1.5R_1)^3}{s+3}\left[\frac{1.5R_1(P_2 - P_3)}{4\,m\,L}\right]^s$$

Section 3: $$Q = \frac{\pi R_2^3}{s+3}\left[\frac{R_2(P_2 - 0)}{4\,m\,L}\right]^s$$

Section 4: $$Q = \frac{\pi R_1^3}{s+3}\left[\frac{R_1(P_3 - 0)}{4\,m\,L}\right]^s$$

The unknown parameters, P_1, P_2, P_3, and R_2, can be obtained using the above equations. For the given values, a radius, R_2, of 2.34 mm would result in a balanced runner system, with pressures P_1 = 562 bar, P_2 = 460 bar and P_3 = 292 bar. For comparison, if we assume a Newtonian model with μ=m, a radius R_2 of 2.76 mm would have resulted, with much higher required pressures of P_1=63030 bar, P_2=49120 bar and P_3=35210 bar.

6.2 You are to determine the maximum clamping force and injection pressure required to mold an ABS suitcase with a filling time, t_f, of 2.5 seconds. Use the dimensions shown in Fig. 6.24, an injection temperature, T_i, of 227 °C (500K), and a mold temperature, T_m, of 27 °C (300K). The properties necessary for the calculations are also given below.

Properties for ABS

$n = 0.29$	$\rho = 1020\ kg/m^3$
$m_0 = 29x10^5\ Pa - s^n$	$C_p = 2343\ J/kg/K$
$a = 0.01369/K$	$k = 0.184\ W/m/K$

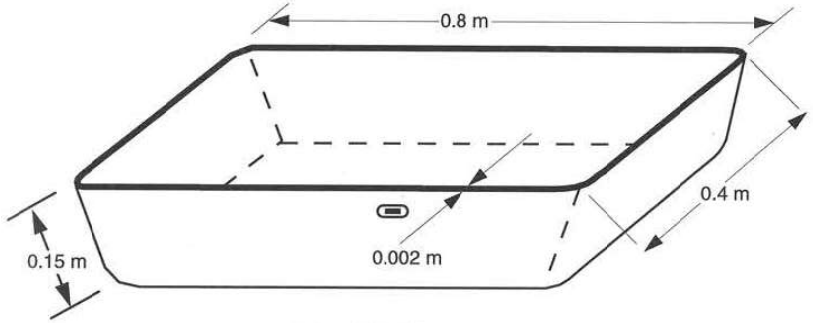


Figure 6.24 Suitcase geometry

We start this problem by first laying the suitcase flat and determining the required geometric factors (Fig. 6.25). From the suitcase geometry, the longest flow path, R, is 0.6 m and the radius of the projected area, R_p, is 0.32 m. We can now compute the dimensionless parameters given in Eqs. (6.5 to 6.7),

$$\beta = 0.01369(500 - 300) = 2.74$$

$$\tau = \frac{2.5(0.184)}{(0.001)^2(1020)(2343)} = 0.192$$

$$Br = \frac{(29x10^6)e^{-0.01369(500)}(0.001)^2}{0.184(500 - 300)}\left(\frac{0.6}{2.5(0.001)}\right)^{0.29+1} = 0.987$$

The isothermal injection pressure and clamping force are computed using Eqs. (6.8 to 6.9)

EG_000216585

ClearCorrect Exhibit 1038, Page 76 of 125

$$\Delta p_I = \frac{29x10^6 e^{-0.01369(500)}}{1-0.29}\left[\frac{1+2(0.29)}{2(0.29)}\frac{0.6}{2.5(0.001)}\right]^{0.29}\left(\frac{0.6}{0.001}\right) = 171\ MPa$$

$$F_I = \pi(0.6)^2\left(\frac{1-0.29}{3-0.29}\right)(17.1x10^7) = 50.7x10^6\ N$$

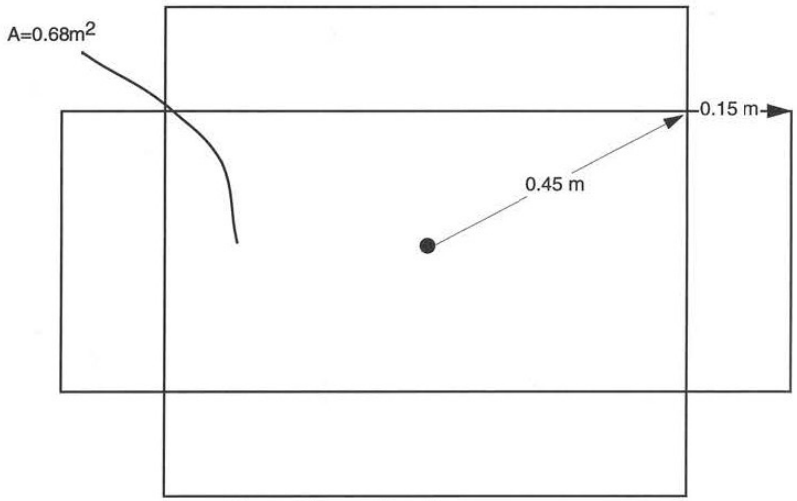


Figure 6.25 Layed-flat suitcase

We now look up $\Delta p/\Delta p_I$ and F/F_I in Figs. (6.8 to 6.11). Since little change occurs between n = 0.3 and n = 0.5, we choose n = 0.3. However, for other values of n we can interpolate or extrapolate. For $\beta = 2.74$, we interpolate between 1 and 3 as

$$\beta = 1 \rightarrow \Delta p/\Delta p_I = 1.36 \text{ and } F/F_I = 1.65$$

$$\beta = 3 \rightarrow \Delta p/\Delta p_I = 1.55 \text{ and } F/F_I = 2.1$$

$$\beta = 2.74 \rightarrow \Delta p/\Delta p_I = 1.53 \text{ and } F/F_I = 2.04$$

$$\Delta p = \left(\Delta p/\Delta p_I\right)\Delta p_I = 262\ MPa = 2{,}620\ bar$$

$$F = \left(F/F_I\right)F_I = 10.3x10^7\ N = 10{,}300\ metric\ tons$$

The clamping force can be corrected for an $R_p = 0.32\ m$ using Fig. 6.12 and $R_p/R = 0.53$.

$$F_{projected} = (0.52)10{,}300 = 5{,}356\ metric\ tons$$

For our suitcase cover, where the total volume is 1,360 cc and total part area is 0.68 m^2, the above numbers are too high. A usefull rule-of-thumb is a maximum allowable clamping force of 2 tons/in^2. Here, we have greatly exceeded that number. Normally, around 3,000 metric tons/m^2 are allowed in commercial injection molding machines. For example, a typical injection molding machine* with a shot size of 2,000 cc has a maximum clamping force of 630 metric tons with a maximum injection pressure of 1,400 bar. A machine with much larger clamping forces and injection pressures is suitable for much larger parts. For example, a machine with a shot size of 19,000 cc allows a maximum clamping force of 6,000 metric tons with a maximum injection pressure of 1,700 bar. For this example we must reduce the pressure and clamping force requirements. This can be accomplished by increasing the injection and mold temperatures or by reducing the filling time. Recommended injection temperatures for ABS are between 210 and 240 °C and recommended mold temperatures are between 40 and 90 °C.** As can be seen, there is room for adjustment in the processing conditions, so one must repeat the above procedure using new conditions.

Problems

6.1 A thin polyamide 66 component is injection molded under the following conditions:

- The melt is injected at 275 °C to a maximum pack/hold pressure of 800 bar.
- The 800 bar pack/hold pressure is maintained until the gate freezes off, at which point the part is at an average temperature of 175 °C.
- The pressure drops to 1 bar as the part cools inside the cavity.
- The part is removed from the mold and cooled to 25 °C.

- Draw the whole process on the PvT diagram.

- Estimate the final part thickness if the mold thickness is 1 mm. For thin injection molded parts, most of the shrinkage leads to part thickness reduction.

* MINIFLOW, Injection Molding Simulation, The Madison Group: PPRC, Madison, WI.
** A good reference for such values is the CAMPUS® material data bank. Books such as H. Dominighaus, *Plastics for Engineers*, Hanser Publishers (1992), Munich are also recommended

EG_000216586

ClearCorrect Exhibit 1038, Page 77 of 125

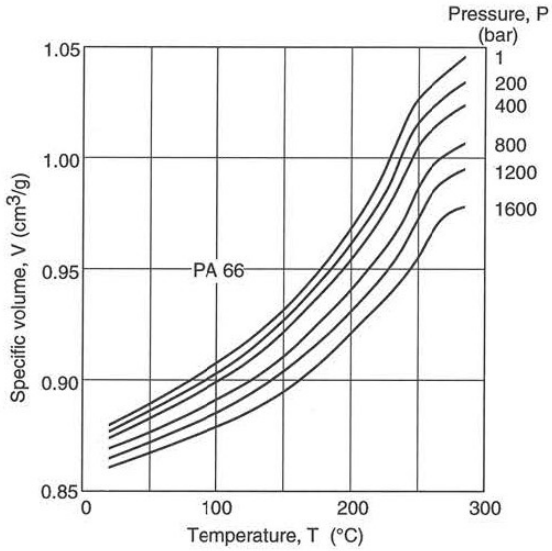


Figure 6.26 PvT diagram for PA66

6.2 Design a balanced runner system for the mold in Example 1 if you are to injection mold a polystyrene product. Assume a power-law model with a consistency index, m, of 2.8×10^4 Pa-s^n, and a power-law index, n, of 0.28.

6.3 Estimate the cooling time for the ABS suitcase presented in Example 6.2 if demolding occurs when the average part temperature is below 60 °C.

6.4 What are the required clamping force and injection pressure if the filling time in Example 6.2 is increased from 2.5 seconds to 3 seconds?

6.5 What are the required clamping force and injection pressure if the mold temperature in Example 6.2 is increased from 27°C to 90°C ?

6.6 What are the required clamping force and injection pressure if the injection temperature in Example 6.2 is increased from 227 to 240 °C?

6.7 What is the residual stress on the surface of a 1 mm thick injection molded polystyrene ruler with a glass transition temperature of 100 °C and a mold temperature of 40 °C? Assume a modulus of 3.2 GPa.

References

1. Pötsch, G., and W. Michaeli, Injection Molding: An Introduction, Hanser Publishers (1995), Munich
2. Greener, J., *Polym. Eng. Sci.* (1986), *26*, 886
3. Michaeli, W., and M. Lauterbach, *Kunststoffe* (1989), *79*, 852
4. Stevenson, J.F., *Polym. Eng. Sci.*((1978), *18*, 577
5. Osswald, T.A., and G. Menges, *Materials Science of Polymers for Engineers,* Hanser Publishers (1996), Munich
6. Wimberger-Friedl, R., *Polym. Eng. Sci.* (1990), *30*, 813
7. Ehrenstein, G.W., *Polymer Kunststoffe,* Hanser Publishers (1978), Munich
8. Verleye, V., and F. Dupret, *Proc. ASME WAM* (1993), New Orleans
9. Crochet, M.J., F. Dupret, and V. Verleye, *Flow and Rheology in Polymer Composites Manufacturing*, Ed. S.G. Advani, Elsevier (1994), Amsterdam
10. Hele-Shaw, H.S., *Proc. Roy. Inst.* (1899), *16,* 49

EG_000216587

ClearCorrect Exhibit 1038, Page 78 of 125

7 Secondary Shaping

Secondary shaping operations such as extrusion blow molding, film blowing, and fiber spinning occur immediately after the extrusion profile emerges from the die. The thermoforming process is performed on sheets or plates previously extruded and solidified. In general, secondary shaping operations consist of mechanical stretching or forming of a preformed cylinder, sheet, or membrane.

7.1 Fiber Spinning

Fiber spinning is used to manufacture synthetic fibers. During fiber spinning, a filament is continuously extruded through an orifice and stretched to diameters of 100 μm and smaller. The process is schematically depicted in Fig. 7.1. The molten polymer is first extruded through a filter or *screen pack*, to eliminate small contaminants. The melt is then extruded through a spinneret, a die composed of multiple orifices. A spinneret can have between one and 10,000 holes. The fibers are then drawn to their final diameter, solidified, and wound onto a spool. The solidification takes place either in a water bath or by forced convection. When the fiber solidifies in a water bath, the extrudate undergoes an adiabatic stretch before cooling begins in the bath. The forced convection cooling, which is more commonly used, leads to a non-isothermal spinning process.

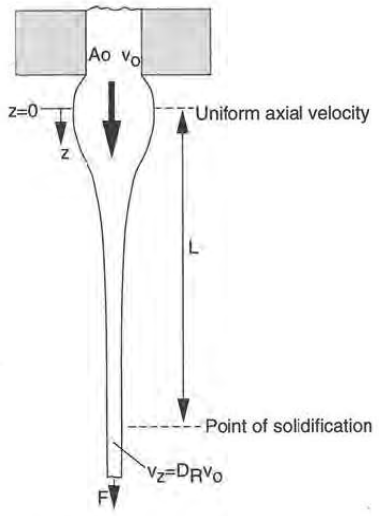


Figure 7.1 The fiber spinning process

EG_000216588

ClearCorrect Exhibit 1038, Page 79 of 125

The drawing and cooling processes determine the morphology and mechanical properties of the final fiber. For example, ultra high molecular weight HDPE fibers with high degrees of orientation in the axial direction can have the stiffness of steel with today's fiber spinning technology.

Of major concern during fiber spinning are the instabilities that arise during drawing, such as brittle fracture, Rayleigh disturbances, and draw resonance. Brittle fracture occurs when the elongational stress exceeds the melt strength of the drawn polymer melt. The instabilities caused by Rayleigh disturbances are like those causing filament break-up during dispersive mixing as discussed in Chapter 5. Draw resonance appears under certain conditions and manifests itself as periodic fluctuations that result in diameter oscillation.

STABILITY ANALYSIS OF FIBER SPINNING

Fisher and Denn [1] performed a stability analysis of isothermal, viscoelastic spinning. Figure 7.2 [1] presents the stable and unstable regions in a draw ratio, D_R, versus $De^{1/n}$ graph. The draw ratio is defined by

$$D_R = \frac{v_0}{v_f} \tag{7.1}$$

and for this case the Deborah number is given by

$$De = \frac{m(3)^{(n-1)/2}}{G}\left(\frac{v_0}{L}\right) \tag{7.2}$$

where n is the power-law index, m the consistency index, G the shear modulus of the fiber, v_0 the material speed as it emerges from the spinneret orifice, v_f the fiber speed at the take-up roll and, L the distance between the spinneret and the first contact take-up wheel.

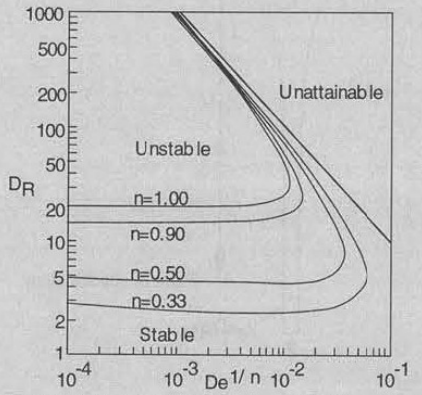


Figure 7.2 Stable and unstable regions during fiber spinning

7.2 Film Production

7.2.1 Cast Film Extrusion

In a cast film extrusion process, a thin film is extruded through a slit onto a chilled, highly polished, turning roll where it is quenched from one side. The speed of the roller controls the draw ratio and final film thickness. The film is then sent to a second roller for cooling of the other side. Finally, the film passes through a system of rollers and is wound onto a roll. A typical film casting process is depicted in Fig. 7.3. The cast film extrusion process exhibits stability problems similar to those encountered in fiber spinning [2].

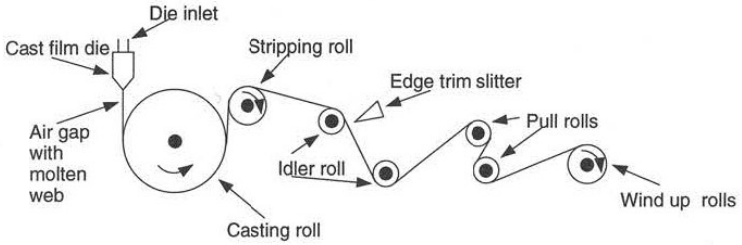


Figure 7.3 Schematic of a film casting operation

Thicker polymer sheets are manufactured similarly. A sheet is distinguished from a film by its thickness; by definition a sheet has a thickness exceeding 250 μm; otherwise, it is called a film.

STABILITY ANALYSIS OF FILM CASTING

Anturkar and Co [2] performed a stability analysis of isothermal, viscoelastic film casting depicted in Fig. 7.4. In their analysis, they used the White-Metzner viscoelastic model and represented the viscosity with the Bird-Carreau model as

$$\eta = \eta_0\left(1+\lambda_v^2\dot{\gamma}^2\right)^{n-1/2} \tag{7.3}$$

If we relate the time constant of the White-Metzner model to first normal stress differences and viscosity using $\lambda = \frac{\Psi_1}{2\eta}$, we end with a similar relation for the relaxation time:

$$\lambda = \lambda_0\left(1+\lambda_t^2\dot{\gamma}^2\right)^{n-1/2} \tag{7.4}$$

EG_000216589

ClearCorrect Exhibit 1038, Page 80 of 125

Figures 7.5 and 7.6[2] present the stable and unstable regions in a draw ratio, D_R ,versus De graph. Here, the Deborah number is defined by

$$De = \frac{\lambda_0 v_0}{L}\left(2\frac{\lambda_r v_0}{L}\right)^{n'-1} \qquad (7.5)$$

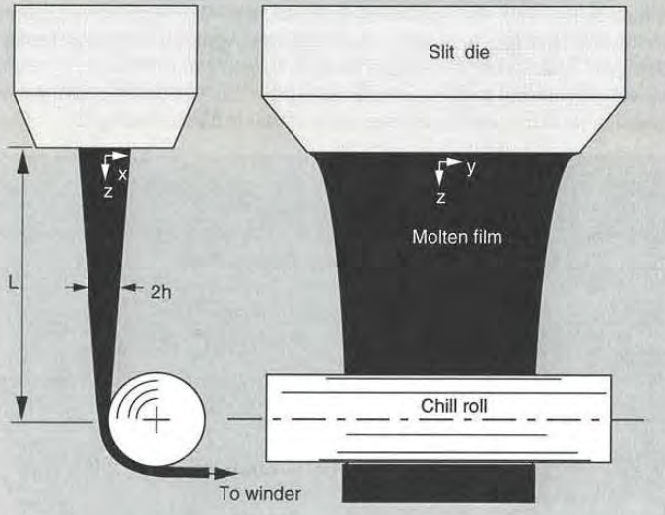


Figure 7.4 Film casting

The curves in Figs. 7.5 and 7.6 show the effect of the exponent n and n', respectively.

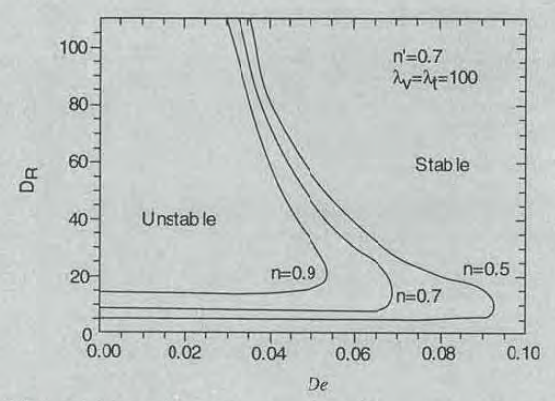


Figure 7.5 Stable and unstable regions during film casting (constant n')

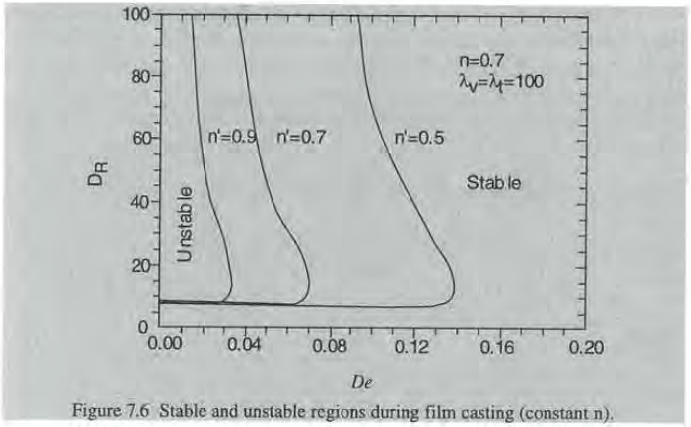


Figure 7.6 Stable and unstable regions during film casting (constant n).

7.2.2 Film Blowing

In film blowing, a tubular cross-section is extruded through an annular die, normally a spiral die, and is drawn and inflated until the *freezing line* is reached. Beyond this point, the stretching is practically negligible. The process is schematically depicted in Fig. 7.5 [3]. The advantage of film blowing over casting is that the induced biaxial stretching renders a stronger and less permeable film.

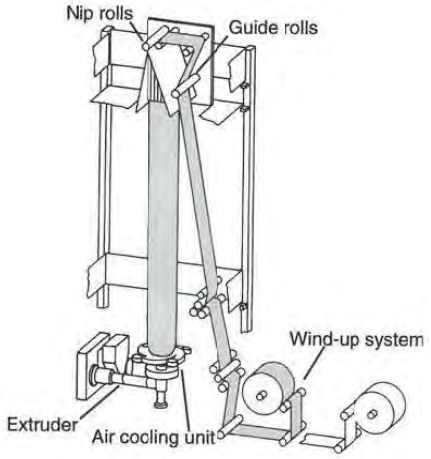


Figure 7.5 Film blowing

EG_000216590

ClearCorrect Exhibit 1038, Page 81 of 125

The extruded tubular profile passes through one or two air rings to cool the material. The tube interior is maintained at a certain pressure by blowing air into the tube through a small orifice on the die mandrel. The air is retained in the tubular film, or bubble, by collapsing the film well above its freeze-off point and tightly pinching it between rollers. The size of the tubular film is calibrated between the air ring and the collapsing rolls.

FILM BLOWING ANALYSIS

The important outcome of a film blowing process (Fig. 7.6) is the size or diameter of the tubular film defined by the dimensionless blow-up ratio

$$B_R = \frac{R_f}{R_0} \tag{7.6}$$

and the dimensionless draw ratio

$$D_R = \frac{v_f}{v_0} \tag{7.7}$$

Conservation of mass leads to a dimensionless thickness defined by

$$\frac{h_0}{h_f} = B_R D_R \tag{7.8}$$

Pearson and Petrie [4] developed and solved a Newtonian model of film blowing and plotted their results in dimensionless graphs. In addition to dimensionless blow-up ratio, draw ratio, and thickness, they introduced a dimensionless pressure, P,

$$P = \frac{\pi R_0^3 \Delta p}{\mu Q} \tag{7.9}$$

a dimensionless take-up force, F,

$$F = \frac{R_0 f_z}{\mu Q} \tag{7.10}$$

and a dimensionless freeze-off point, X,

$$X = \frac{Z}{R_0} \tag{7.11}$$

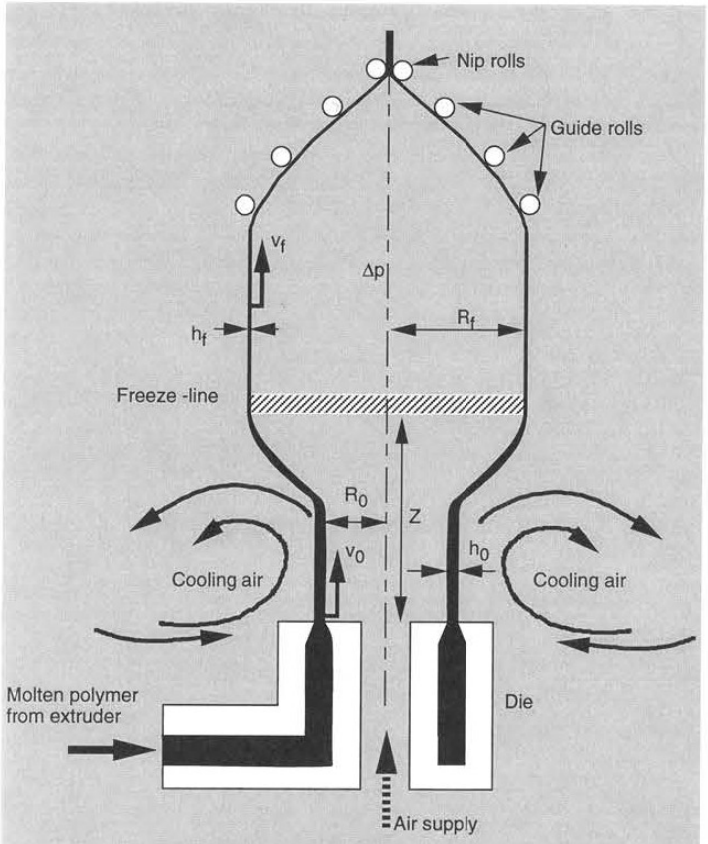


Figure 7.6 Film blowing

where μ is the Newtonian viscosity, R_0 is the radius of the extruded tube, R_f is the radius of the final tubular film, v_0 is the velocity of the material at the exit of the die, v_f is the take-up speed, Q is the volumetric material throughput, Δp is the pressure difference across the film, and f_z is the film take-up force. Figures 7.7[4] and 7.8[4] present results from the isothermal Newtonian film blowing calculations using the above dimensionless parameters. These graphs are helpful when determining effect of processing conditions on film size and thickness.

EG_000216591

ClearCorrect Exhibit 1038, Page 82 of 125

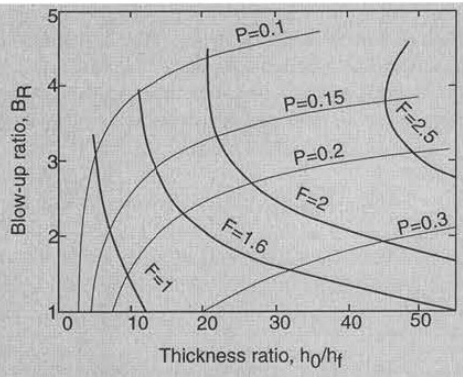


Figure 7.7 Film blowing processing conditions for X=10

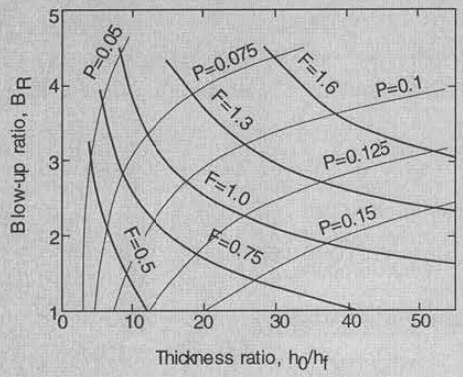


Figure 7.8 Film blowing processing conditions for X=20

7.3 Blow Molding

The predecessor of the blow molding process was the blowing press developed by Hyatt and Burroughs in the 1860s to manufacture hollow celluloid articles. Polystyrene was the first synthetic polymer used for blow molding during World War II and polyethylene was the first material to be implemented in commercial applications. Until the late 1950s, the main application for blow molding was the manufacture of LDPE articles such as squeeze bottles.

Blow molding produces nearly hollow articles that do not require a homogeneous thickness distribution. Today, HDPE, LDPE, PP, PET, and PVC are the most common materials used for blow molding.

7.3.1 Extrusion Blow Molding

In extrusion blow molding, a *parison* or tubular profile is extruded and inflated into a cavity with the specified geometry. The blown article is held inside the cavity until it is sufficiently cool. Figure 7.9 [5] presents a schematic of the steps in blow molding.

During blow molding, one must generate the appropriate parison length such that the trim material is minimized. Another means of saving material is by generating a parison of variable thickness, usually referred to as *parison programming*, such that an article with an evenly distributed wall thickness is achieved after stretching the material. An example of a programmed parison and finished bottle thickness distribution is presented in Fig. 7.10 [6].

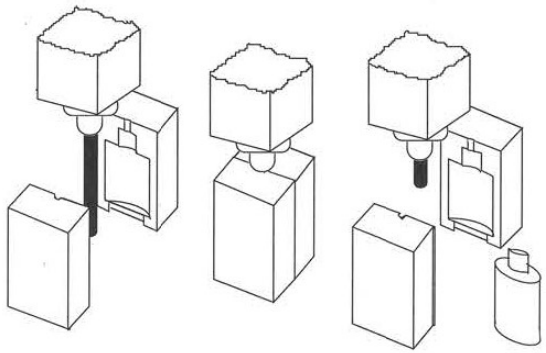


Figure 7.9 Schematic of the extrusion blow molding process

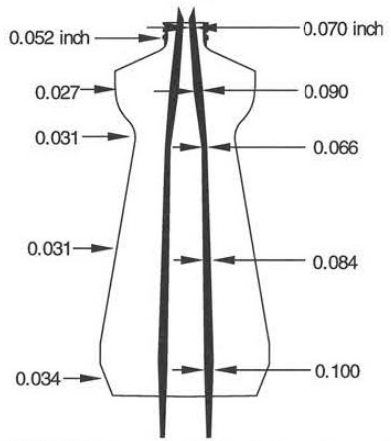


Figure 7.10 Wall thickness distribution in the parison and the part

EG_000216592

ClearCorrect Exhibit 1038, Page 83 of 125

A parison of variable thickness can be generated by moving the mandrel vertically during extrusion as shown in Fig. 7.11. A thinner wall not only results in material savings but also reduces the cycle time due to the shorter required cooling times.

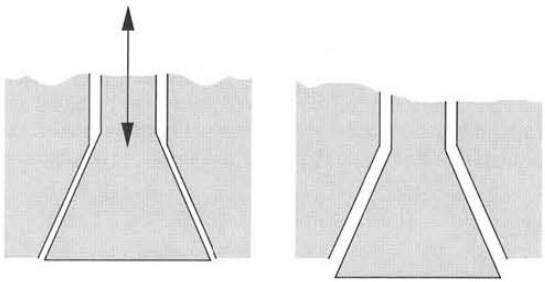


Figure 7.11 Moving mandrel used to generate a programmed parison

As expected, the largest portion of the cycle time is the cooling of the blow molded container in the mold cavity. For this reason, for high volume applications, rotary molds are often used in conjunction with vertical or horizontal rotating tables (Fig. 7.12 [5]).

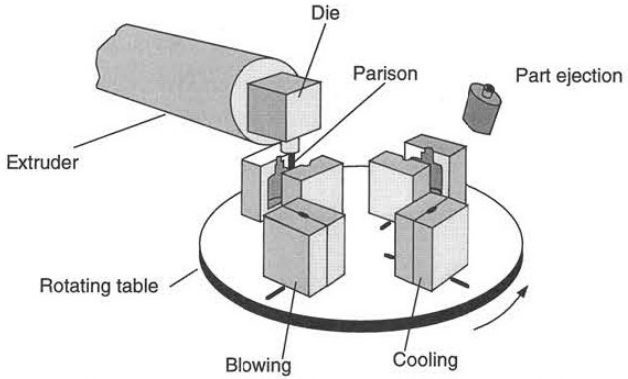


Figure 7.12 Schematic of an extrusion blow molder with a rotating table

COOLING TIME FOR BLOW MOLDING

The same procedure used for injection molding can be used to estimate the cooling time during blow molding. Since the article is cooled from one side only, the inner surface can be considered insulated. The modified Eq. (6.3) now becomes

$$t_{cooling} = \frac{4h^2}{\pi\alpha} \ln\left(\frac{8}{\pi^2}\frac{T_m - T_w}{T_D - T_w}\right) \qquad (7.12)$$

7.3.2 Injection Blow Molding

Injection blow molding depicted in Fig. 7.13 [5], begins by injection molding the parison onto a core and into a mold with finished bottle threads. The formed parison has a thickness distribution that leads to reduced thickness variations throughout the container. Before blowing the parison into the cavity, it can be mechanically stretched to orient molecules axially, Fig. 7.14 [5]. The subsequent blowing operation introduces tangential orientation. A container with biaxial molecular orientation exhibits higher optical (clarity) and mechanical properties and lower permeability. In the injection blow molding process one can go directly from injection to blowing or one can have a re-heating stage in-between.

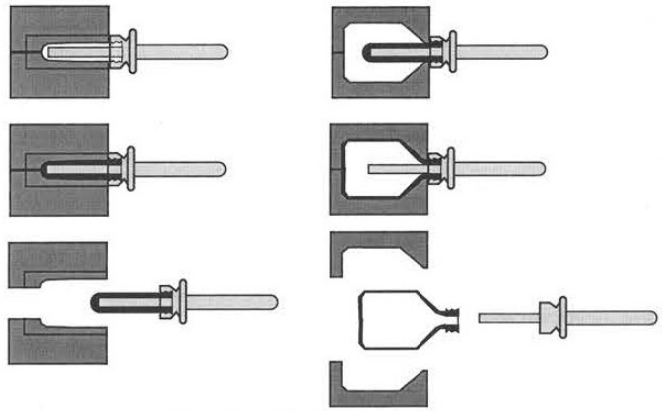


Figure 7.13 Injection blow molding

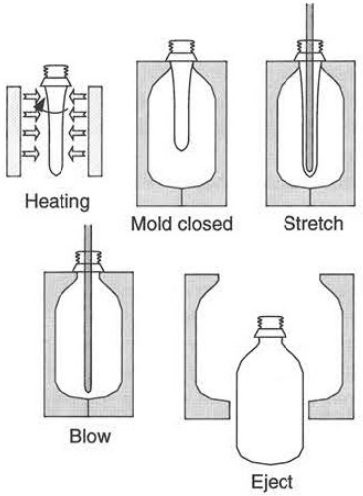


Figure 7.14 Stretch blow molding

EG_000216593

The advantages of injection blow molding over extrusion blow molding are:

- Pinch-off and therefore post-mold trimming are eliminated
- Controlled container wall thickness
- Dimensional control of the neck and screw-top of bottles and containers

Disadvantages include higher initial mold cost and the need for both injection and blow molding units.

7.4 Thermoforming

Thermoforming is an important secondary shaping of plastic film and sheet. Thermoforming consists of warming the plastic sheet and forming it into a cavity or over a tool using vacuum, air pressure, and mechanical means. During the 18th century, tortoiseshells and hooves were thermoformed into combs and other shapes. The process was refined during the mid-19th century to thermoform various cellulose nitrate articles. During World War II, thermoforming was used to manufacture acrylic aircraft cockpit enclosures, canopies, and windshields, as well as translucent covers for outdoor neon signs. During the 1950s, the process made an impact in the mass production of cups, blister packs, and other packaging commodities. Today, in addition to packaging, thermoforming is used to manufacture refrigerator liners, pick-up truck cargo box liners, shower stalls, bathtubs, as well as automotive trunk liners, glove compartments, and door panels.

A typical thermoforming process is presented in Fig. 7.15 [3]. The process begins by heating the plastic sheet slightly above the glass transition temperature, for amorphous polymers, or slightly below the melting point, for semi-crystalline materials. Although, both amorphous and semi-crystalline polymers are used for thermoforming, the process is easiest with amorphous polymers because they have a wide rubbery temperature range above the glass the transition temperature. At these temperatures the polymer is easily shaped, but still has enough rigidity to hold the heated sheet without much sagging. Most semi-crystalline polymers lose their strength rapidly once the crystalline structure breaks up above the melting temperature.

The heating is achieved using radiative heaters and the temperature reached during heating must be high enough for sheet shaping, but low enough so the sheets do not droop into the heaters. One key requirement for successful thermoforming is to bring the sheet to a uniform forming temperature. The sheet is then shaped into the cavity over the tool. This can be accomplished in several ways. Most commonly a vacuum sucks the sheet onto the tool, stretching the sheet until it contacts the tool surface. The main problem here is the irregular thickness distribution that arises throughout the part. Hence, the main concern of the process engineer is to optimize the system such that the differences in thickness throughout the part are minimized. This can be accomplished many ways but most commonly by plug-assist. Here, as the plug pushes the sheet into the cavity, only the parts of the sheet not touching the plug-assist stretch. Since the unstretched portions of the sheet must remain hot for subsequent stretching, the plug-assist is made of a low thermal

conductivity material such as wood or hard rubber. The initial stretch is followed by a vacuum for final shaping. Once cooled, the product is removed.

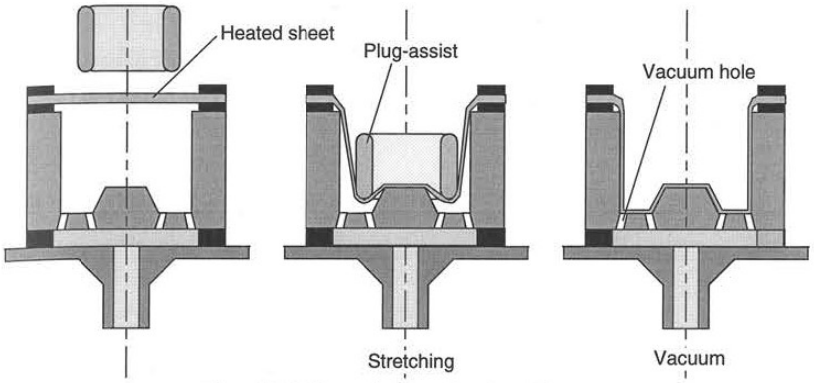


Figure 7.15 Plug-assist thermoforming using vacuum

To reduce thickness variations in the product, the sheet can be prestretched by forming a bubble at the beginning of the process. This is schematically depicted in Fig. 7.16 [3]. The mold is raised into the bubble, or a plug-assist pushes the bubble into the cavity, and a vacuum finishes the process.

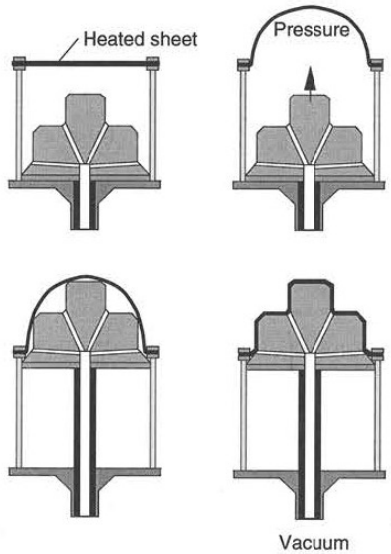


Figure 7.16 Reverse draw thermoforming with plug-assist and vacuum

EG_000216594

ClearCorrect Exhibit 1038, Page 85 of 125

One of the main reasons for the rapid growth and high volume of thermoformed products is that the tooling costs for a thermoforming mold are much lower than for injection molding.

ANALYSIS OF THERMOFORMING

The thickness distribution in various thermoformed shapes can be predicted using a simple volume or mass balance. For a thermoformed conical shape, shown in Fig. 7.17, the final thickness distribution is given by

$$h = h_0 \frac{1+\cos\alpha}{2}\left[1-\frac{s}{H}\sin\alpha\right]^{\sec\alpha-1} \tag{7.13}$$

This equation can also be used to estimate the thickness distribution in a truncated cone or cup. The thickness distribution in the cylindrical shape shown in Fig. 7.18 is given by

$$h = \frac{h_0}{2} e^{-\frac{s}{R}} \tag{7.14}$$

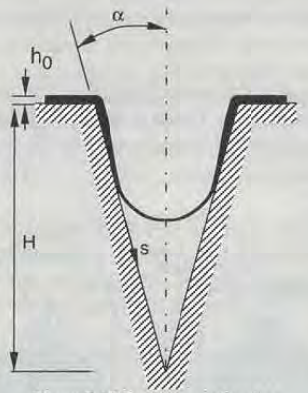


Figure 7.17 Cone thermoforming

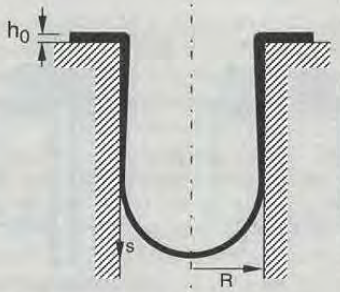


Figure 7.18 Cylinder thermoforming

Examples

7.1 Polyethylene fibers are spun to a draw ratio, D_R, of 10 through 500 μm diameter orifices at mass flow rates, $\dot{m}$, of 0.18 kg/hr per fiber. For the data below, will draw resonance occur for a spinning length of 2 m?

Material data: $n = 0.5$, $m = 2000\ Pa-s^n$, $G = 3000\ Pa$, and $\rho = 960\ kg/m^3$.

To solve this problem, we must first compute the speed of the polyethylene as it emerges from the spinneret

$$v_0 = \dot{m}/(A\rho) = \frac{0.18}{(60)(60)\pi(0.00025)^2(960)} = 0.265\ m/s$$

We can now compute the Deborah number using Eq. (7.2)

$$De = \frac{2000(3)^{(n-1)/2}}{3000}\left(\frac{0.265}{2}\right) = 0.067$$

This gives $De^{1/n} = 0.0045$ which lies in the unstable regime in Fig. 7.2. For a draw ratio of 10 and n = 0.5, the stable regime of $De^{1/n}$ lies between 0.035 and 0.1. To eliminate draw resonance, the distance between the spinneret and the take-up wheel must be decreased to 0.72 m, which requires faster cooling.

7.2 An LLDPE film is blown to a thickness of 50 μm from a 25 mm diameter annular die with a 1 mm thick slit. Determine the required bubble pressure and take-up force for an extruder mass throughput of 100 kg/hr and draw-down ratio, D_R, of 4. The freezing point is 200 mm above the die exit; the polymer is assumed to be Newtonian with a viscosity of 1000 Pa-s; and the density is 920 kg/m^3. What is the take-up speed?

We start the solution by calculating the dimensionless freezing point, X, and the thickness ratio, h_0/h_f, as

$$X = \frac{200}{12.5} = 16$$

$$h_0/h_f = \frac{0.001}{50x10^{-6}} = 20$$

From Eq. (7.8), we can compute the blow-up ratio as

$$B_R = \frac{h_0/h_f}{D_R} = \frac{20}{4} = 5$$

EG_000216595

ClearCorrect Exhibit 1038, Page 86 of 125

Figures 7.7 and 7.8 represent the film blowing process for dimensionless freezing points of 10 and 20, respectively. We can get P and F from the figures and iterpolate for a dimensionless freezing point of 16:

$X = 10 \rightarrow P = 0.08$ and $F = 1.95$

$X = 20 \rightarrow P = 0.055$ and $F = 1.50$

$X = 16 \rightarrow P = 0.065$ and $F = 1.68$

Using Eqs. (7.9) and (7.10), we can now solve for the bubble pressure and the take-up force as:

$$\Delta p = \frac{0.065(1000)(100)(1/60)(1/60)(1/920)}{\pi(0.0125)^3} = 319\ Pa$$

$$f_z = \frac{1.68(1000)(100)(1/60)(1/60)(1/920)}{(0.0125)} = 4.06\ N$$

The take-up speed can be computed using

$$v_f = \frac{(100)(1/60)(1/60)(1/920)}{(50x10^{-6})(0.025)(5)\pi} = 1.54\ m/s$$

7.3 Derive Eq. (7.14) which describes the thickness distribution in a long cylindrical thermoformed container.

The first step in the drawing process is the formation of a spherical bubble of thickness h_1. Through conservation of mass we can equate

$$\pi R^2 h_0 = 2\pi R^2 h_1$$

which results in $h_1 = \frac{h_0}{2}$. At any time, the bubble thickness as it travels down the cylinder is h. As the contact point in Fig. 7.18 travels from S to $S + dS$, it deposits a cylindrical strip of thickness h and width dh on the cylinder wall. A mass balance would result in

$$2\pi R^2 h = 2\pi R^2 (h + dh) + 2\pi R h ds$$

which reduces to

$$\frac{dh}{h} = -\frac{ds}{R}$$

which can be integrated with a boundary condition $h = h_1$ at $s = 0$ to give

$$h = \frac{h_0}{2} e^{-\frac{s}{R}}$$

Problems

7.1 Polyethylene fibers are spun to a draw ratio, D_R, of 20 through 300 μm diameter orifices at mass flow rates, $\dot{m}$, of 0.10 kg/hr per fiber. Using the data in Example 7.1, find the range of allowable distances between the spinneret and the take-up wheel.

7.2 A polyethylene film is cast as shown in Fig. 7.4 at a speed of 0.3 m/s with a draw ratio of 10. Use Figs. 3.2 and 3.7 to determine the constants in Eqs. (7.3) and (7.4).

7.3 In Example 7.2, a faster cooling rate results in a freezing point of 130 mm above the die. What is the new bubble pressure requirement?

7.4 What is the bubble pressure required for the process presented in Example 7.2, but with a blow-up ratio requirement of 4? What is the take-up speed?

7.5 What is the cooling time required for a 0.5 mm thick HDPE blow molded bottle. The extrudate temperature is 150 °C, and the mold temperature is 40 °C. The bottle can be safely removed from the cavity when the average temperature is 60 °C. Material data: $\rho = 950\ kg/m^3$, $C_p = 2300\ J/kg/K$ and $k = 0.63\ W/m/K$

7.6 Derive Eq. (7.13) which describes the thickness distribution in a thermoformed conical container.

7.7 Plot the thickness distribution along the wall of a 100 mm diameter, 400 mm deep cylindrical container thermoformed out of a polystyrene sheet initially 2 mm thick.

7.8 Plot the thickness distribution along the wall of a thermoformed 100 mm deep polystyrene juice cup. The cup mouth and bottom are 70 and 40 mm in diameter, respectively. The sheet was initially 1 mm thick.

References

1. Fisher, R.J., and M.M. Denn, *AIChE J.* (1976), 22, 236
2. Anturkar, N.R., and A. Co, *J. Non-Newtonian Fluid Mech.* (1988), *28*, 287
3. Menges, G., *Einführung in die Kunststoffverarbeitung*, Hanser Publishers (1986), Munich
4. Pearson, J.R.A., and C.J.S. Petrie, *Plastics & Polymers* (1970), *38*, 85
5. Rosato, D.V, and D.V. Rosato, *Blow Molding Handbook*, Hanser Publishers (1989), Munich
6. Modern Plastics Encyclopedia, 53, McGraw-Hill (1976), New York

EG_000216596

ClearCorrect Exhibit 1038, Page 87 of 125

8 Other Important Polymer Processes

8.1 Calendering

In a calender line, the polymer melt is transformed into films and sheets by squeezing it between pairs of co-rotating high precision rollers. Calenders are also used to produce certain surface textures which may be required for different applications. Today, calendering lines are used to manufacture PVC sheet, floor covering, rubber sheet, and rubber tires. They are also used to texture or emboss surfaces. When producing PVC sheet and film, calender lines have a great advantage over extrusion processes because of the shorter residence times, resulting in a lower requirement for stabilizer. This can be cost effective since stabilizers are a major part of the overall expense of processing these polymers.

Figure 8.1 [1] presents a typical calender line for manufacturing PVC sheet. A typical system is composed of:

- Plasticating unit
- Calender
- Cooling unit
- Accumulator
- Wind-up station

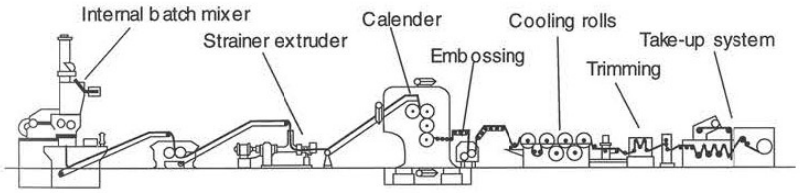


Figure 8.1 Schematic of a typical calendering process (Berstorff GmbH)

In the plasticating unit, the material is melted and mixed by an internal batch mixer or a roll-mill before it is fed between the nip of the first two rolls. Here, the first pair of rolls control the feeding rate, while subsequent rolls in the calender calibrate the sheet thickness. Most calender systems have four rolls as does the one in Fig. 8.1, which is an inverted L- or F-type system. Other typical roll arrangements are shown in Fig. 8.2. After the main calender, the sheet can be passed through a secondary calendering operation for embossing. The sheet is then passed through a series of chilling rolls where it is cooled from both sides in an alternating fashion. After cooling, the film or sheet is wound.

EG_000216597

One of the major concerns in a calendering system is generating a film or sheet with a uniform thickness distribution with tolerances as low as ± 0.005 mm. To achieve this, the dimensions of the rolls must be precise. It is also necessary to compensate for roll bowing resulting from high pressures in the nip region. Roll bowing is a structural problem that can be mitigated by placing the rolls in a slightly crossed pattern, rather than completely parallel, or by applying moments to the roll ends to counteract the separating forces in the nip region.

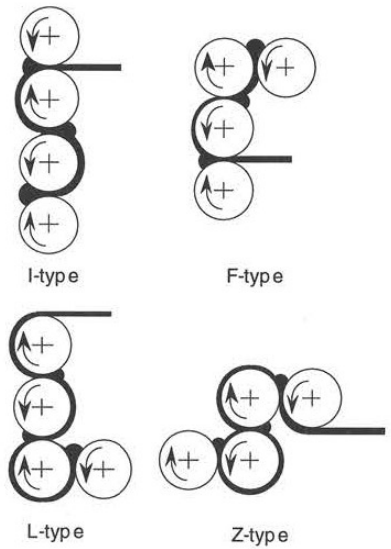


Figure 8.2 Calender arrangements

ANALYSIS OF CALENDERING

Calendering can be modeled by assuming steady state, laminar flow and isothermal conditions. Such an analysis is presented by Middleman [2] and the main results are shown here. Assuming a power-law viscosity model given by

$$\eta = m|\dot{\gamma}|^{n-1} = m_0 e^{-a(T-T_0)}|\dot{\gamma}|^{n-1} \tag{8.1}$$

and the notation presented in the schematic shown in Fig. 8.3, the maximum pressure in the nip region can be calculated using

$$p_{max} = m\sqrt{\frac{2R}{h_0}}P(n) \tag{8.2}$$

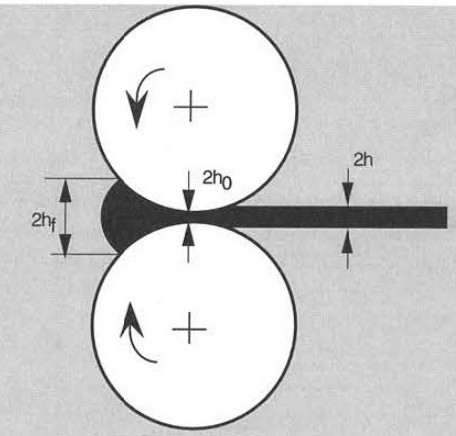


Figure 8.3 Schematic of the calendering process

where $P(n)$ is presented in Fig. 8.4[2]. The roll separating force caused by the pressure distribution between the nip can be calculated using

$$f = m\left(\frac{v}{h_0}\right)^n RWF(n) \tag{8.3}$$

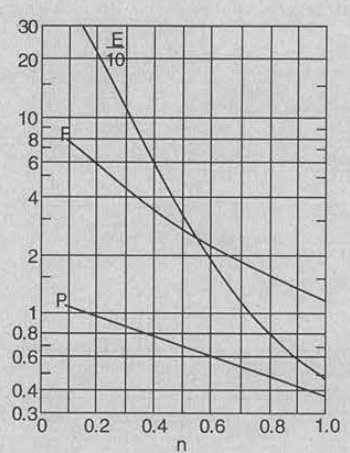


Figure 8.4 Pressure, force, and power functions versus power-law index

where W is the width of the sheet between the rolls and the quantity $F(n)$ can be found in Fig. 8.4[2]. The power transmitted to the sheet between the nips can also be calculated using

EG_000216598

ClearCorrect Exhibit 1038, Page 89 of 125

$$\dot{S} = mv^2\left(\frac{v}{h_0}\right)^{n-1} W\sqrt{\frac{R}{h_0}}E(n) \tag{8.4}$$

where $E(n)$ is presented in Fig. 8.4 [2].

The sheet thickness, $2h$, as it emerges from the rolls is also a function of the power-law index and is presented in Fig. 8.5 for a system with a large amount of material accumulated at the entrance of the nip region. For the case where a finite sheet of thickness $2h_{feed}$ is fed through the nip region, the thickness of the film or sheet can be calculated using the curves presented in Fig. 8.6 [3].

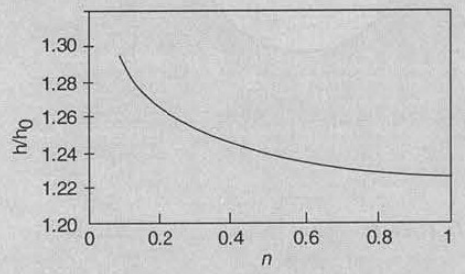


Figure 8.5 Sheet thickness as a function of power-law index for a large reservoir thickness

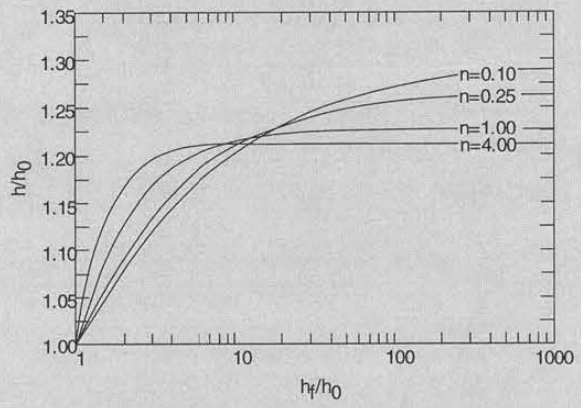


Figure 8.6 Sheet thickness as a function of upstream reservoir thickness for various power-law indices

8.2 Coating

In coating a liquid film is continuously deposited on a moving, flexible or rigid substrate. Coating is done on metal, paper, photographic films, audio and video tapes, and adhesive tapes. Typical coating processes include *wire coating*, *dip coating*, *knife coating*, *roll coating*, *slide coating*, and *curtain coating*.

In wire coating, a wire is continuously coated with a polymer melt by pulling the wire through an extrusion die. The polymer resin is deposited onto the wire using the drag flow generated by the moving wire and sometimes a pressure flow generated by the back pressure of the extruder. The process is schematically depicted in Fig. 8.7.* The second normal stress differences, generated by the high shear deformation in the die, help keep the wire centered in the annulus [4].

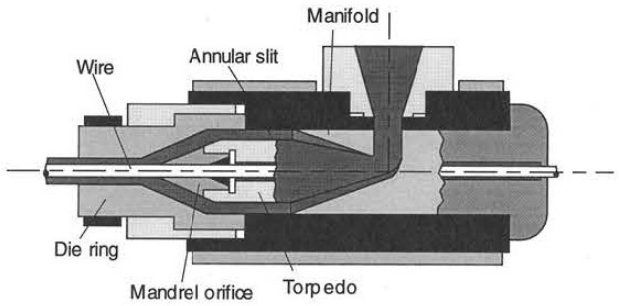


Figure 8.7 Wire coating process

Dip coating is the simplest and oldest coating operation. Here, a substrate is continuously dipped into a fluid and withdrawn with one or both sides coated with the fluid. Dip coating can also be used to coat individual objects that are dipped and withdrawn from the fluid. The fluid viscosity and density and the speed and angle of the surface determine the coating thickness.

Knife coating, depicted in Fig. 8.8, consists of metering the coating material onto the substrate from a pool of material, using a fixed rigid or flexible knife. The knife can be normal to the substrate or angled and the bottom edge can be flat or tapered. The thickness of the coating is nearly half the gap between the knife edge and the moving substrate or web. A major advantage of a knife edge coating system is its simplicity and relatively low maintenance.

Roll coating consists of passing a substrate and the coating simultaneously through the nip region between two rollers. The physics governing this process is similar to calendering, except that the fluid adheres to both the substrate and the opposing roll. The

* Other wire coating processes extrude a tubular sleeve which adheres to the wire via stretching and

EG_000216599

ClearCorrect Exhibit 1038, Page 90 of 125

coating material is a low viscosity fluid, such as a polymer solution or paint and, is picked up from a bath by the lower roll and applied to one side of the substrate. The thickness of the coating can be as low as a few μm and is controlled by the viscosity of the coating liquid and the nip dimension. This process can be configured as either forward roll coating for co-rotating rolls or reverse roll coating for counter-rotating rolls (Fig. 8.9). The reverse roll coating process delivers the most accurate coating thicknesses.

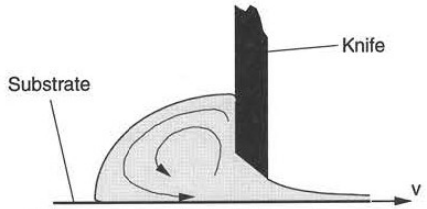


Figure 8.8 Schematic of a knife coating process

FILM THICKNESS IN FORWARD ROLL COATING

Using the nomenclature in Fig. 8.9, the thickness ratio of the film traveling with the rolls after they split can be calculated using [5]

$$\frac{T_2}{T_1}=\left(\frac{U_2}{U_1}\right)^E \tag{8.5}$$

where the exponent E is related to the shear thinning effect of the polymer melt. Figure 8.10 [5] presents E as a function of the power-law index.

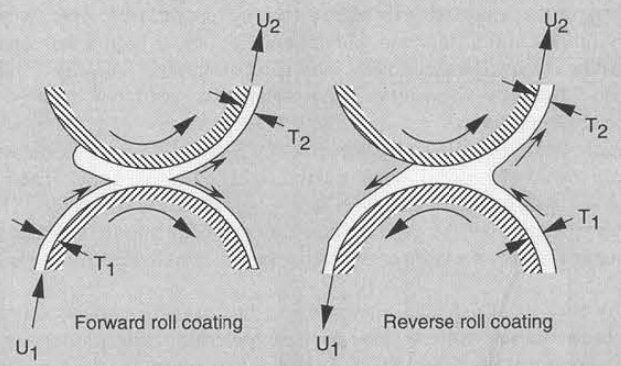


Figure 8.9 Schematic of forward and reverse roll coating processes

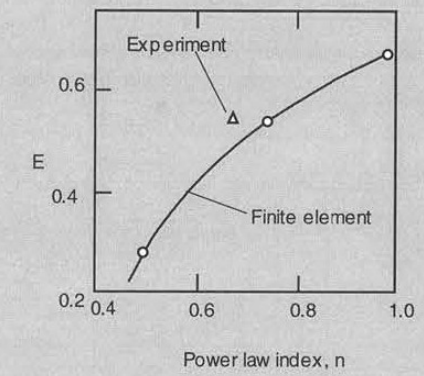


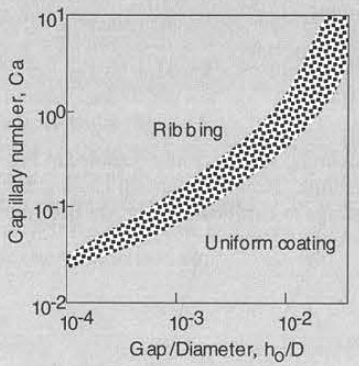
Figure 8.10 Constant E for Eq. (8.5) used to compute coating thickness in forward roll coating

RIBBING IN ROLL COATING

A defect that often forms during roll coating is caused by the ribbing instability. Here, sinusoidal waves across the web form, leaving so called rake lines in the moving direction of the substrate. Figure 8.11[5] presents the critical capillary number, which determines the onset of instabilities during forward roll coating as a function of roll geometry. The capillary number in Fig. 8.11 is defined by

$$Ca=\frac{\mu\bar{v}}{\sigma_s} \tag{8.6}$$

where μ is the viscosity of the coating fluid, $\bar{v}$ is the average roll speed, and σ_s is the surface tension of the fluid in air.



EG_000216600

ClearCorrect Exhibit 1038, Page 91 of 125

FILM THICKNESS IN REVERSE ROLL COATING

Using the nomenclature used in Fig. 8.9, the film thickness in a reverse roll coating operation can be computed using the graph presented in Fig. 8.12 [5].

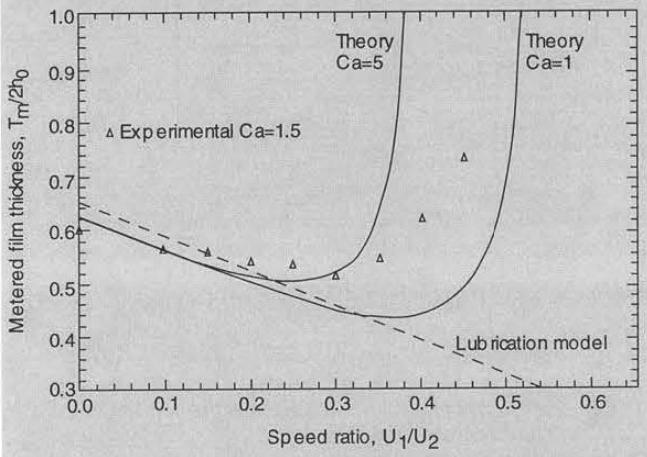


Figure 8.12 Film thickness versus roll speed ratio for various capilary numbers

Here, the capillary number is calculated using

$$Ca = \frac{\mu U_2}{\sigma_s} \tag{8.7}$$

where U_2 is the speed of the applicator roll. The figure shows how well theory agrees with experiments.

Slide coating and curtain coating, schematically depicted in Fig. 8.13, are commonly used to apply multi-layered coatings. However, curtain coating has also been widely used to apply single layers of coatings to cardboard sheet. In both methods, the coating fluid is pre-metered.

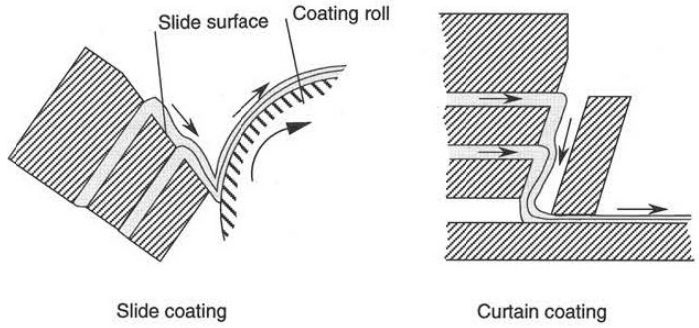


Figure 8.13 Slide and curtain coating

8.3 Processing Reactive Polymers

Reactive polymers, such as thermosets, undergo a chemical reaction during solidification. In processing, thermosets are often grouped into three distinct categories, namely those that undergo a *heat activated cure,* those dominated by a *mixing activated cure*, and those activated by the absorption of humidity or ultra violet radiation. Examples of heat activated thermosets are phenolics; examples of mixing activated cure are epoxy resins and polyurethane. Similarly to thermoplastics, thermosets either cure via *condensation polymerization* or *addition polymerization.*

Condensation polymerization is the growth process that results from combining two or more monomers with reactive end-groups, and leads to by-products such as alcohol, water and acid. The by-product of the reaction when making phenolics is water. Another well known example of a thermoset that cross links via condensation polymerization is the co-polymerization of unsaturated polyester with styrene molecules, also called free radical reaction, as shown in Fig. 8.14. The molecules contain several carbon-carbon double bonds which act as cross linking sites during curing. An example of the resulting network after the chemical reaction is shown in Fig. 8.15.

No matter which category of thermoset, its curing reaction can be described by the reaction between two chemical groups denoted by A and B which link two segments of a polymer chain. The reaction can be followed by tracing the concentration of unreacted As or Bs, C_A or C_B, respectively. If the initial concentrations of As and Bs are defined as C_{Ao} and C_{Bo}, the degree of cure can be described as

$$c = \frac{C_{Ao} - C_A}{C_{Ao}} \tag{8.8}$$

EG_000216601

ClearCorrect Exhibit 1038, Page 92 of 125

The degree of cure or conversion, c, equals zero when there has been no reaction and equals one when all As have reacted and the reaction is complete. It is difficult to monitor reacted and unreacted As and Bs during the curing reaction of a thermoset polymer. However, the heat released during curing can be used to monitor the conversion, c. When small samples of an unreacted thermoset polymer are placed in a differential scanning calorimeter (DSC), each at a different temperature, every sample releases nearly the same amount of heat, Q_T. This occurs because every cross link that occurs during a reaction releases a little heat. For example, Fig. 8.16 [6] shows the heating rate during isothermal cure of a vinyl ester at various temperatures.

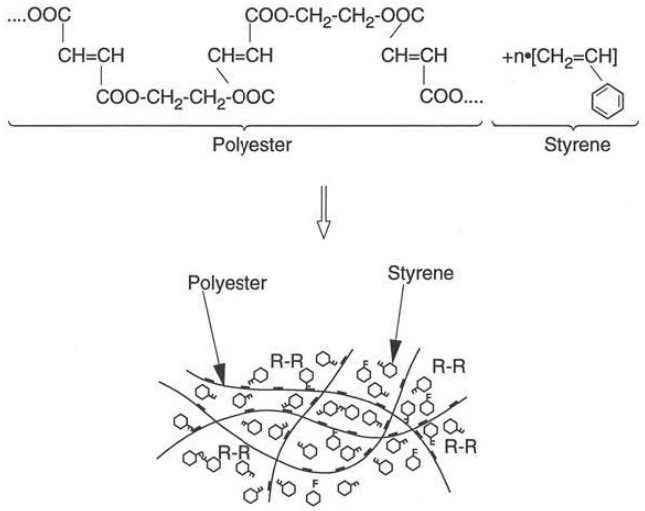


Figure 8.14 Symbolic and schematic representations of uncured unsaturated polyester

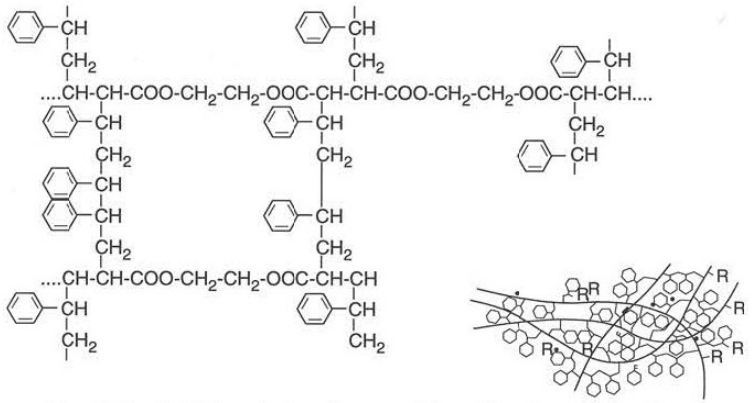


Figure 8.15 Symbolic and schematic representations of cured unsaturated polyester

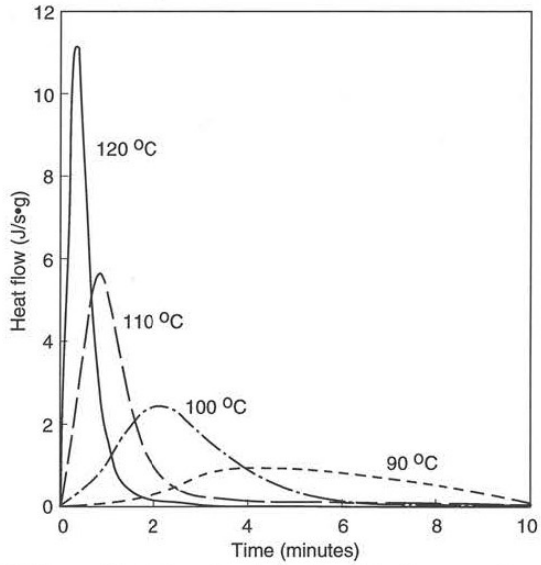


Figure 8.16 DSC scan of the isothermal curing reaction of vinyl ester at various temperatures

CURING REACTION MODELS

The degree of cure of a thermoset resin can be defined by the following relation

$$c = \frac{Q}{Q_T} \tag{8.9}$$

where Q is the heat released up to an arbitrary time t. DSC data is commonly fitted to empirical models that accurately describe the curing reaction. Hence, the rate of cure can be described by the exotherm, $\dot{Q}$ and the total heat released during the curing reaction, Q_T. The curing kinetics for many heat activated cure materials, such as vinyl esters and unsaturated polyesters, can be described fairly well using the Kamal-Sourour Model [7] given by

$$\frac{dc}{dt} = \frac{\dot{Q}}{Q_T} = \left(a_1 e^{-\frac{b_1}{RT}} + a_2 e^{-\frac{b_2}{RT}} c^m \right)(1-c)^n \tag{8.10}$$

where the six constants can be fit to DSC data.

On the other hand, mixing activated cure materials such as polyurethanes instantly start releasing exothermic heat after the mixture of its two

EG_000216602

ClearCorrect Exhibit 1038, Page 93 of 125